

VIII AUSE CONGRESS AND III ALBA USER'S MEETING

9th - 11th October 2017

Campus of the Consejo Superior de Investigaciones Científicas (CSIC)
Serrano 117-123, 28006 Madrid



VIII AUSE Congress and III ALBA User's Meeting
Madrid 9th-11th October 2017



Sponsors



greateyes

DISCOVER WHAT
THE EYE CAN'T SEE



Contents

Organizing Committee	4
Scientific Program	5
Oral contributions	8
Poster contributions	59
Author index	101

Organizing Committee

CONFERENCE CHAIR

Mari Cruz García-Gutiérrez / *maricruz@iem.cfmac.csic.es*

LOCAL COMMITTEE

Ana Cámara / *acamara@ual.es*

Tiberio A. Ezquerro / *t.ezquerro@csic.es*

Juan de la Figuera / *juan.delafiguera@iqfr.csic.es*

Edgar Gutiérrez / *edgar.gutierrez@iem.cfmac.csic.es*

Amelia Linares / *linares@iem.cfmac.csic.es*

Aurora Nogales / *aurora.nogales@csic.es*

Inmaculada Ramos / *iramos@cells.es*

Esther Rebollar / *e.rebollar@csic.es*

Álvaro Rodríguez-Rodríguez / *alvaro.rodriguez@iem.cfmac.csic.es*

SCIENTIFIC COMMITTEE

Caterina Biscari / *cbiscari@cells.es*

Aurelio Cabeza / *aurelio@uma.es*

Ana Cámara / *acamara@ual.es*

Salvador Ferrer / *sferrer@cells.es*

Miguel A.G. Aranda / *g.aranda@cells.es*

Mari Cruz García-Gutiérrez / *maricruz@iem.cfmac.csic.es*

José Luis García-Muñoz / *garcia.munoz@icmab.es*

Olga López / *oloesi@cid.csic.es*

Juan Rubio / *juan.rubio@esrf.fr*

Gonzalo Santoro / *gonzalo.santoro@icmm.csic.es*

Gloria Subías / *gloria@unizar.es*

Scientific Program

MONDAY - 9th of October (AUSE)

Room A

12:30 - 14:30	Welcome Party: Registration & lunch; sponsor exhibition (cloister)
14:30 - 15:00	Opening Ceremony
15:00 - 15:20	Caterina Biscari "ALBA general status"
15:20 - 16:10	Plenary Lecture: Francesco Sette, European Synchrotron ESRF. 45' + 5'.
16:10 - 16:30	Marta Martínez-Sanz - 15' + 5'.
16:30 - 16:50	Jordi Fraxedas - 15' + 5'.
16:50 - 17:10	Álvaro Rodríguez-Rodríguez - 15' + 5'.
17:10 - 17:30	Ernesto Pérez - 15' + 5'.

Room B

16:10 - 16:30	Víctor de la Peña O'Shea - 15' + 5'
16:30 - 16:50	Enrique V. Ramos-Fernández - 15' + 5'
16:50 - 17:10	Carlos Frontera - 15' + 5'
17:10 - 17:30	Carmen Sánchez de Rojas - 15' + 5'

Cloister

17:30-19:00	Coffee & poster discussion: ALBA users and AUSE members; sponsor exhibition
-------------	---

Authors should be present to answer the questions/comments from the awarding committee. Authors entitled for the prizes must be 'young researchers' as defined by being 30 years old (or younger) 09/10/2017.

AUSE price to the best poster (300 € & diploma), secondary award 'accésit' (150 € & diploma)

ALBA price to the best poster (300 € & diploma), secondary award 'accésit' (150 € & diploma)

Scientific Program

TUESDAY - 10th of October (AUSE)

Room A

09:00 - 09:50	Plenary Lecture: Massimo Altarelli European XFEL 45' + 5'
09:50 - 10:10	Mark van Raaij 15' + 5'
10:10 - 10:30	Inmaculada Martínez-Rovira 15' + 5'
10:30 - 10:50	Verónica Moner 15' + 5'
10:50 - 11:20	Coffee break
11:20 - 11:50	June Ereño. Talk based on the Ph.D. thesis award AUSE – 2015/2016 25' + 5'
11:50 - 12:10	Lourdes Marcano 15' + 5'
12:10 - 12:30	Ilaria Carlomagno 15' + 5'
12:30 - 12:50	Gema Martínez-Criado 15' + 5'
12:50 - 13:10	María Ángeles Subirana 15' + 5'
13:10 - 13:30	Juan Vilatela 15' + 5'

Cloister

13:30 - 15:00	Lunch; sponsor exhibition
---------------	---------------------------

Room A

15:00 - 15:50	Plenary Lecture: Christoph Quitmann MAX IV Laboratory 45' + 5'
15:50 - 16:10	José Abad 15' + 5'
16:10 - 16:30	Alicia de Andrés 15' + 5'
16:30 - 16:50	Eduardo Salas-Colera 15' + 5'
16:50 - 17:10	María Vila 15' + 5'

Room B

15:50 - 16:10	Alicia Gomis-Berenguer 15' + 5'
16:10 - 16:30	Juan Angel Sans 15' + 5'
16:30 - 16:50	Adrián Andrada-Chacón 15' + 5'
16:50 - 17:10	Ana Cuesta 15' + 5'

17:10 - 17:30	Coffee break
17:30 - 18:00	Key-note contribution: SpLine ESRF" 25' + 5'
18:00 - 19:30	AUSE general assembly

Scientific Program

WEDNESDAY - 11th of October (ALBA Users)

Room A

09:00 - 09:30	Caterina Biscari - ALBA strategic Plan and European LEAPS initiative 20' + 10'
09:30 - 09:50	Montse Pont - Five years of ALBA Accelerator Operation and outlook 15' + 5'
09:50 - 10:20	Marc Malfois - Upgrade of the SAXS BL: NCD-SWEET 25' + 5'
10:20 - 10:40	Ibraheem Yousef - The new Synchrotron Infrared Microspectroscopy BL-MIRAS 25' + 5'
10:40 - 11:00	Federico Bisti - LOREA: the ARPES BL under construction at ALBA 15' + 5'
11:00 - 11:30	Coffee break
11:30 - 12:00	Jordi Juanhuix - Update and recent developments at XALOC and MISTRAL BLs. 25' + 5'
12:00 - 12:30	Francois Fauth - Update and recent developments at MSPD and CLAESS BLs. 25' + 5'
12:30 - 12:50	Dino Tonti 15' + 5'
12:50 - 13:10	Laura Simonelli 15' + 5'
13:10 - 13:30	Oriol Vallcorba 15' + 5'

Room B

12:30 - 12:50	Juan Pedro Espinós 15' + 5'
12:50 - 13:10	Frederik Schiller 15' + 5'
13:10 - 13:30	Eva Mateo-Marti 15' + 5'

Cloister

13:30 - 15:00	Lunch; sponsor exhibition
---------------	---------------------------

Room A

15:00 - 15:30	Eric Pellegrin. Update and recent developments at CIRCE and BOREAS BLs 25' + 5'
15:30 - 15:50	Michael Foerster 15' + 5'
15:50 - 16:10	Juan de la Figuera 15' + 5'
16:10 - 16:30	Miguel Angel Valbuena 15' + 5'
16:30 - 17:00	Miguel A. G. Aranda. Possibilities for collaboration with ALBA synchrotron 20' + 10'

Room B

15:30 - 15:50	Javier Bartolomé 15' + 5'
15:50 - 16:10	Pierluigi Gargiani 15' + 5'
16:10 - 16:30	Stefano Agrestini 15' + 5'

Cloister

17:00 - 19:00	Coffee and poster discussion; sponsor exhibition Continue the selection for the prizes to the best posters
---------------	---

21:00	Conference Dinner, including the awarding of the best poster prizes and oral contributions
-------	--

Oral Contributions

Monday 9th October 15:00 - 15:20

ALBA General Status

C. Biscari

ALBA Synchrotron, Carrer de la Llum, 2-26, Cerdanyola del Valles, 08290, Barcelona (Spain);
cbiscari@cells.es

ALBA Synchrotron, the Spanish photon source, is an interdisciplinary instrument and a research laboratory where cutting edge experiments are daily realized by a wide variety of user groups, both public and private.

Nationally funded and fully committed to serve the Spanish community, it still has an international character, expressed in its staff, usage and collaborations.

The successful operation period since 2012, the available beamlines as well as those in construction, will be described. Scientific and technological excellences will be highlighted.

The ESRF EBS Programme: a new X-ray source for synchrotron science

Francesco Sette

ESRF, 71 Avenue des Martyrs, Grenoble 38043 – France

The presentation reviews the ongoing Upgrade Programme (UP) of the ESRF, which was launched in 2009 in two phases and will be concluded by 2022. The first phase is concluded, and it delivered 19 new instruments aiming to develop X-ray science in the study of the structure and dynamics of condensed and living matter with improved microscopy and imaging capacity, down to nanometer space resolution, and time-scales down to the nanosecond. The ongoing second phase is centred on the construction of the first of a new generation of storage rings for synchrotron science. This new hybrid multiple bend achromat storage ring lattice design efficiently enables the delivery of diffraction limited hard X-rays by drastically reducing the electron beam horizontal emittance; its adaptation to the existing ESRF storage ring tunnel will improve today's performances by 100 in terms of brightness and transverse coherence. This project, following the footsteps of the MAX-IV multiple bend storage ring implemented in Lund, is under construction at the ESRF since two years and will be operational in 2020. This ESRF new Extremely Brilliant Source (EBS) programme has attracted worldwide attention, triggering similar conceptual studies in almost all existing and future synchrotron laboratories on the planet. The ESRF Orange Book (http://www.esrf.eu/Apache_files/Upgrade/ESRF-orange-book.pdf) describes the whole ESRF EBS programme including the new scientific investigation opportunities. The ESRF-EBS will deliver a new and first-of-a-kind storage ring, new adapted beamlines, and an ambitious instrumentation programme centred on X-ray detector developments and data handling strategies.

THE POTENTIAL OF SCATTERING TECHNIQUES TO INVESTIGATE THE STRUCTURE AND MOLECULAR INTERACTIONS OF POLYSACCHARIDES

M. Martínez-Sanz, M.J. Fabra, L.G. Gómez-Mascaraque and A. López-Rubio

Food Quality and Preservation Department, IATA-CSIC, Avda. Agustín Escardino 7, 46980 Paterna, Valencia (Spain); mmartinez@iata.csic.es

Scattering techniques represent an excellent tool for the structural characterization of natural polysaccharides since they involve minimal sample preparation and do not require drying processes which can strongly affect the native structure of hydrated systems. However, the application in this field is still a largely unexploited area due to their specificity and the complexity of data manipulation and interpretation.

In this work, we present the application of small angle X-ray techniques (WAXS and SAXS), in combination with complementary methods such as small angle neutron scattering (SANS), differential scanning calorimetry (DSC), spectroscopy and morphological characterisation, to investigate the structure and molecular interactions of polysaccharides in hydrated systems with different practical applications, such as plant cell wall (PCW) materials, and starch-microalgae blends.

The characterisation of PCWs by SAXS and SANS and the application of a suitable model to describe the experimental data, revealed the multi-phase structure of cellulose, as well as the essential role of water at the different structural levels. Furthermore, the presence of matrix polysaccharides such as arabinoxylan, xyloglucan, mixed linkage glucans and pectins during synthesis in model cellulose hydrogels evidenced their distinct structural role and interaction mechanism with cellulose.

The structural changes undergone by starch during gelatinisation were studied by temperature-resolved simultaneous SAXS-WAXS experiments, combined with DSC characterisation. The incorporation of microalgae had a significant impact on the gradual disruption of the crystalline and lamellar structure of starch during gelatinisation. The impact on the gelatinisation process was seen to be different depending on the starch amylose ratio and the lipidic profile and content of the diverse microalgae species utilised.

These results highlight the potential of X-ray scattering techniques, especially when combined with complementary methods, to provide valuable insights on the structure and molecular interactions of polysaccharides in a wide variety of hydrated systems.

SELF-ASSEMBLY OF BLOCK COPOLYMER THIN FILMS AS REVEALED BY GISAXS

J. Fraxedas^a, L. Evangelio^{a,b}, M. Fernández-Regúlez^b, S. Gottlieb^b, G. Rius^b, F. Pérez-Murano^b, H. Amenitsch^c, E. Gutiérrez^d, A. Nogales^d, M. C. García-Gutiérrez^d and T. Ezquerro^d

^a Catalan Institute of Nanoscience and Nanotechnology (ICN2), CSIC and The Barcelona Institute of Science and Technology, Campus UAB, Bellaterra 08193, Barcelona, Spain; jordi.fraxedas@icn2.cat

^b Institut de Microelectrònica de Barcelona (IMB-CNM, CSIC), Campus UAB, Bellaterra 08193, Barcelona, Spain; francesc.perez@imb-cnm.csic.es

^c Institute of Inorganic Chemistry, Graz University of Technology, Stremayrgasse 9/5, A-8010 Graz, Austria

^d Instituto de Estructura de la Materia, IEM-CSIC, Serrano 121, Madrid 28006, Spain; t.ezquerro@csic.es

Directed self-assembly (DSA) of block co-polymers (BCP) is one of the main alternative lithography methods to continue with the miniaturization trend in micro/nano semiconductor electronics industry. The main advantage of DSA is the capability to create sub-10 nm line-width patterns in large areas with simpler processes and lower line edge roughness. Understanding the self-assembly mechanisms is essential in order to find the optimal process conditions, such as the kinetics of self-assembly and the control of the density of defects. We use the GISAXS technique to investigate different aspects related to DSA.^{1,2} The information will be used to optimize process conditions and to determine the quality and properties of the DSA patterns. We report GISAXS experiments on the self-assembly of BCP which were performed at the Austrian SAXS beamline at ELETTRA (Trieste, Italy). 0.154 nm X-rays with a beam size of $400 \times 200 \mu\text{m}$ (H \times V) was used. Scattered intensity was recorded by a Pilatus 1M detector with a sample-to-detector distance of 1878 mm. We will show how GISAXS provides useful information on the following aspects: (i) dimensions of the self-assembled patterns and their modification after pattern transfer (see figure 1), (ii) role of surface properties on the morphology of the self-assembled patterns, and (iii) influence of the guiding patterns dimensions on the self-assembled patterns. In addition, we have characterized the self-assembly process in real time by in-situ annealing the samples while being exposed to the x-ray beam.

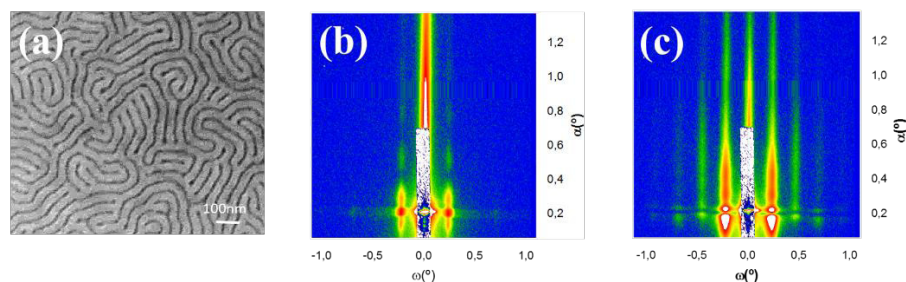


Figure 1. (a) SEM image of a PS-b-PMMA BCP thin film. Dark and bright domains correspond to PS and PMMA, respectively. The average pitch of the pattern is 37 nm. (b) GISAXS image of the same sample. (c) GISAXS image of the same BCP film after selective removal of the PMMA domain. The higher contrast in the GISAXS spectra provides richer information of the sample properties.

Acknowledgements. We thank S. Bernstorff and B. Marmiroli for assistance during the experiments and to Sincrotrone Trieste, Elettra, for beam time allocation.

¹ M. Fernández-Regúlez *et al.*, *ACS Appl. Mater. Interfaces* **2014**, *6*, 21596.

² D. R. Rueda *et al.*, *J. Appl. Crystallography* **2012**, *45*, 1038-1045.

NANOPHASE SEPARATION IN LASER INDUCED PERIODIC SURFACE STRUCTURES (LIPSS) ON BULK HETEROJUNCTION PHOTOVOLTAIC THIN FILMS AS REVEALED BY RESONANT SOFT X-RAY SCATTERING

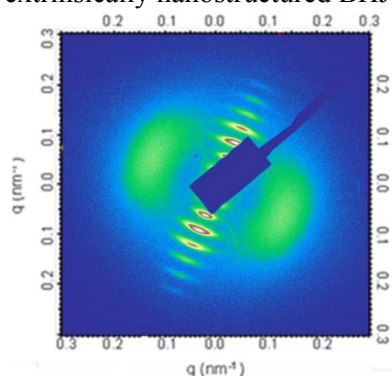
Álvaro Rodríguez-Rodríguez^a, Mari-Cruz Garcia-Gutiérrez^a, Tiberio A. Ezquerro^a, Michael A. Brady^b, Cheng Wang^b and Esther Rebollar^c

^aInstituto de Estructura de la Materia (IEM-CSIC), Serrano 121, 28006 Madrid, Spain.

^bAdvanced Light Source, Lawrence Berkeley National Laboratory, Berkeley, California 94720 USA.

^cInstituto de Química Física Rocasolano (IQFR-CSIC), Serrano 119, 28006 Madrid, Spain.

Organic photovoltaics have raised a great deal of attention as an alternative to the well-established photovoltaic solar cells based on silicon¹. In this respect, the most efficient polymer cell design is based on the so called bulk heterojunction architecture (BHJ) which are blends formed by two organic phases, one being the electron donor and the other being the electron acceptor². Besides new materials, one strategy to further improve solar cell performance consists of the fabrication of periodic micro and nanostructures on the surface of the BHJ in order to improve light harvesting by enhancing both optical path length and light trapping³. LIPSS have been recently applied to produce grating-like nanostructures on the surface of a BHJ⁴. LIPSS can be an alternative to lithography processes avoiding the necessity of using clean rooms, high vacuum systems or mask fabrication⁵. In addition to the effort in the development of new approaches, it is evident that further advance requires also the ability to characterize the nanomorphology typically exhibiting a complex hierarchy of length scales. If the characterization of the intrinsic nanomorphology of BHJ is still a cumbersome issue it becomes even more complicated upon dealing with extrinsically nanostructured BHJ systems.



In this work, Resonant Soft X-ray Scattering at the carbon K edge is shown to be an adequate approach to evaluate the phase segregation between donor and acceptor phases across the grooves of a Laser Induced Periodic Surface nanostructure on a paradigmatic poly(3-hexylthiophene)/fullerene bulk heterojunction. The results provide direct evidence that the formation of the nanostructure on the surface of the BHJ induces not only additional phase separation of the two components but also a preferential directional arrangement of the different phases.

Figure 1. 2D RSoXS pattern of the LIPSS P3HT/PC71BM thin film at $E = 284.2$ eV.

Acknowledgements. This work has been supported by Spanish Ministry of Economy and Competitiveness under the projects MAT2014-59187-R, MAT2015-66443-C02-1-R and CTQ2016-75880-P. E.R. and A.R-R thank MINECO for the tenure of a Ramón y Cajal contract (No. RYC-2011-08069) and FPI (BES-2013-062620) contracts, respectively. The authors thank the Soft X-ray Scattering team at Beamline 11.0.1.2 of the ALS at LBNL, Berkeley, USA.

¹ H. Hoppe and N. S. Sariciftci, *Journal of Materials Research* **19**, 1924 (2004).

² S. Günes, H. Neugebauer, and N. S. Sariciftci, *Chemical Reviews* **107**, 1324 (2007).

³ S.-I. Na, S.-S. Kim, J. Jo, S.-H. Oh, J. Kim, and D.-Y. Kim, *Advanced Functional Materials* **18**, 3956 (2008).

⁴ J. Cui *et al.*, *ACS Applied Materials & Interfaces* **8**, 31894 (2016).

⁵ E. Rebollar, M. Castillejo, and T. A. Ezquerro, *Eur. Polym. J.* **73**, 162 (2015).

SYNCHROTRON STUDY OF THE ROTATOR PHASES AND POLYMORPHISM IN *n*-PARAFFINS

**E. Pérez^a, E. Blázquez-Blázquez^a, R. Barranco-García^a, M. L. Cerrada^a
and J. C. Martínez^b**

^a*Instituto de Ciencia y Tecnología de Polímeros (ICTP-CSIC), Juan de la Cierva 3, 28006 Madrid (Spain); ernestop@ictp.csic.es*

^b*ALBA Synchrotron Light Source, Carrer de la Llum 2-26, 08290 Cerdanyola del Vallès, Barcelona, (Spain).*

Many studies have been devoted to the phase behavior of *n*-paraffins. This considerable interest has been partly due to the fact that these simple compounds can be considered as models for the structure of many other more complicated systems in different fields, such as liquid crystals, surfactants, membranes, lipids and other biological compounds.^{1,2,3} Not forgetting the implications in the crystalline structure of a polymer as relevant as polyethylene.

These *n*-paraffins exhibit a rather complicated and interesting phase behavior, showing different crystalline polymorphs depending on the number of carbons, on the parity, and, of course, on temperature.^{4,5} Moreover, different solid–solid phase transformations are observed, especially for homologues with $n > 22$.

Interestingly, between those polymorphs with perfect crystalline order and the fully disordered liquid phase there are the so called rotator phases, yet exhibiting a typically crystalline long range three-dimensional positional order, but accompanied by a rotational freedom of the molecules about its long axis.^{1,2} The result is a layered organization with a certain disorder, so that these phases are also named as plastic crystals, resembling the structure of highly ordered smectics. Up to five different rotator phases have been described, the two most important ones being the rotator I, showing a pseudohexagonal symmetry, and the rotator II, with a hexagonal symmetry.

We present here a synchrotron study of the rotator phases and polymorphism in several *n*-paraffins with different lengths and parity. For that, real-time variable-temperature SAXS/WAXS experiments with synchrotron radiation were performed at beamline BL11-NCD at ALBA (Cerdanyola del Vallés, Barcelona, Spain) at a fixed wavelength of 0.1 nm. The WAXD profiles were acquired with a Rayonix LX255-HS detector, placed at about 16 cm from sample and a tilt angle of around 30 degrees, and the SAXS ones with a Pilatus 1M detector (at a distance of around 300 cm from sample). The temperature control unit was a Linkam hot stage, connected to a cooling system working with liquid nitrogen.

Particular attention has been paid to the low-angle diffractions, and the corresponding comparison of the correlation lengths deduced for the rotator and crystalline phases.

Acknowledgements. The financial support from project MAT2016-79869-C2-1-P (AEI/FEDER, UE) is greatly acknowledged. RBG also thanks her pre-doctoral funding (BES-2014-070972). The synchrotron experiments were performed at beamline BL11-NCD at ALBA Synchrotron Light Facility with the collaboration of ALBA staff.

¹G. Ungar, N. Masic, *J. Phys. Chem.* **1985**, *89*, 1036.

²E. B. Sirota, H. E. King, D. M. Singer, H. H. Shao, *J. Chem. Phys.* **1993**, *98*, 5809.

³J. Doucet, I. Denicolo, A. Craievich, *J. Chem. Phys.* **1981**, *75*, 1523

⁴M. G. Broadhurst, *J. Res. Natl. Bur. Stand.* **1962**, *A66*, 241.

⁵A. E. Smith, *J. Chem. Phys.* **1953**, *21*, 2229.

INSIGHTS IN THE CO₂ PHOTO-ACTIVATION OVER HYBRID PHOTOCATALYSTS FOR ARTIFICIAL PHOTOSYNTHESIS

P. Reñones^a, I. Villar^a, E. Alfonso^a, F. Fresno^a, A. García^a, C. García^a, M. Liras^a, M. Barawi^a, R. Pérez^a, V. Perez-Dieste^b, C. Escudero^b, L. Simonlelli^b, W. Wojciech^b Olszewski, V. A. de la Peña O'Shea^{a*}

^a Photoactivated Processes Unit, IMDEA Energy Institute, Móstoles Technology Park, Avenida Ramón de la Sagra, 3, 28935 Móstoles, Madrid, (Spain); victor.delapenya@imdea.org

^b Alba Synchrotron Light Source, Carretera BP 1413, Km. 3.3, 08290 Cerdanyola del Vallès, Barcelona, Spain (Spain).

An interesting route for the valorization of CO₂ consists on its photocatalytic conversion into fuels and/or chemicals in the presence of water and suited photocatalysts¹; this process is also known as Artificial Photosynthesis (AP). Such conversion is a quite challenging process since CO₂ is a very stable compound and its reduction involves a series of multi-electron reactions. Extensive efforts are focused on improving the photocatalytic efficiencies, especially when using water as the electron donor. Generally, this process suffers from very low quantum yields and non-selective product distributions, due to the complexity of the involved multi-step reactions.

During the last years, a series of innovative materials with versatile properties and multifunctional character, known as hybrid materials, have been developed. Synergistic effects between their components provide these materials with exciting properties for light harvesting and charge separation, fundamental issues in artificial photosynthesis. Therefore, the development of new hybrid multifunctional photocatalysts using sunlight to produce fuels and chemicals is considered as a cornerstone for CO₂ valorisation technologies

In this work we report different strategies and modifications photocatalysts to increase process performance. The modification of optoelectronic properties of through the use of band gap engineering strategies, allow controlling the absorption of incident photons, redox capabilities and subsequently the photocatalytic performance. In addition, metal nanoparticles act as electron scavenger and as co-catalyst^{2,3} [2-4]. Finally, the use of novel hole transport materials maximize the light harvest and charge separation. On the other hand, efforts are devoted to shed light on mechanistic aspects of the reaction. In order to clarify the effect of different parallel and competitive reactions in the activity and products distribution, a series of photocatalytic experiments in combination with operando characterization using synchrotron radiation and laboratory techniques and theoretical calculations were performed.

These studies show that introduction of SPR NPs as co-catalyst or conductive polymers as hole transports leads to changes in the conversion and enhanced selectivity to higher demand electron products, such as CH₄, while the CO and H₂ concentrations decrease

Acknowledgements. Authors acknowledge financial support from the Spanish Ministry of Economy and Competitiveness through the project (CTM2011-25093) and HyMAP project, receiving funding from the European Research Council (ERC) under the European Union's Horizon 2020 research and innovation programme (grant agreement No. 648319).

¹ V. A. de la Peña O'Shea, D. P. Serrano, J. M. Coronado, *From Current challenges of CO₂ photocatalytic reduction over semiconductors using sunlight*, in *Molecules to Materials—Pathway to Artificial Photosynthesis*, Ed. E. Rozhkova, K. Ariga (Eds.), Springer, London, **2015**.

² L. Collado, P. Jana, B. Sierra, J.M. Coronado, P. Pizarro, D.P. Serrano V.A. de la Peña O'Shea, *Chem. Eng. J.* **2013**, *128*, 224.

³ L. Collado, A. Reynal, J.M. Coronado, D.P. Serrano, J.R. Durrant, V.A. de la Peña O'Shea, *Appl. Catal. B: Environ.* **2015**, *177*.

Mixed-valence Ce/Zr MOFs: controlling the oxidation state of cerium in one-pot synthesis approach

M. Ronda¹, I. Pellicer-Carreño¹, R. Boada², Sofía Díaz-Moreno², A. Sepúlveda-Escribano¹, Enrique V. Ramos-Fernandez¹,

¹Laboratorio de Materiales Avanzados. Instituto Universitario de Materiales de Alicante-Departamento de Química Inorgánica. Universidad de Alicante. Apartado 99, E-03080 Alicante, Spain

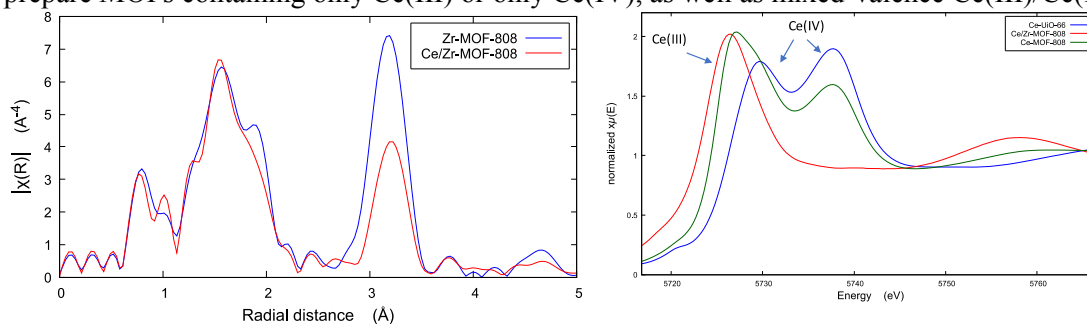
²Diamond Light Source, Didcot OX11 0DE, United Kingdom

For a catalyst to be useful in redox reactions, the presence of metal species that can easily exchange their oxidation state is of paramount importance. A classic example is ceria, in which Ce(IV) can readily be reduced to Ce(III) under adequate environment, and vice versa. Although there have been some attempts to prepare Ce-containing MOFs, their stability is limited. However, it can be enhanced by introducing Zr cations in the same cluster, in a way that can be compared with the ceria-zirconia mixed oxides. Another important point, which is the main objective of the work reported here, is the tailoring of the oxidation state of ceria cations which are present in the MOF. Stock's group¹ and others have reported the preparation of Ce or Ce/Zr MOFs with the same topology in which the Ce(IV)/Ce(III) pair is introduced to work as redox functionality. Actually, they have already reported UiO and MOF-808 structures containing both pure Ce and Ce/Zr. However, the preparation and characterization of these mixed-metal MOFs is far from being trivial, since we can find different situations such as the formation of segregated phases (Ce-MOF and Zr-MOF), clusters having only Ce or Zr in the same crystal and finally the desired one, all clusters containing both cations (true mixed-metal MOF). Besides the true mixed-metal nature of the MOF, it is also crucial to control the oxidation state of Ce. Ce(III) and Ce(IV) are both stable at ambient conditions depending on their environment, and both of them have the same coordination with carboxylic acid groups; thus, both can be used for producing MOFs with the same topology. The tailoring of the oxidation state of the Ce cations is expected to lead to a fine control of the redox properties.

In this work we have developed a synthesis method that can be used to prepare Ce/Zr-MOFs (UiO and MOF-808 structures) having only Ce(III), mixed-valence Ce(IV)/Ce(III), or only Ce(IV) cations, as desired. In order to check the success of the synthesis, we have used a large number of characterization techniques such as: UV-Vis, XRD, N₂ adsorption at 77 K, TGA, Raman spectroscopy, XRF, XPS and EXAFS.

The Fourier transform of the Zr K-edge EXAFS spectra which provides a pseudo-radial distribution function (left), shows that the first shell (Zr-O_a 1.6 Å, and Zr-O_b 1.9 Å contributions) is modified when Ce is added to the framework. This indicates that oxygen vacancies are created in the Zr hexanuclear clusters due to the alteration caused by Ce cations. Additionally, the drastic decrease of intensity of the second shell peak (Zr-Zr/Ce 3.2 Å) can only be explained by the successful substitution of Zr by Ce in the Zr₆ cluster since the contribution arising from Ce atoms interferes destructively with the one coming from Zr.

On the other hand, the XANES region of the Ce L₃-edge confirms that we have been able to prepare MOFs containing only Ce(III) or only Ce(IV), as well as mixed-valence Ce(III)/Ce(IV).



X-RAY ABSORPTION SPECTROSCOPY STUDY OF MAGNETIC ANISOTROPY AND VALENCE STATES IN $\text{La}_2\text{Co}_{1-x}\text{Mn}_{1+x}\text{O}_6$ ($x \approx 0.23$) THIN FILMS

L. López-Mir^a, R. Galceran^a, J. Herrero-Martín^b, B. Bozzo^a, J. Cisneros-Fernández^a, E.V. Pannunzio Miner^a, Ll. Balcells^a, B. Martínez^a, and C. Frontera^a

^a*Institut de Ciència de Materials de Barcelona-CSIC, C. dels Til·lers s/n (Campus UAB), E-08193 Cerdanyola del Vallès, Spain*

^b*ALBA Synchrotron Light Source, C. de la Llum 2-26, E-08920 Cerdanyola del Vallès, Spain*

Ferromagnetic insulators may play an important role in spintronics as spin sources, spin conductors¹, or as potential candidates for magnetically active barriers or spin filters². Ferromagnetic insulating materials are scarce since in many cases ferromagnetic interactions are of exchange-type and driven by carriers. Among these rare materials, $\text{La}_2\text{CoMnO}_6$ and $\text{La}_2\text{NiMnO}_6$ double perovskites have been reported to be ferromagnetic insulators when cationic ordering (Co/Mn, Ni/Mn) is achieved. In the case of $\text{La}_2\text{CoMnO}_6$ FMI character extends beyond the 1:1 Mn:Co ratio³.

In the last years we have been investigating magnetic and transport properties of $\text{La}_2\text{Co}_{1-x}\text{Mn}_{1+x}\text{O}_6$ (LCMOx with $x \approx 0.23$) thin films grown by RF-sputtering on top of different substrates. We have found very good magnetic properties (saturation magnetization and Curie temperature similar to bulk samples), signaling a good Co/Mn cationic ordering. Moreover, films present a strong magnetic anisotropy that can be tuned by the strain induced by the substrate: compressive strain leads to in-plane easy axis while tensile strain leads to perpendicular magnetic anisotropy⁴.

Under this stoichiometry, the substitution of Co by Mn opens the question of which is the valence of the substituting Mn and how cationic order is achieved. To shed light into these questions, we have performed X-ray absorption spectroscopy at the Mn and Co $L_{2,3}$ edges, known to be very sensitive to the $3d$ electronic configurations. To understand the origin of magnetic anisotropy and its strain dependence, we have studied samples grown on top of SrTiO_3 with different oxygen contents (inducing a change in strain⁴) and on top of $(\text{LaAlO}_3)_{0.3}(\text{Sr}_2\text{AlTaO}_6)_{0.7}$ and LaAlO_3 substrates using X-ray magnetic circular dichroism (XMCD). This is a unique tool allowing studying separately, in an element-specific way, the orbital and spin contributions to the atomic magnetic moment. We have shown that LCMOx behavior has a magnetocrystalline origin that must be attributed to the combination of the large spin orbit coupling in Co^{2+} ions with the modification of the crystal field due to the strain⁵.

Acknowledgements. We thank financial support from the Spanish Ministry of Economy and Competitiveness through the “Severo Ochoa” Programme for Centres of Excellence in R&D (SEV-2015-0496), and projects MAT2012-33207 and MAT2015-71664-R.

¹ Y. Kajiwara, K. Harii, S. Takahashi, J. Ohe, K. Uchida, M. Mizuguchi, H. Umezawa, H. Kawai, K. Ando, K. Takanashi, S. Maekawa, E. Saitoh, *Nature* **2014**, *464*, 262.

² M. Bibes, J. E. Villegas, A. Barthélémy, *Adv. Phys.* **2011**, *60*, 5.

³ S. N. Barilo, V. I. Gatal'skaya, S. V. Shiryayev, L. A. Kurochkin, S. N. Ustinovich, H. Szymczak, R. Szymczak, M. Baran, *Phys. Status Solidi* **2003**, *199*, 484.

⁴ R. Galceran, L. López-Mir, B. Bozzo, J. Cisneros-Fernández, J. Santiso, L. Balcells, C. Frontera, B. Martínez, *Phys. Rev. B* **2016**, *93*, 144417.

⁵ L. López-Mir, R. Galceran, J. Herrero-Martín, B. Bozzo, J. Cisneros-Fernández, E. V. Pannunzio Miner, A. Pomar, Ll. Balcells, B. Martínez¹, C. Frontera, *Phys. Rev. B* **2017** (in press).

CHEMICAL COMPATIBILITY OF A MICRO-FLUIDIC CELL FOR X-RAY MICROSCOPY

**Carmen S. de Rojas Candela^a, Simon Washbrook^b, Kylash Makenji^b,
Matthew T. Shand^a, Peter A. F. Anastasi^a**

^a*Silson Ltd, Insight Park, Welsh Road East, Southam, Warwickshire, CV47 1NE, United Kingdom; carmen.sanchezderojas@silson.com*

^b*Warwick Manufacturing Group, University of Warwick, Coventry, CV4 7AL, United Kingdom; S.Washbrook@warwick.ac.uk*

There is increasing demand to examine specimens within a wet environment using x-ray microscopy. Simple static or active enclosures can be prepared using an assembly of thin silicon nitride membranes, with a pre-determined separation controlled by a suitable spacer. The environmental cell structure produced by Silson is shown in figure Figure.

Spacers are typically made from SU-8 photoresist as it is widely considered to be chemically stable when fully crosslinked¹. It has become apparent however, that for certain extremely sensitive analyses, the specimen media could be mixed with unknown contaminants transferred from the spacer layer into the solvent. Measurement and quantification of the contaminant composition will provide an invaluable recommendation for future users of the cells.

A method for testing the physical characteristics of SU-8 layers when exposed to a range of organic solvents is proposed. The solvents identified are typically used in the preparation of biological and materials science samples and are qualitatively grouped into non-polar, polar aprotic and polar protic. Examples chosen include Acetonitrile and Toluene which are commonly used for crystallisation and further x-ray Analysis. Investigation of the mass change and material thickness due to the solvent attack has been made to identify the most stable solvents available for use with SU-8.

Subsequent spectroscopic analysis of each sample has also been performed to characterise the composition. This testing will identify any material from the spacer taken into the sample solution which has the potential to contaminate any future results. Recommendations can then be made to determine the solvents which are the most compatible for use, along with potential by-products that may be detected as part of an experiment.

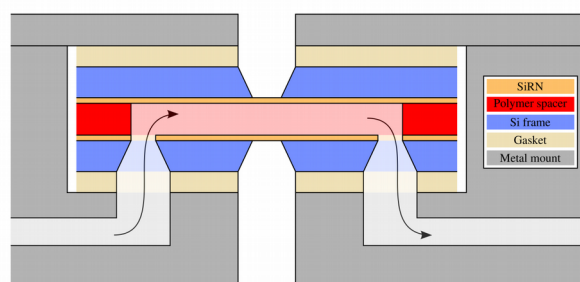


Figure 1: Structure of the SU-8 liquid cell.

1 Marc J. Madou, in "Fundamentals of microfabrication and nanotechnology" (Ed. 3), Vol. 2, CRC Press, Taylor & Francis Group, 2012; pp. 35.

THE EUROPEAN X-RAY FREE-ELECTRON LASER IN THE HAMBURG REGION

M. Altarelli^a

^a *Max-Planck Institute for Structure and Dynamics of Matter, 22761 Hamburg, Germany;*
massimo.altarelli@mpsd.mpg.de

The European XFEL is ready to welcome first users this year. This talk summarizes the scientific motivations and the main features of the new source and the accompanying commissioning with beam of the 17.5 GeV superconducting linac accelerator, almost 2 km long, started in early 2017, with first lasing in the soft X-ray region at 0.8 nm wavelength in early May. When fully commissioned it shall distribute up to 27 000 ultrashort (~ 10 fs) electron bunches per second to three different undulators (later to be upgraded to five). The two hard X-ray undulators should provide coherent radiation in a 3 to 25 keV range of photon energy in the first harmonic, while the soft X-ray undulator should cover the range from 250 eV up to 3 keV. The aim for full operation is to have three experiments performed in parallel and to maximise scientific output by optimised x-ray optics, optical lasers, diagnostics, detectors and data acquisition.

First users were selected last spring by a peer-reviewed proposal screening process, for the earliest two of the overall six instruments, namely the Single Particle and Biomolecules/Serial Femtosecond Crystallography (SPB/SFX) instrument, and the Femtosecond X-ray Experiment (FXE) instrument. The former is devoted mostly to bio-structural studies and the latter to pump-probe experiments on photochemical reactions and photoinduced phase transitions. Both shall allow time-dependent studies in the ~ 100 fs time scale. Four additional experiments will come on line in 2018.

The leading position of this new European facility in the worldwide context of X-ray free-electron lasers, and some of the scientific expectations it rises shall be discussed.

CRYSTAL STRUCTURES OF VIRAL RECEPTOR-BINDING PROTEINS

M. J. van Raaij^a

^a *Department of Macromolecular Structures, Centro Nacional de Biotecnología - CSIC, E28049 Madrid (Spain); mjvanraaij@cnb.csic.es*

Both adenoviruses and bacteriophages use fibre proteins to recognize their host cells. Bacteriophages have specialized proteins for initial, reversible, host cell wall recognition. Once a suitable host is found, the phage commits to infection by irreversible attachment via a secondary receptor interaction. The crystal structures of several of these receptor-binding proteins have been solved using data collected at the Xaloc beamline and other synchrotron beamlines, and have been shown to be mainly beta-structured, but structurally highly diverse and containing several new protein folds. Structures of the receptor-binding proteins of the coli-phages T4, T5 and T7, of the *Salmonella* phage epsilon15 and of the *Staphylococcus* phages S24-1 and K will be shown.

Adenoviruses fibre proteins also serve as primary host cell recognition proteins and we have recently determined structures of the first atadenovirus and siadenovirus fibre head domains. We also discovered that the atadenovirus LH3 capsid protein contains a bacteriophage tailspike fold.

Ongoing structural, mutational and binding analysis of virus receptor-binding proteins with receptors and receptor analogues will be discussed. Bacteriophage receptor-recognizing proteins may be used for bacterial detection, while modification by natural or experimental mutation of bacteriophage receptor-binding domains may allow retargeting of phages to alternative host bacteria. Their shape and stability may also allow their use in nanotechnological applications.

Acknowledgements. I am grateful to present and former research group members for performing the work described. The staff of the Xaloc beamline and several ESRF and Diamond beamlines are thanked for their expert assistance. This research has been funded by grants from the Spanish Ministry of Economy, Industry and Competitiveness and the European Union.

INFRARED MICROSPECTROSCOPY: A BIO-ANALYTICAL TOOL FOR UNDERSTANDING AND IMPROVING RADIOTHERAPY

**I. Martínez-Rovira^a, O. Seksek^b, M. Kreuzer^c, J. Gómez^a, T. Ducic^c, J. Puxeu^d,
R. Perea^c, G. Cinque^e, J. Sulé-Suso^f, M.J. Ferreres^g, M. Artigués^d, Y. Prezado^b,
I. Yousef^c**

^a Ionizing Radiation Research Group, Universitat Autònoma de Barcelona (E08193, Cerdanyola del Vallès, Spain); immamartinez@gmail.com

^b Laboratoire d'Imagerie et Modélisation en Neurobiologie et Cancérologie, Centre National de la Recherche Scientifique (F91405, Orsay, France)

^c MIRAS beamline BL01, ALBA Synchrotron (E08290, Cerdanyola del Vallès, Spain)

^d Hospital Universitari Sant Joan de Reus (E43204, Reus, Spain)

^e MIRIAM beamline B22, Diamond Light Source (OX11 0DE, Didcot, UK)

^f Keele University (ST5 5BG, Keele, UK)

^g Laboratori ASPCAT Tortosa (E43500, Tortosa, Spain)

Radiotherapy is one of the main modalities for cancer therapeutics. However, it remains unsatisfactory for certain tumours and localizations, where the tolerance of normal tissues to radiation limits the possibility of delivering higher (potentially curative) doses to the tumour. This is especially critical in the case of radio-resistant tumours, such as gliomas. High-grade gliomas have still a poor prognosis and most of the treatments remain palliative. In the quest for ways to improve the therapeutic index, innovative radiotherapy approaches are being explored. Within this context, we are working on the development of spatially fractionated radiotherapy using several beam qualities, and in the use of nanoparticles as tumour radio-sensitizers¹.

Although the potential of these two innovative approaches, the biochemical mechanisms are not fully understood yet. Within this context, we used synchrotron-based Fourier-transform infrared microspectroscopy (SFTIRM) as a powerful tool to disentangle the biochemical processes inside glioma cells induced by these radiotherapy treatments². The intense infrared light produced at ALBA and DIAMOND synchrotrons was used, leading to a clear advantage in spectral quality at subcellular level. A large population of single cell spectra was acquired to overcome biological variability and to have statistical significance. The SFTIRM data obtained provided valuable information on cell functionality, cell cycle and cell death modes. Results showed clear treatment-induced variations in the main cell biomolecules (Amide I and II protein bands; CH₂ and CH₃ lipid stretching modes; and phosphodiester DNA modes), after Principal Component Analysis (PCA).

An overview on spatially fractionated radiotherapy and on the use of nanoparticles as tumour radio-sensitizers will be given. Detailed PCA results with focus on how SFTIRM contributed to understand the underlying biology of these cutting-edge radiotherapy techniques will be presented.

¹ I. Yousef, *et al.*, *Analyst*. **2016**, *141*, 2238-2249;

I. Martínez-Rovira *et al.*, *Med. Phys.*, **2015**, *42*, 685-693.

² M. J. Baker *et al.*, *Nat. Protoc.* **2014**, *9*, 1771-1791.

SYNCHROTRON INFRARED SPECTROSCOPY TO ANALYSE THE PENETRATION OF DIFFERENT LIPID SYSTEMS IN THE SKIN AND TO STUDY SKIN CONDITIONS

V. Moner^a, E. Fernández^b, M. Cócera^b, I. Yousef^c, A. de la Maza^a and O. López^a

^a Department of Chemical and Surfactants Technology, Institute of Advanced Chemistry of Catalonia, CSIC, Carrer Jordi Girona 18-26, 08034 Barcelona (Spain); ymmtqt@iqac.csic.es

^b Bicosome S.L, Carrer Jordi Girona 18-26, 08034 Barcelona (Spain); info@bicosome.com

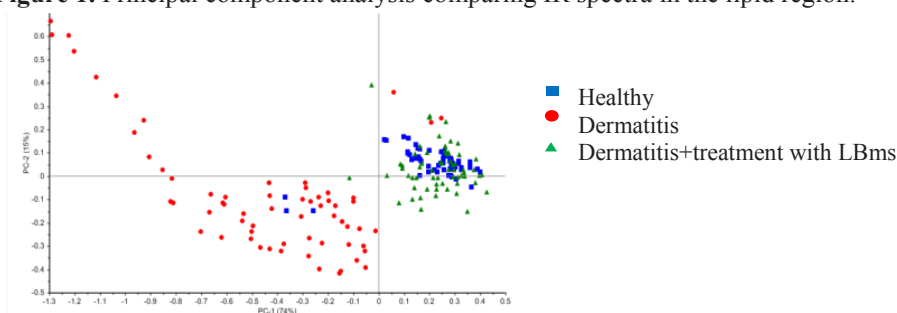
^c Alba Synchrotron, Carrer de la llum 2-26, 08290 Cerdanyola del Vallès, Barcelona (Spain); iyousef@cells.es

Epidermal lamellar bodies are organelles that secrete their content, mainly lipids and enzymes, into the intercellular space of the stratum corneum (the outermost layer of the skin) to form the lamellar structure of this tissue. A large number of skin diseases are associated with dysfunctional lamellar bodies¹. Consequently, diseased skin is characterized by reduced barrier function and alterations in lipid composition and organization. The lamellar body mimetic system (LBms) is a lipid system based on bicosomes² that mimics the morphology, structure and composition of epidermal lamellar bodies³.

In this work the infrared microscopy with synchrotron radiation was used to study the penetration and distribution of the LBms in the different layers of the skin, generating a map of the sample. The results indicate that the system penetrates and remains mainly in the stratum corneum. In addition this technique allows to study different skin conditions: healthy skin, skin affected by dermatitis and, dermatitis skin after treatment with LBms.

Principal component analysis (PCA) using Unscrambler® programme helps to find out in what respect one sample is different from another. In this work we compare IR spectra focusing in the lipid region (3100-2800 cm⁻¹). PCA reveals clear differences between healthy and dermatitis samples, showing that dermatitis affects dramatically the skin lipids. It is interesting to note that after treatment with LBms the skin recovered IR spectra features characteristics to healthy skin (figure 1). This fact could be associated with a modification in the lipid region by effect of the treatment that would lead to an improvement of the disease.

Figure 1. Principal component analysis comparing IR spectra in the lipid region.



Acknowledgements: These experiments were performed at Miras beamline at ALBA Synchrotron with the collaboration of ALBA staff. This work was supported by funds from Comisión Interministerial de Ciencia y Tecnología from Spain (CTQ 2013-44998-P).

¹ P. M. Elias and J. S. Wakefield, *J Allergy Clin. Immunol.* **2014**, *134*, 781-791.

² E. Fernández, S. Hostachy, C. Sandt, G. Rodríguez, H. C. Bertrand, S. Clède, M. Cócera, A. de la Maza, F. Lambert, C. Polícar, O. López, *RSC Adv.* **2016**, *6*, 72559-72567.

³ V. Moner, E. Fernández, G. Rodríguez, M. Cócera, L. Barbosa-Barros, A. de la Maza, O. López, *Int. J. Pharm.* **2016**, *510*, 135-143.

STRUCTURAL BASIS OF THE ALLOSTERIC ACTIVATION OF HUMAN CYSTATHIONINE BETA SYNTHASE BY S-ADENOSYLMETHIONINE

J. Ereño-Orbea^a, T. Majtan^b, I. Oyenarte^a, J.P. Kraus^b and L.A. Martínez-Cruz^a

^a*Structural Biology Unit, Center for Cooperative Research in Biosciences (CIC bioGUNE), 48160 Bizkaia, Spain; amartinez@cicbiogune.es*

^b*Department of Pediatrics, School of Medicine, University of Colorado, Aurora, CO 80045; Jan.kraus@ucdenver.edu*

Cystathionine β -synthase (CBS) is a mammalian enzyme responsible for catalyzing the first step of the transsulfuration pathway that converts methionine to cysteine. The human CBS (*hCBS*) condenses serine and homocysteine to cystathionine with the help of two co-factors, heme and pyridoxal-5'-phosphate (PLP). Mutations in *hCBS* result in homocystinuria, an autosomal recessive disorder characterized by a combination of connective tissue and vascular defects, skeletal deformities and mental retardation. The structural basis underlying the allosteric regulation mechanism and oligomerization of the enzyme has remained elusive until we solved the crystal structure of the full-length *hCBS* in its “basal” and “activated” states^{1,2}.

hCBS is a homotetrameric enzyme composed of three functional domains. N-terminal heme binding region, central catalytic core and the C-terminal region which consists of a tandem pair of CBS motifs (CBS1 and CBS2) that bind to the allosteric activator S-adenosylmethionine (AdoMet). Crystallization of *hCBS* was facilitated by an engineered construct lacking the flexible loop located in CBS2. The crystal structure of *hCBS* in its basal state revealed a basket-shaped symmetrical dimer in which the catalytic core of each subunit interacts with both the catalytic core and the regulatory domain of the complementary subunit¹. The relative arrangement of the catalytic core and regulatory domain places the latter just above the entrance of the catalytic site, thus hampering the access of substrates into this cavity. Binding of AdoMet promotes a sharp rotation of the two CBS motifs towards the formation of a disk-shaped antiparallel “CBS module” that allows the access of substrates into the catalytic site². Based on the structures of both the “basal” and the “activated” states, we have elucidated the mechanism of *hCBS* activation by AdoMet and the properties of the AdoMet binding site. The availability of the *hCBS* structures helps to understand the pathogenicity of the numerous missense mutations causing inherited homocystinuria and will allow for the rational design of compounds modulating CBS activity.

Acknowledgements. We thank the staff at beamlines ID23.1 and ID29 of the European Synchrotron Radiation Facility and XALOC of ALBA synchrotron. This work was supported by Postdoctoral Fellowship 0920079G from the American Heart Association; National Institutes of Health Grant HL065217; American Heart Association Grant-In-Aid 09GRNT2110159; Basque Government (PI2010-17, IE05-147 and IE07-202); Bizkaia County (Exp.7/13/08/2006/11 and 7/13/08/2005/14); Spanish Government (BFU2010-17857 and BFU2013-47531-R); and Spanish Ion Channel Initiative Program (SICI CONSOLIDER CSD 2008-00005).

¹J. Ereño-Orbea, T. Majtan, I. Oyenarte, J.P. Kraus and L.A. Martínez-Cruz, *Structural basis of regulation and oligomerization of human cystathionine β -synthase, the central enzyme of transsulfuration*. Proc. Natl. Acad. Sci. USA. 110 (40): 3790-3799, **2013**.

²J. Ereño-Orbea, T. Majtan, I. Oyenarte, J.P. Kraus and L.A. Martínez-Cruz, *Structural insight into the molecular mechanism of allosteric activation of human cystathionine beta-synthase by S-adenosylmethionine*. Proc. Natl. Acad. Sci. USA. 111 (37): 3845-3852, **2014**.

THE EFFECT OF COBALT INCORPORATION IN THE MAGNETIC ANISOTROPY OF MAGNETOSOMES

L.Marcano^a, D.Muñoz^b, A. García-Prieto^{c,d}, J.Alonso^d, R. Martín Rodríguez^e, A. Serrano^{f,g}, L.Simonelli^h, S.Valenciaⁱ, I.Orue^j, A.Muela^{b,d}, M.L. Fdez-Gubieda^{a,d}

^a Departamento de Electricidad y Electrónica, UPV/EHU, Leioa (Spain)-

lourdes.marcano@ehu.eus

^b Departamento de Inmunología, Microbiología y Parasitología, UPV/EHU, Leioa (Spain)

^c Departamento de Física Aplicada I, UPV/EHU, Bilbao (Spain)

^d BCMaterials, Building No.500, Technological Park of Biscay, Derio (Spain)

^e QUIPRE Department, University of Cantabria, Santander (Spain)

^f SpLine, Spanish CRG Beamline at the ESRF, Grenoble (France)

^g Instituto de Ciencia de Materiales de Madrid-ICMM/CSIC, Madrid (Spain)

^h CELLS - ALBA Synchrotron Radiation Facility, Cerdanyola del Valles, Barcelona (Spain)

ⁱ Helmholtz-Zentrum Berlin für Materialien und Energie, Berlin (Germany)

^j SGIker, UPV/EHU, Leioa (Spain)

Magnetotactic bacteria are a group of microorganisms able to orient in and navigate along geomagnetic fields thanks to the presence of one or more chains of magnetic nanoparticles, also called magnetosomes. The high biological control imposed in the synthesis bestows well-defined properties on the biomineralized particles suitable for numerous applications^{1,2}. Moreover, aiming to widen the range of applications of magnetosomes, in the last few years numerous works have focused on modifying the main properties by adding small amounts of new elements as dopant^{3,4,5}. In this sense, Co has received a lot of attention because of the drastic changes in the magnetic response of the magnetosomes even at low doping contents. In this work, we present a complete characterization of Co-doped magnetosomes synthesized by the bacterium *Magnetospirillum gryphiswaldense*. This species synthesizes cubo-octahedral shaped magnetite magnetosomes with a mean diameter of 45 nm⁶. In order to dope them with Co, we have added 100 μM of Co(II)-citrate into the bacterial growth medium.

By means of X-ray Absorption Near Edge Structure (XANES) spectroscopy and X-ray Magnetic Circular Dichroism (XMCD) we have determined the position of Co into the magnetite structure. Both techniques indicate that Co is incorporated as Co²⁺ through the substitution of Fe²⁺ located in octahedral sites. On the other hand, the hysteresis loops measured with SQUID magnetometer and X-ray Photoemission Electron Microscopy (XPEEM) carried out on the Fe L-edge at different applied magnetic fields reveals the magnetic hardening as a consequence of the Co incorporation, attributed to an increment of the magnetic anisotropy.

¹ A. Muela, D. Muñoz, R. Martín-Rodríguez, I. Orue, E. Garaio, A. Abad Díaz de Cerio, J. Alonso, J. Á. García, and M. L. Fdez-Gubieda, *J. Phys. Chem. C* **120**, 24437 (2016)

² A. M. Huizar-Félix, D. Muñoz, I. Orue, C. Magén, A. Ibarra, J. M. Barandiarán, A. Muela, and M. L. Fdez-Gubieda, *Appl. Phys. Lett.* **108**, 063109 (2016).

³ M. Tanaka, R. Brown, N. Hondow, A. Arakaki, T. Matsunaga, and S. Staniland, *J. Mater. Chem.* **22**, 11919 (2012)

⁴ S. Staniland, W. Williams, N. Telling, G. Van Der Laan, A. Harrison, B. Ward, *Nat. Nanotechnol.* **3**, 158 (2008).

⁵ J. Li, N. Menguy, M.-A. Arrio, P. Sainctavit, A. Juhin, Y. Wang, H. Chen, O. Bunau, E. Otero, P. Ohresser, and Y. Pan, *J. R. Soc. Interface* **13**, 20160355 (2016).

⁶ M. L. Fdez-Gubieda, A. Muela, J. Alonso, A. García Prieto, L. Olivi, R. Fernández-Pacheco, and J. M. Barandiarán, *ACS Nano*, **7** (4), 3297-3305 (2013).

Combining XANES and XES to probe the magnetic and structural nature of complex nanoparticles

I. Carlomagno^a, C. Meneghini^a, F. Porcaro^b, C. Marini^c, L. Simonelli^c, L. Marcano^d, M.L. Fdez-Gubieda^{d,e}, J. Alonso^{e,f}, Z. Nemati^f, R. Das^f, M.H. Phan^f, and H. Srikanth^f

^a Dipartimento di Scienze, Università Roma Tre, via della Vasca Navale 84, 00146 Roma Italy
ilaria.carlomagno@uniroma3.it

^b CNRS, Institut National de Physique Nucléaire et de Physique des Particules (IN2P3),
 CENBG, UMR 5797, F-33170 Gradignan, France

^c CELLS - ALBA Synchrotron Radiation Facility, Carrer de la Llum 2-26, 08290, Cerdanyola del Valles, Barcelona, Spain

^d Departamento de Electricidad y Electrónica, Universidad del País Vasco, Barrio Sarriena s/n 48940 Leioa, Spain

^e BCMaterials, Edificio No. 500, Parque Tecnológico de Vizcaya, 48160 Derio, Spain

^f Department of Physics, University of South Florida, Tampa, FL 33620, USA

Magnetic nanoparticles (NPs) with spinel structure have been studied for a variety of applications as their functionality can be tuned through chemical and physical properties. Fe@Fe-oxide core@shell NPs, for instance, are appealing for biomedical applications because their magnetic response can be adjusted by acting on core and shell composition [1].

Inner-shell spectroscopies, being element specific, sensitive to oxidation, spin state, and local geometry of the sample, can provide valuable information on the coupling between the NPs structure and physical properties. In this work, we exploit the high photo flux available at CLÆSS (Core Level Absorption and Emission Spectroscopies) beamline, combined with the high resolution of the CLEAR spectrometer to achieve complementary information on the local electronic, magnetic, and structural properties of spherical Fe@Fe₃O₄+γ-Fe₂O₃ (15 nm) and Fe₃O₄@CoFe₂O₄ (9 nm) core@shell nanoparticles together with FeO+Fe₃O₄ (28 nm) nanocomposites.

Combining Fe K-edge X-ray Emission and high-resolution X-ray Absorption Near Edge Structure Spectroscopies (XES and XANES) we identify different de-excitation channels of Fe atoms. Focussing on the K_β and K_{β1,3} channels (Fig. 1a), it is possible to obtain details on the average magnetic moment of Fe in different environments. The high-resolution XANES spectra collected in partial fluorescence yield allow one to distinguish the different Fe atoms in the coexisting phases/sites on the basis of the different K_β regions (Fig. 1b) and to assess differences in the local structure of Fe as a function of its magnetic state.

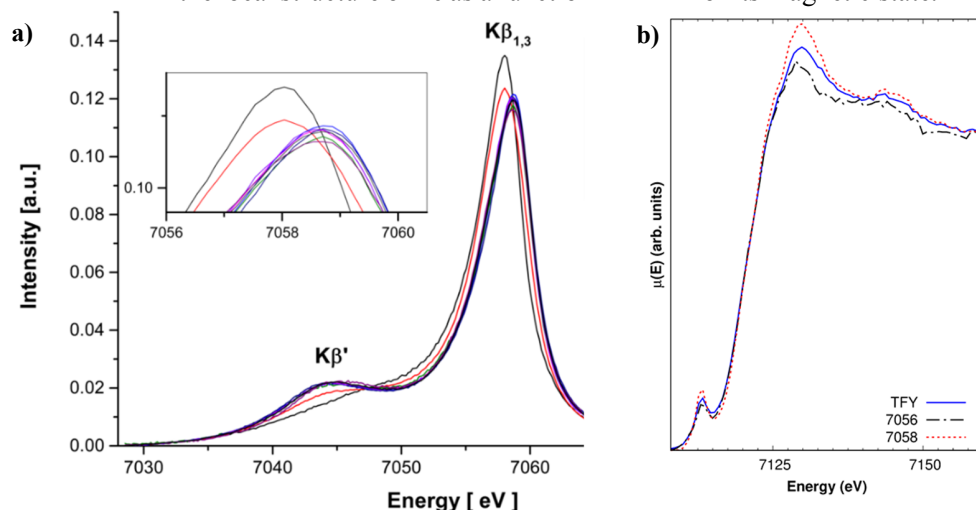


Fig 1. a) Fe K_β XES of different reference compounds and NPs. The K_β emission can be used to derive the average Fe magnetic moment. **b)** XANES of Fe@FeO NPs collected in Total Fluorescence Yield (TFY) and in partial fluorescence yield allow to selectively probe different Fe ions in the sample.

PICOSECOND DYNAMICS IN SINGLE CORE-SHELL NANOWIRES BY SYNCHROTRON EXCITED OPTICAL LUMINESCENCE

Jaime Segura-Ruiz^a, Benito Alén^b, Andrei Rogalev^c, Damien Salomon^c, Joël Eymery^d, Gema Martínez-Criado^{c,e}

^a *Institute Laue-Langevin, 38043 Grenoble (France); jasegur@ill.fr*

^b *IMM, Instituto de Microelectrónica de Madrid (CNM, CSIC), 28760 Tres Cantos (Spain); benito.alen@csic.es*

^c *European Synchrotron Radiation Facility, 38043 Grenoble (France); andrei.rogalve@esrf.fr*

^d *Université Grenoble Alpes, Equipe mixte CEA-CNRS-UJF “Nanophysique et semiconducteurs”, CEA, INAC, 38054 Grenoble (France); joel.eymery@cea.fr*

^e *Instituto de Ciencia de Materiales de Madrid (CSIC), 28049 Cantoblanco (Spain); gema.martinez.criado@csic.es*

Core-multishell GaN/InGaN nanowires are subject to threefold quantum confinement effects owing to their lateral size, polarization-induced electrostatic fields (Stark effect), and cross-sectional geometry. We have already provided experimental evidence for the latter carrier localization phenomena at the hexagon corners by combining synchrotron excited optical luminescence with simultaneous X-ray fluorescence spectroscopy at the nanoscale. Due to the strong built-in electric fields commonly present in c-plane InGaN quantum wells, the quantum confined Stark effect plays a detrimental role on the radiative recombination processes. Improved optical properties are conversely expected from InGaN quantum wells grown on nonpolar or semipolar planes. In the present work, the ultrafast photocarrier dynamics in nonpolar m-plane GaN/InGaN strained multiquantum wells is investigated using an enhanced experimental approach. By means of a pulsed hard X-ray nanobeam, the decay pathways within individual nanowires are analyzed applying a time-resolved multimode imaging tool. Our development not only extends the capabilities of the previous setup, but offers a unique combination of high chemical sensitivity and spectral luminescence selectivity (\sim meV) with concurrent spatial and temporal resolutions based on a synchrotron nanoprobe (about 50 nm and 20 ps, respectively). We anticipate that our scheme can contribute to a greater understanding of the underlying design concepts not only on photonic nanodevices, but also on emitting molecules in life sciences.

Spatially resolved selenium speciation in fortified wheat grain

**M. A. Subirana^a, M. Llugany^b, I. H. Valido^a, A. Pell^a, G. E. Brown^c, S. M. Webb^d,
C. Marini^e, L. Simonelli^e and M. Valiente^a**

^a Centre Grup de Tècniques de Separació en Química (GTS), Departament de Química, Universitat Autònoma de Barcelona, Cerdanyola del Vallès (Spain)

^b Unitat de Fisiologia Vegetal, Fac. Biociències, Universitat Autònoma de Barcelona, Cerdanyola del Vallès (Spain)

^c Department of Geological Sciences, School of Earth, Energy & Environmental Sciences, Stanford University, Stanford (USA)

^d Stanford Synchrotron Radiation Lightsource, Menlo Park (USA)

^e CLAEISS beamline, ALBA Synchrotron Light Facility, Cerdanyola del Vallès (Spain)

Selenium is an essential micronutrient for humans. This element is incorporated into proteins in the form of selenoamino acids, and it takes part in metabolic processes as the active site of enzymes. Among other properties, it is antioxidant, anti-viral, anti-carcinogenic and beneficial for cardiovascular diseases¹. However, Se-poor soils produce Se-deficient food for humans, and therefore it is insufficiently consumed by population worldwide. The elaboration of functional foods through soil Se-enrichment in edible plants has been proposed as a solution for this problem². Wheat has been chosen as an ideal candidate because it is commonly consumed in the diet of many cultures. The popularity of selenium biofortification practices has increased, consequently, a proper characterization of the Se uptake, metabolism, translocation and accumulation in the plants is critical to avoid toxicity risks and to target determined health benefits.

Wheat plants have been cultivated hydroponically, and exposed to different Se(IV)/Se(VI) conditions. These inorganic species are toxic to both plants and humans in excessive amounts. However, they are taken up and transformed through the plant metabolism into selenoamino acids, which are incorporated into proteins. The transformation occurs to a different extent depending on the conditions during the hydroponics, and the specie of selenium used in the fortification³. For these reasons, it is necessary to characterize the selenium uptake by the plant, and the distribution and speciation in the different plant organs. Special interest has been paid to the distribution of Se species in wheat grain, which is more relevant to human consumption.

Plants and grains grown in different conditions have been studied with synchrotron light in CLAEISS beamline at ALBA and in 2-3 and 10-2 beamlines at SSRL. X-ray fluorescence mapping was performed on the grains at chosen energies around the Se K-edge, in order to distinguish the distribution of different species. Furthermore, spatially resolved μ XAS spectra were measured in several points inside the grain, including germ, bran and endosperm. The non-homogeneous distribution of the selenium species is clearly depicted, which provide novel significant results on wheat physiology and selenium enrichment.

Acknowledgements

The present work has been financially supported by the project CHENEXUS (Ref CTM2015-65414-C2-1-R) from the Spanish Ministry MINECO.

¹ M. P. Rayman, *The Lancet*, **2000**, 356, 233-241

² M.J. Poblaciones, S. Rodrigo, O. Santamaría, Y. Chen, S.P. McGrath, *Food Chemistry*, **2014**, 378-384

³ B. Guerrero, M. Llugany, O. Palacios, M. Valiente. *Plant Physiology and Biochemistry*, **2014**, 83, 300-307

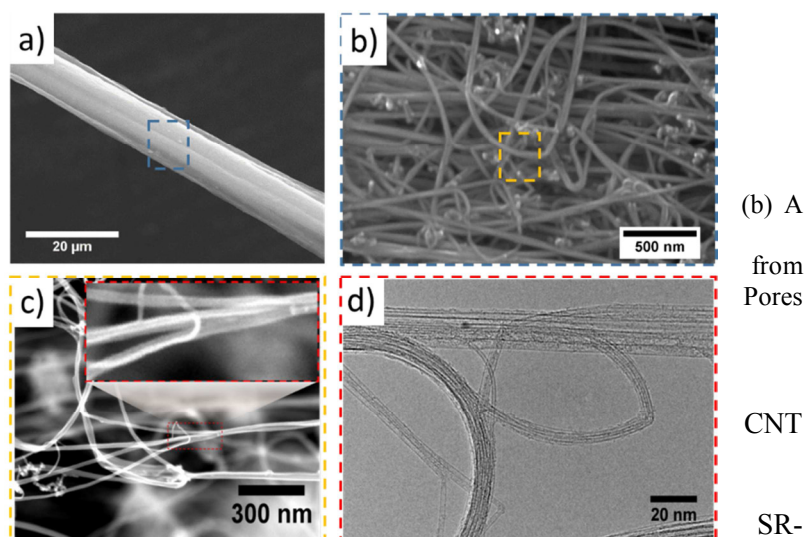
WAXS/SAXS studies of nanostructured hybrids for composites and energy managing devices

J. J. Vilatela^a, V. Reguero^a, E. Senokos^{a,b}, A. Monreal-Bernal^a, B. Alemán^a, J.C. Fernández^a, J.P. Fernández-Blázquez^a, R. Marcilla^b

^a IMDEA Materials (Spain); juanjose.vilatela@imdea.org ^b IMDEA Energy, (Spain)

One of the most exciting challenges of the last decade in material sciences is the controlled assembly of nanostructured building blocks into macroscopic structures that efficiently exploit their properties and thus lead to bulk properties superior to those of current engineering materials. An archetypical example is macroscopic textile fibres made up of aligned carbon nanotubes (Figure 1), which have been shown to have bulk mechanical properties¹ higher than carbon fibre and higher conductivity than copper.

Figure 1—Electron micrographs showing the hierarchical structure of CNT fibres: (a) Individual CNT fibre filament. (b) Porous network. (c) Mesoporous structure arising from imperfect bundle packing. (d) CNTs that branch out of bundles.



An interesting feature of fibres is their hierarchical structure resulting from imperfect packing of CNTs. WAXS/SAXS studies

(NCD-Alba) on these materials have exposed the coexistence of a large porosity and extended crystalline domains between CNT “molecules”. This combination is unusual and makes CNT fibre fabrics a superb electrode in a range of energy storage and optoelectronic devices with augmented mechanical properties, such as flexibility, toughness and ultimately structural properties². Static and in-situ mechanical tests during WAXS/SAXS measurements have shown that these fibres can be treated as polymeric fibrillary crystallites with mechanical properties determined the bundles of CNTs. On the other hand, their porous structure leads to fractional Porod slopes in SAXS, arising from the surface fractal structure of the fibres³. Density fluctuations in the material can be deconvoluted from the data following the formalism developed by Ruland and co-workers. With the view of using these fibres in composites, in-situ WAXS/SAXS during crystallization of thermoplastics have shown accelerated crystallization in the presence of CNTs. This is due to the high thermal conductivity of the fibres, assisted by preferential folding of polymer chains parallel to the CNTs, irrespective of polymer chemistry.⁴ Finally, this presentation discusses in-situ WAXS/SAXS during electrochemical measurements of CNTs fibres in ionic liquids as well as combined with polymeric electrolytes. Such experiments provide pointers for further improvement of flexible supercapacitors⁵ and other energy storage devices produced by the group.

1. Alemán, B., Reguero, V., Mas, B. & Vilatela, J. J. *ACS Nano* **9**, 7392–7398 (2015).
2. Vilatela, J. J. & Marcilla, R. *Chem. Mater.* **27**, 6901–6917 (2015).
3. Yue, H. *et al. Carbon* **accepted**,
4. Yue, H., Monreal-Bernal, A., Fernández, J. P., Llorca, J. & Vilatela, J. J. *Sci. Rep.* **5**, (2015).
5. Senokos, E. *et al. Adv. Mater. Technol.* 1600290 (2017). doi:10.1002/admt.201600290

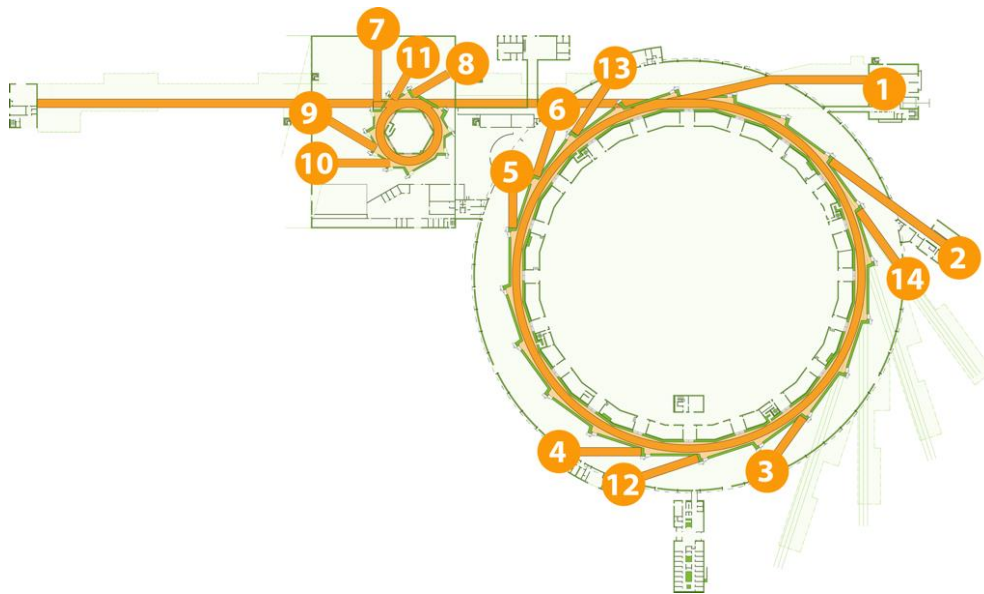
MAX IV: Options with a new light source

C. Quitmann^a on behalf of the MAX IV team

^a MAX IV Laboratory, Lund University, S-22100 Lund (Sweden);
christoph.quitmann@maxiv.lu.se

MAX IV Laboratory has completed building three dedicated new light sources in Lund, Sweden. These are a 3 GeV linac acting as an injector and a source of ultra-short (ca 100fs) hard-x-ray pulses; a 1.5 GeV storage ring optimized as a source of soft X-rays (ca 5 – 500 eV) for up to beamlines; an ultra-low emittance 3 GeV ring serving up to 19 beamlines with hard X-rays. All beamlines will be based on insertion devices.

These new sources open new opportunities for science¹, in particular by exploiting the coherent X-rays offered at the 3 GeV ring with a emittance of only 350 pmrad. I will summarize the present status and plans for expansion beyond the present 14 funded beamlines.



Layout of the MAX IV facility showing the linac (top left to top right), the 1.5 GeV ring (top center) and the 3 GeV ring (right) with the first set of 14 funded beamlines.

Today 4 beamlines are accepting commissioning experts or regular users. By the beginning of 2018 five more will open to users.

In the second part of the presentation I will introduce LEAPS - the League of European Accelerator-based Photon Sources². This initiative unites the Synchrotron and free electron laser facilities throughout Europe in a partnership to coordinate ongoing activities in science, instrumentation, education, and outreach. In the future it hopes to generate EU-funding for common projects at EU light sources.

Acknowledgements. The MAX IV team gratefully acknowledges the many institutions, which have contributed to building the facility. The ALBA team was most helpful in several software collaborations, for motion control and in licensing electrometers.

¹ Mikael Eriksson, J. Friso van der Veen and Christoph Quitmann, *Special issue on Diffraction-Limited Storage Rings and New Science Opportunities, Journal of Synchrotron Radiation*, Volume 21, Issue 5, pages 837–842, September 2014. And other articles in the same volume.

² <https://www.leaps-initiative.eu/>.

HAXPES TECHNIQUE APPLIED TO DEVICES FOR THE PRODUCTION AND STORAGE OF ENERGY

J. Abad^{a,f}, R. López-Vicente^b, C. Toledo^b, J. Colchero^c, A. Urbina^b, J. Rubio-Zuazo^{d,e}, G. R. Castro^{d,e}, J. Padilla^{a,f} and A. J. Fernández-Romero^f

^a Department of Applied Physics, Technical University of Cartagena (UPCT), 30202 Cartagena (Spain); jose.abad@upct.es, javier.padilla@upct.es

^b Department of Electronics, Technical University of Cartagena (UPCT), 30202 Cartagena (Spain); rodolfo.lopez@upct.es, carlos.toledo@upct.es, antonio.urbina@upct.es

^c Department of Applied Physics, University of Murcia, 30100 Murcia (Spain); colchero@um.es

^d SpLine, Spanish CRG beamline at the ESRF, 71 Avenue des Martyrs, 38043 Grenoble (France)

^e Institut of Materials Science of Madrid-CSIC, Sor Juana Inés de la Cruz 3,28049 Madrid (Spain); rubio@esrf.fr, castro@esrf.fr

^f Research Group of Advanced Materials for the Production and Storage of Energy, Technical University of Cartagena (UPCT), 30202 Cartagena (Spain); antonioj.fernandez@upct.es

The interest in Hard X-ray photoelectron spectroscopy (HAXPES) technique has grown rapidly in the past few years, due to the possibility to study the composition and electronic properties of buried interfaces in the bulk and of multilayers, as well as, measure the core-level binding energy shifts of bulk atoms. At high electron kinetic energy, e.g. 15 keV, the information depth can reach several tens of nanometres¹ and using the advantage of tuneable synchrotron X-ray radiation the photoelectron kinetic energy and therefore the information depth can be changed and consequently electronic and compositional depth profiles can be obtained.²

Our research group is devoted to the study of advanced materials for the production and storage of energy. In this work we present the application of the HAXPES technique to different materials, in bulk, layered samples and even in functional devices. The experiments were carried out at the Spanish CRG SpLine beamline at the ESRF.³ The first example is the analysis of the Zn anode in Zn/MnO₂ ionic liquid based gel polymer electrolyte batteries, which have been discharged or charged reaching different states of charge. The second example deals about the vertical segregation of PCBM within the active layers of standard and inverted organic solar cells, analyzing the influence of temperature and electrode composition of functional devices. Blends of P3HT and PCBM are the benchmark materials for the active layers of plastic solar cells. These experiments are a challenge since the photo-active layer of this kind of devices is not a staking of two layers but it is a blend of two organic materials, where one material acts as electron acceptor and the other as electron donor: their mixture creates a distributed “bulk heterojunction”. Nevertheless, the PCBM tends to aggregate and therefore destroy the path needed for *n*-type carrier transport; furthermore, the vertical segregation creates an inconvenient depth profile for PCBM in standard architecture.

Acknowledgements. Authors acknowledge the financial support by the Spanish Ministry of Economy through the project (ENE2016-79282-C5-5-R), the Consejo Superior de Investigaciones Científicas (CSIC) under grant PIE 201060E013 and Fundación Séneca-Murcia, grant 19882/GERM/15.

¹ J. Rubio-Zuazo, G. R. Castro, *J. Electron Spectros. Relat. Phenom* **2011**, 184, 384–390.

² J. Rubio-Zuazo, P. Ferrer, G. R. Castro, *J. Electron Spectros. Relat. Phenom* **2010**, 180, 27–33.

³ J. Rubio-Zuazo, G.R. Castro, *Nucl. Instrum. Methods Phys. Res. A*, **2005**, 547, 64–72.

OXIDATION MECHANISMS OF COPPER UNDER GRAPHENE

Leo Álvarez-Fraga¹, Juan Rubio-Zuazo^{1,2}, Félix Jiménez-Villacorta¹, Esteban Climent-Pascual¹, Rafael Ramírez-Jiménez^{1,3}, Carlos Prieto¹ and Alicia de Andrés¹

¹ *Instituto de Ciencia de Materiales de Madrid, Consejo Superior de Investigaciones Científicas. Cantoblanco, 28049 Madrid, Spain.*

² *BM25-SpLine The Spanish CRG Beamline at the ESRF, 38043 Grenoble Cedex 9, France.*

³ *Departamento de Física, Escuela Politécnica Superior, Universidad Carlos III de Madrid, Avenida Universidad 30, Leganés, 28911 Madrid, Spain.*

The oxidation and corrosion of copper are fundamental issues studied for many decades due to their ubiquitous and transversal impact. However, the oxidation of copper used as catalyst for graphene synthesis has opened a singular problem not solved yet. Since graphene is an impermeable one-atom thick membrane, it was foreseen to efficiently protect copper against oxidation; however contradictory results about this protection have been published. In some cases graphene is demonstrated to protect copper at a short time, several hours, in others, also for days and weeks. However, in other publications a significant enhancement of copper oxidation when covered by graphene has been reported and a mechanism for this enhancement was proposed. In order to understand these contradictory results, we studied the oxidation of different types of copper substrates with and without graphene for about one year comparing the oxidation of highly textured copper thin films with that of copper foils. Graphene is demonstrated to act either protecting or favoring oxidation depending on the morphology and the initial oxygen content of copper. Synchrotron x-ray diffraction and resonant Raman spectroscopy are used to determine structural aspects and to follow the formation of copper oxide. Morphological aspects are observed by scanning electron microscopy (SEM), atomic force microscopy (AFM) and optical microscopy.

We propose a novel mechanism to explain the enhanced oxidation of polycrystalline copper originated by oxygen encapsulated by the graphene impermeable layer during graphene growth. The initial oxygen content and the existence of grain boundaries are the main factors that determine the relevance of this process. Graphene is shown to prevent oxidation from atmosphere for any of the copper substrates but also promotes slow oxidation derived by the release of out-of equilibrium encapsulated oxygen. The formation of bubbles after several months [¹] evidences this slow release. By using hard (11KeV) x-ray photoemission spectroscopy (HAXPES), we studied the oxygen content at different depths inside copper for graphene covered samples and graphene free one [²]. The apparently contradictory reported results are understood in the frame of the presence of two oxidation mechanisms, the well known atmospheric oxidation and the here proposed novel process.

Acknowledgements: We acknowledge funding from MINECO (MAT2015-65356-C3-1-R and for provision of synchrotron facilities) and from Comunidad de Madrid (S2013/MIT-2740).

¹ R. Ramírez-Jiménez, L. Álvarez-Fraga, E. Climent-Pascual, F. Jimenez-Villacorta, C. Prieto and A. de Andrés. *Carbon*, **105**, 556-565 (2016)

² L. Álvarez-Fraga, J. Rubio-Zuazo, F. Jiménez-Villacorta, E. Climent-Pascual, R. Ramírez-Jiménez, C. Prieto, and A. de Andrés. *Chem. Mater.* **29**, 3257-3264 (2017)

STUDY OF OXYGEN VACANCIES GENERATION PROCESS IN La_{0.7}Ca_{0.3}MnO_{3-x} PEROVSKITE BY POLARIZED X-RAY ABSORPTION SPECTROSCOPY

E. Salas-Colera^{a,b}, J. Rubio-Zuazo^{a,b} and G. R. Castro^{a,b}

^a Spanish CRG BM25-SpLine Beamline, The European Synchrotron (ESRF), 71 Avenue des Martyrs, F38043, Grenoble, (France);

^b Instituto de Ciencia de Materiales de Madrid (ICMM), Sor Juana Inés de la Cruz 3, E28049 Cantoblanco, Madrid (Spain);

eduardo.salas-colera@esrf.fr

Complex oxides systems show notable superconductivity, colossal magnetoresistance, ferroelectricity and multiferroicity properties. These properties are consequence of combination of charge, spin, chemical composition and lattice features. La_{0.7}Ca_{0.3}MnO₃ perovskite material shows a ferromagnetic-paramagnetic phase transition with a metal-insulator transition and colossal magnetoresistance behaviour near to room temperature. This material has been studied in ultra-thin films form to be used in magneto-electronic devices¹. The magnetic and electronic properties of this mixed-valence manganite deteriorate when it is grown in thin film form. In mixed-valence manganites magnetoresistance properties are managed by the amount of oxygen content in the sample². Oxygen vacancies induce lattice distortions and how the interaction between Mn³⁺ and Mn⁴⁺ ions are produced.

Previous experiments³ were carried out by X-Ray Diffraction and Hard X-Ray Photoelectron Spectroscopy synchrotron techniques. It was obtained that oxygen defects produce important changes in the crystal structure and electronic properties of manganite samples. The Mn valence is reduced and the metal-insulator transition is shifted to lower temperatures due to the modifications in the Mn-O bonds produced by oxygen defects.

In this work we aim to study how the structural and magneto-electronic properties are modified and correlated by the generation of oxygen vacancies in La_{0.7}Ca_{0.3}MnO₃ perovskite material. Polarized X-Ray Absorption Spectroscopy (P-XAS) experiment was carried out to study the oxygen vacancies generation process in 20 nm La_{0.7}Ca_{0.3}MnO₃ thin films grown on SrTiO₃ substrate by Pulsed Laser Deposition. XAS technique allow to study the structural properties of the first coordination shell. The polarized X-Ray source from synchrotron is used to distinguish between in-plane and out-of-plane contributions⁴ to XAS signal from octahedral MnO₆ structure.

Polarized-XAS characterization show clear evidences that the formation of oxygen vacancies is produced in the basal plane of the MnO₆ block. This results confirm that the magnetoresistance properties are managed by the amount of oxygen content and where the vacancies are produced in the crystal structure. These results have been correlated with previous structural and electronic properties characterized by synchrotron techniques.

¹ Y. Lu, X. W. Li, G. Q. Gong, G. Xiao, A. Gupta, P. Lecoeur, J. Z. Sun, Y. Y. Wang and V. P. Dravid, *Phys. Rev. B* **1996**, *54*, R8357.

² S. Mercone, C. A. Perroni, V. Cataudella, C. Adamo, M. Angeloni, C. Aruta, G. De Filippis, F. Miletto, A. Oropallo, P. Perna, A. Y. Petrov, U. Scotti di Uccio and L. Maritato, *Phys. Rev. B* **2005**, *71*, 064415.

³ J. Rubio-Zuazo, L. Onandía, P. Ferrer and G. R. Castro, *Appl. Phys. Lett.* **2014**, *104*, 212404.

⁴ S. Lafuerza, J. García, G. Subías, J. Blasco and V. Cuartero, *Phys. Rev. B* **2014**, *89*, 045129.

STRAIN STUDY OF Cr₂O₃ THIN FILMS GROWN BY PULSED LASER DEPOSITION

M.Vila^{a,b}, J. Rubio – Zuazo^{a,b}, E. Salas - Colera^{a,b},
A. Prados^{c,d} and G. R. Castro^{a,b}

^a*SpLine CRG BM25 Beamline, European Synchrotron Radiation Facility, 71, Avenue des Martyrs, 38000, Grenoble, France*

^b*Instituto de Ciencia de Materiales de Madrid, Consejo Superior de Investigaciones Científicas (ICMM-CSIC) 28049, Madrid, Spain*

^c*Departamento de Física de Materiales, Facultad de Ciencias Físicas, Universidad Complutense de Madrid, E-28040 Madrid, Spain*

^d*Instituto de Sistemas Optoelectrónicos y Microtecnología (ISOM), Universidad Politécnica de Madrid, 28040, Madrid, Spain.*
vilasant@esrf.fr

Transition metal sesquioxide, chromia, α - Cr₂O₃, is a corundum-type crystal (space group R3⁻c, $a = 4.96$ Å, $c = 13.59$ Å, $c/a = 2.74$). The structure consists of alternating oxygen layers and chromium bilayers along the c-axis of the hexagonal lattice. Bulk Cr₂O₃ present antiferromagnetic properties ($T_N = 307$ K), and is also the first room temperature magnetoelectric material reported in the same phase¹. In addition, it exhibits uniaxial magnetic anisotropy along [111]. These magnetic properties make Cr₂O₃ suitable for spintronic applications². However, Cr₂O₃ grown as thin film can result in a modification of its magnetic properties, strain on thin films can cause ferromagnetism³, and therefore it is crucial to fully understand structural modifications of the thin films in comparison with the bulk.

We have grown, for the first time, crystalline α -Cr₂O₃ thin films onto SrTiO₃(111) substrates by Pulsed Laser Deposition (PLD), as well as on Al₂O₃, due to their similar lattice parameters. In situ Reflection High-Energy Electron Diffraction (RHEED) patterns were obtained, showing smooth diffraction stripes, representative of a smooth and homogeneous layer. Crystallinity is observed from the first laser shoot. The crystallographic properties of the thin films grown on both substrates have been studied using grazing incidence surface X – Ray diffraction and X-ray reflectivity (GIXRD/XRR) in beamline BM25-SpLine (Branch B) at the European Synchrotron Radiation Facility (ESRF). A study of the coupling of the Cr₂O₃ lattice in both substrates has been fulfilled. Reciprocal Space Mapping (RSM) performed in Cr₂O₃ thin films, for the Cr₂O₃/SrTiO₃(111) thin films, reveal an in-plane rotation of 30° of the layer respect to the underlying substrate. However, Cr₂O₃/Al₂O₃ are epitactical. The morphology of the film surface has been studied by Atomic Force Microscopy (AFM), revealing good coverage and homogeneity, as well as a very flat surface (rms ~ 1 nm). Extended X – Ray Absorption fine structure (EXAFS) and X – Ray Absorption Edge Structure (XANES) measurements have been also performed in BM25 – SpLine (Branch A) in the thin layers to study the local coordination environment of Cr and O atoms. Atomic distances in both Cr₂O₃/SrTiO₃(111) and Cr₂O₃/Al₂O₃ are shorter than bulk values, specially Cr – Cr distances.

¹ D. N. Astrov, B. I. Al'shin, R. V. Zorin, and L.A. Drobyshev, Soviet Physics JETP. 6 (1969) 28

² A. Kirfel, K. Eichhorn, Acta Crystallogr. Sect. A: 46 (1990) 271

³ S.Punugupati, J. Narayan and F.Hunte, JAP 117, (2015) 193907

UNRAVELING THE GAS-INDUCED STRUCTURAL CHANGES ON NANOPOROUS SOLIDS COUPLING GAS ADSORPTION AND IN SITU SYNCHROTRON XRD

A. Gomis-Berenguer^a, E. Salas-Colera^b, J.B. Parra^c, S. García-Granda^d, G.R. Castro^b and C.O. Ania^a

^aCEMHTI, CNRS, UPR 3079, 45071 Orléans (France); alicia.gomis-berenguer@cnrs-orleans.fr, conchi.ania@cnrs-orleans.fr

^bSpLine, Spanish CRG BM25 Beamline, ESRF, 38000 Grenoble (France); Instituto de Ciencia de Materiales de Madrid (ICMM), CSIC, c. Sor Juan Inés de la Cruz 3, E-28049 Madrid, Spain. eduardo.salas-colera@esrf.fr; german.castro@esrf.fr

^cInstituto Nacional del Carbon (INCAR-CSIC), P.O. 63, 33011 Oviedo (Spain); jbparra@incarcsic.es

^dDepartamento de Química Física y Analítica, Facultad de Química, Universidad de Oviedo, 33071 Oviedo (Spain); sgg@uniovi.es

Our studies on equilibrium gas adsorption on different families of nanoporous materials (such as MOFs, ZIFs and zeolites) using different gases and temperatures have revealed unusual structural modifications (so called gate-opening and/or breathing effects) depending on the size and polarizability of the gas probe and the interactions with the solid host¹. In this regard, useful information can be obtained combining powerful experimental gas and computation tools, including high resolution gas adsorption and in-situ synchrotron XRD measurements during the gas loading and release from the nanoporous voids.

In this work we provide insights on the mechanisms governing structural deformations during gas adsorption of various nanoporous solids (i.e., ZIF-8, ZIF-67 and MFI zeolite), combining in-situ adsorption and high resolution powder diffraction. The in-situ synchrotron high resolution powder XRD measurements combining various probes (e.g. N₂, Ar, O₂) and temperatures (from cryogenic to ambient) were conducted at the Spanish CRG at ESRF (Grenoble), in a controlled environment chamber specially designed for these experiments, and that allowed the fine control of the gas dosage, sample outgassing under vacuum, temperature control and simultaneous recording².

In the case of ZIF-8, we have shown that the gas-induced deformation does not affect the cell structure of the pristine material, although it does modify its gas uptake. This process is governed by the polarizability, molecular size and shape of the gas adsorbed, and it is originated in the rearrangement of the moieties inside the cavities when a threshold gas pressure is attained upon adsorption. A similar effect was detected for an isomorphic material with a different cation, showing that this phenomenon is not affected by the electronic structure of the metal defining the structure of the framework. We have also explored all silica MFI zeolite, since this material has a bi-stable behavior controlled by the gas pressure as external stimulus, provoking an outstanding structural transformation^{3,4}. Data has evidenced that the origin of the gas-induced structural changes, would be attributed to changes in the gas phase rather than to a solid phase transition from the monoclinic to orthorhombic phase.

Acknowledgements. This work was supported by the Spanish MINECO and the Spanish National Research Council (CSIC).

¹ Ania CO, García-Pérez E, Haro M, Gutiérrez-Sevillano JJ, Valdés-Solís T, Parra JB, Calero S, *J. Phys. Chem. Lett.* **2012**, 3, 1159.

² Salas-Colera E, Muñoz-Noval A, Heyman C, Ania CO, Parra JB, García-Granda S, Calero S, Rubio-Zuazo J, Castro GR, *J. Synch. Radiation* **22**, **2015**, 42.

³ García-Pérez E, Parra JB, Ania CO, Dubbeldam D, Vlucht TJH, Castillo JM, Merklings PJ, Calero S, *J. Phys. Chem. C* **112**, **2008**, 9976.

⁴ Snurr RQ, Bell AT, Theodorou DN, *J. Phys. Chem.* **1993**, 97, 13742.

Pressure-induced structural transitions in molecular compounds based on sesquioxides of group 15

J.A. Sans^a, F. J. Manjón^a, C. Popescu^b, V. P. Cuenca-Gotor^a, A. Muñoz^c, P. Rodríguez-Hernández^c, A. L. J. Pereira^d, V. Monteseuro^e and J. Ibañez^f

^a *IDF, Universitat Politècnica de València, 46022 Valencia (Spain); juasant2@upv.es*

^b *ALBA-CELLS, 08290 Cerdanyola (Spain)*

^c *Departamento de Física, Universidad de La Laguna, 38205 La Laguna (Spain)*

^d *Lab. de Materiais Cerâmicos Avançados, U. F. da Grande Dourados, Dourados (Brazil)*

^e *ESRF, F-38043 Grenoble (France)*

^f *Institute of Earth Sciences Jaume Almera, CSIC, 08028 Barcelona (Spain)*

Pressure is an important thermodynamic parameter similar in importance to temperature. Application of high pressure to solid-state compounds leads to an overall increase of density and the decrease of interatomic and intermolecular distances. Consequently, high-pressure research has allowed us to explore in detail atomic and molecular interactions and has improved our fundamental understanding of these interactions in solids. Understanding interactions in solids has benefited largely from synchrotron-based angle-dispersive x-ray diffraction which provides structural data to study the evolution of materials at extreme conditions of pressure and temperature. In this work, we present a brief description of the recent discoveries in sesquioxide compounds (A_2O_3) with molecular structure covering different pressure-induced structural phase transitions. In particular, the different polymorphs of sesquioxides formed by elements of the group 15 (As, Sb and Bi) have recently attracted an increasing interest with the aim to understand the effect of the lone electron pair of these cations in the molecular character of the sesquioxides.

Among them, α -As₂O₃ is one of the most compressible solid inorganic compounds in absence of hydrogen bonding and crystallizes in a cubic structure.¹ This compound presents a pressure-induced amorphization, only avoided by the pressure-induced helium trapping and bonding that provides an unexpected mechanical stability to the structure.² Nevertheless, isostructural α -Sb₂O₃ shows two second-order phase transitions; i.e., structural transitions without volume change and driven by dynamical instabilities, below 10 GPa and a first-order phase transition at higher pressure.^{3,4} On the other hand, intermediate symmetric structures such as orthorhombic β -Sb₂O₃ and tetragonal β -Bi₂O₃ seem to be more prone to suffer second-order phase transitions.^{5,6} In particular, β -Sb₂O₃ has an internal second-order phase transition in the molecular structure which is hidden by the larger compressibility of the structural voids in the bulk. Finally, α -Bi₂O₃ that crystallizes in a monoclinic structure, the least symmetric structure despite having the smaller lone electron pair, leads to a common first-order phase transition at high pressures.⁷

In summary, this work will show some guidelines in the stability of the sesquioxide polymorphs and the effect of the lone electron pair in the formation of the different structures. Furthermore, this study will offer some hints about the influence of the molecular character in the kind of phase transition observed at high pressures.

Acknowledgements. The authors thank the financial support of the grants No. MAT2016-75586-C4-1/2/3-P and MAT2015-71070-REDC (MALTA Consolider). JAS also acknowledges financial support through the Ramon y Cajal fellowship (RYC-2015-17482).

¹ J. A. Sans, F. J. Manjón, C. Popescu, et al., *J. Phys.: Cond. Matter.* **2016**, *28*, 475403.

² J. A. Sans, F. J. Manjón, C. Popescu, et al., *Phys. Rev. B.* **2016**, *93*, 054102.

³ A. L. J. Pereira, L. Gracia, D. Santamaría-Perez et al., *Phys. Rev. B.* **2012**, *85*, 174108.

⁴ Z. Zhao, Q. Zeng, H. Zhang et al., *Phys. Rev. B.* **2015**, *91*, 184112.

⁵ J. A. Sans, F. J. Manjón, A. L. J. Pereira et al., under preparation.

⁶ A. L. J. Pereira, J. A. Sans, R. Vilaplana et al, *J. Phys. Chem. C.* **2014**, *118*, 23189-23201.

⁷ A. L. J. Pereira, D. Errandonea, A. Beltrán et al, *J. Phys.: Cond. Matter.* **2013**, *25*, 475402.

PRESSURE AND TEMPERATURE DEPENDENCE OF THE STRUCTURE AND ANHARMONIC EFFECTS IN HfSe₂

A. Andrada-Chacón, V. G. Baonza and J. Sánchez-Benítez

MALTA-Consolider Team, Physical Chemistry Department, Faculty of Chemical Sciences, Universidad Complutense de Madrid, E-28040 Madrid (Spain); a.andrada@ucm.es

Transition metal dichalcogenides (TMDs) with MX₂ stoichiometry are layered materials formed by stacking of two dimensional layers, commonly linked through weak Van der Waals interlayer interactions (see Figure 1). Although TMDs have acquired during last years an extremely large attention due to their interesting physical properties and phenomena,^{1,2} some materials remain still scarcely studied. Currently, we are particularly interested on HfSe₂, since, to our knowledge, neither high pressure nor thermal evolution studies have been reported in the literature. Additionally, recent first-principles calculations suggest that HfX₂ materials are small gap semiconductors with large work functions and reasonable carrier mobility.³

In this study, we address the structural characterization of 1T-HfSe₂ under pressure and temperature extreme conditions. For this purpose, we have performed several synchrotron x-ray diffraction experiments at MSPD beamline at ALBA facility. Moreover, some other experiments have been completed in our laboratory involving Raman spectroscopy and DFT calculations. We have found for the first time in these materials clear evidences of Fermi Resonance (FR) effect, easily tuned at low pressures and vanishing at around 3 GPa. This phenomenon, clearly observed as a correlation between intensities and frequencies in the Raman spectra, is due to anharmonic coupling between two phonons. Additionally, XRD data acquired at MSPD allowed us to obtain the high pressure and thermal evolution of HfSe₂ structure. Interestingly, this structural evolution also exhibits a perturbation around 3 GPa, in very good agreement with the anharmonic coupling limit found by Raman spectroscopy. Furthermore, the correlation between the structural evolution and the anharmonic coupling is also evidenced through the Se-Se interlayer distances. Finally, as the analysis of XRD data reveals, pressure seems to induce a structural transition in HfSe₂ around 15 GPa, also evidenced by the phonon frequencies evolution through Raman spectroscopy under pressure.

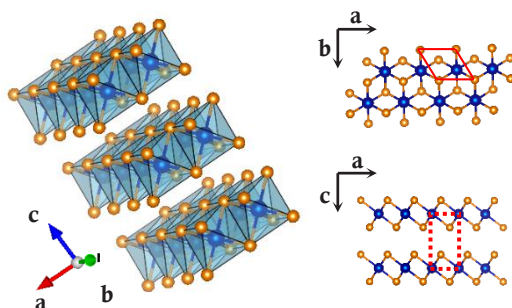


Figure 1. 1T-HfSe₂ crystal structure.

Acknowledgements. This research was supported by the MICINN and MINECO under projects MALTA-Consolider Team (CSD2007-00045, MAT2015- 71070-REDC) and CTQ2015-67755-C2-1-R (MINECO/FEDER). We thank the ALBA Light Source for making their facilities available and the allocated beamtime. A. A-C. acknowledges support from a MINECO-FPI grant (BES-2013-066112).

¹ M. N. Ali, J. Xiong, S. Flynn, J. Tao *et al.*, *Nature* **2014**, *514*, 205-208.

² B. Sipos, A. F. Kusmartseva, A. Akrap, H. Berger, L. Forró, E. Tutis, *Nature Materials* **2008**, *7*, 960-965.

³ C. Gong *et al.*, *Appl. Phys. Lett.* **2013**, *103*, 053513.

PAIR DISTRIBUTION FUNCTION STUDIES IN CEMENTITIOUS SYSTEMS

A. Cuesta^a, J. D. Zea-Garcia^b, D. Londono-Zuluaga^b, A. G. De la Torre^b, I. Santacruz^b, O. Vallcorba^a, M. A. G. Aranda^a

^a ALBA Synchrotron, Carrer de la Llum 2-26, E-08290 Cerdanyola del Vallès, Barcelona, Spain; acuesta@cells.es

^b Departamento de Química Inorgánica, Cristalografía y Mineralogía, Universidad de Málaga, 29071-Málaga, Spain

The analysis of amorphous/nanocrystalline phase(s) within cement matrices that contain high amounts of crystalline phase(s) is very challenging. Synchrotron techniques can be very useful to characterize such complex samples.¹ This work is focused on total scattering Pair Distribution Function (PDF) quantitative phase analyses in selected real-space ranges for a better understanding of the binding gel(s). Powder diffraction data collected in BL04-MSPD beamline have been analyzed by PDF and Rietveld methodologies to determine nanocrystalline and microcrystalline phase contents. The comparison between both methodologies allows us to have a better insight about the nanocrystalline/microcrystalline components which coexist in cement pastes. Three sets of hydrated model samples have been studied: i) monocalcium aluminate, CaAl_2O_4 , the main component of calcium aluminate cements, ii) ye'elimite, $\text{Ca}_4\text{Al}_6\text{SO}_{16}$, the main component of calcium sulfoaluminate cements, and iii) tricalcium silicate, Ca_3SiO_5 , the main component of Portland cements.

For the CaAl_2O_4 paste, the PDF fit shows that the aluminum hydroxide gel has a gibbsite local structure with an average particle size close to 5 nm.² Figure 1 shows the final fit for CaAl_2O_4 paste in two different real-space regions. On the contrary, for $\text{Ca}_4\text{Al}_6\text{SO}_{16}$ paste, it has been found that the particle size of the aluminum hydroxide gel is below 3 nm. Moreover, the Ca_3SiO_5 paste contains a different nanocrystalline gel, C-S-H, which has also been thoroughly studied. Different crystal structures (including Tobermorite, Clinotobermorite and Jennite) have been tested to find the structural model that fits better the experimental data. The results from this ongoing investigation will be reported and discussed.

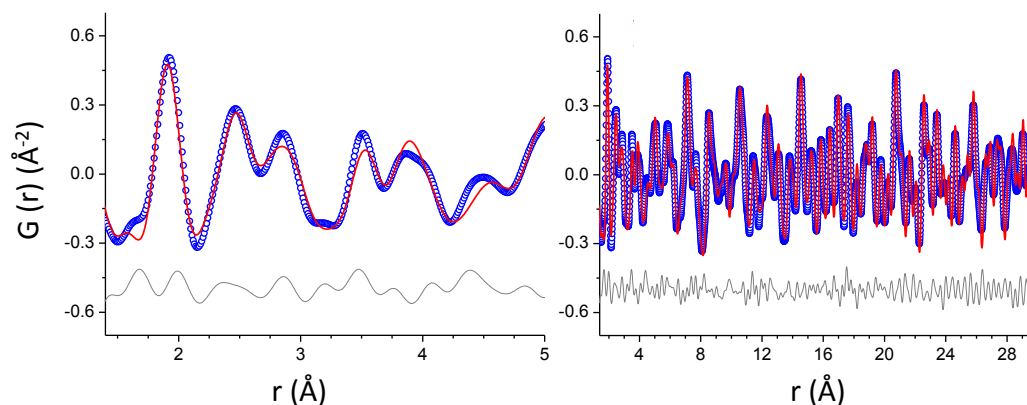


Figure 1. Experimental (blue circles) and fitted (red solid line) PDFs for $\text{Ca}_2\text{Al}_4\text{O}_4$ paste at selected ranges.

Acknowledgements. This work has been supported by Spanish MINECO through BIA2014-57658-C2-1-R and BIA2014-57658-C2-2-R, which is co-funded by FEDER, research grants. We also thank CELLS-ALBA for providing synchrotron beam time at BL04-MSPD.

¹ M.A.G. Aranda, *Cryst. Rev.* **2016**, 22, 150-196.

² A. Cuesta, et al., *Cem. Concr. Res.* **2017**, 96, 1-12.

SpLine Spanish CRG BM25 beamline at the ESRF-The European Synchrotron: Activity report, current status and future challenges

J. Rubio Zuazo^{a,b} and G. R. Castro^{a,b}

^a SpLine Spanish CRG BM235 Beamline at the ESRF, 71 avenue des Martyrs, 38000 Grenoble, France

^b ICMM Instituto de Ciencias de Materiales de Madrid, Consejo Superior de Investigaciones Científicas, Sor Juana Inés de la Cruz, 3, Cantoblanco, 28049 Madrid, Spain; spline@esrf.fr

The main goal of the interdisciplinary and multipurpose Spanish CRG BM25-SpLine beamline is to satisfy the needs of the use of synchrotron radiation in the region of hard X-rays of the Spanish scientific community. The beamline, which started the user's operation in 2005, is dedicated to structural and electronic investigations using hard X-ray scattering mostly in materials science, specialized on X-Ray diffraction techniques, X-Ray absorption spectroscopy and hard X-ray photoemission spectroscopy.

After more than 20 years of excellent achievements, the ESRF has launched, few years ago, an overambitious upgrade program^{1,2}. A major goal of the phase II program is to construct and commission the new Extremely Brilliant Source (ESRF – EBS) storage ring. The new ESRF-EBS design has been conceived with performances multiplied by 100 in terms of brilliance and coherence. For the CRGs beamlines five different “bending magnet/short wiggler” sources will be available in the new EBS-ESRF Source. Additionally, with the new EBS-ESRF machine the electron beam position will be optimized at the Short Wiggler positions, which is not the case for the present Bending Magnet positions, leading to a major increase in stability and beam performances. The EBS-ESRF ring offer exceptional improvement of the beam characteristic in terms of stability, flux and brilliance that will have a huge impact in the science that can be addressed, responding to each time more demanding exigencies of the synchrotron user's community.

In this talk, we will present in the first part the activity report for the last two years, in a second part we will show the huge and exceptional advantages that offer the new EBS-ESRF for the CRGs. We will present the goals of the SpLine development and the upgrade program, which aims to preserve and take advantage of the exceptional characteristics of the new ESRF-EBS source. The refurbishment programme for SpLine will improve actual technical capabilities for users and will be realized during the next four years in order to reduce the economic impact and achieve a better spread of the requested financial resources.

Acknowledgements. We are grateful to the SpLine staff for their valuable help in operation of the beamline and to the financial and administrative support from the Spanish MINECO and Consejo Superior de Investigaciones Científicas.

¹ http://www.esrf.fr/Apache_files/Upgrade/DP_ESRF-2015-En.pdf

² http://www.esrf.fr/Apache_files/Upgrade/ESRF-orange-book.pdf

ALBA strategic plan and European LEAPS initiative

C. Biscari

ALBA Synchrotron, Carrer de la Llum, 2-26, Cerdanyola del Valles, 08290, Barcelona (Spain);
cbiscari@cells.es

ALBA Synchrotron belongs to the national map of ICTS (*Infraestructura Científica y Técnica Singular*), which includes a large variety of scientific infrastructures and is approved by the Consejo de Política Científica, Tecnológica y de Innovación of MINECO.

The ICTS map is evaluated and updated every four years, through a process based on performance indicators and strategy plans. The strategy plan for the period 2017-2020 is presently being prepared.

The LEAPS (League of European Accelerator-based Photon Sources) initiative, aims at coordinating efforts of European photon sources, optimizing resources, prioritizing technological roadmaps, integration, education and innovation. It will be officially presented at the European Commission in November 2017.

ALBA vision, main objectives, and strategies for the future at the national and international level will be presented in the context of both initiatives.

TITLE: FIVE YEARS OF ALBA ACCELERATORS. OPERATION AND OUTLOOK

M.Pont

ALBA-CELLS, Cerdanyola del Vallès, (Spain) pont@cells.es

The ALBA Synchrotron has been in operation for external users for five years. It is a good moment to review the operation of the accelerators as well as to present the plans for the future.

First the ALBA accelerators will be briefly presented, together with the present capabilities of the accelerators in terms of electron beam current, electron beam stability, filling pattern.

The major figure of merit when discussing the operation of an accelerator for a synchrotron light source is the beam availability, understood as the fraction of the scheduled time in which the photon beam has reached the beamlines. This number has been increasing steadily, since day one, reaching more than 99% in the first half of 2017. Other figures of merit, like mean time between failures (MTBF) and time to recover (MTTR) the beam will also be presented and discussed.

The future evolution of the accelerators in order to increase the operational performance as well as the plans to keep the beam availability at the achieved high level will also be discussed.

UPGRADE OF THE SAXS BL: NCD-SWEET

M. Malfois^a, C. S. Kamma-Lorger^b, J.C. Martínez^c and E. Solano^d

^a ALBA, 08290, Cerdanyola del vallès (Spain); mmalfois@cells.es

^b ALBA, 08290, Cerdanyola del vallès (Spain); ckamma@cells.es

^c ALBA, 08290, Cerdanyola del vallès (Spain); guilmar@cells.es

^d ALBA, 08290, Cerdanyola del vallès (Spain); esolano@cells.es

The Small Angle X-ray Scattering (SAXS) beamline at ALBA is currently under a major upgrade. The monochromator, the Beam Conditioning Optics (BCO), the sample platform and the WAXS detector support are being installed and will be available for users in November 2017. A new SAXS detector is already in use since June 2017. The beamline will allow the users to perform state of the art experiments in transmission mode.

The Double Crystal Monochromator will be changed to a channel-cut crystal that will produce a more stable beam and thus with more flux.

The BCO will accommodate an On-Axis camera. This will facilitate the sample alignment. The sample can also be observed while measuring the SAXS/WAXS data. A series of Beryllium lenses will be incorporated into the BCO for focusing the beam to a couple of m horizontally and vertically. A scatterless slits will also be installed for cleaning the direct beam from the parasitic scattering beam.

A new sample platform will be set up with micrometer resolution and will hold 100kg load. A wide variety of in-house sample environment for performing time resolved experiments can then be installed on the beamline.

The WAXS detector support will be independent of the sample stage motion. The nosecone will slide along the beam to reduce the air gap to the minimum for SAXS experiments. If SAXS/WAXS experiments are performed, the optimized distance between the sample and the WAXS detector can be achieved. Rotating the WAXS detector along the beam axis will also be possible.

A new SAXS photon counting detector is available for users since June 2017. The main features of this detector are the frame rate where 25 images can be collected in a second, the low background and the dynamic range.

A new beamline development is under way that should be available for users by the end of 2018: GSAXS.

The New Synchrotron Infrared Microspectroscopy Beamline MIRAS

Ibraheem Yousef^a, Martin Kreuzer^a, Tanja Ducic^a, Nuria Benseny-Cases^a, Carlos Falcon^a and Miguel A. G. Aranda^a

^aALBA Synchrotron, Carrer de la Llum 2-26, 08290, Cerdanyola del Vallès, Barcelona, Spain
iyousef@cells.es

MIRAS is one of the phase II beamlines recently entered in operation at the third generation synchrotron light facility ALBA, located near Barcelona, Spain. Construction of MIRAS was initiated in 2014 and advanced rapidly. The commissioning phase of the beamline started in 2016 with a scheduled plan of welcoming the first users by the end of 2016. MIRAS is dedicated to infrared microspectroscopy, with the aim to deliver world-class performance in terms of a bright and highly stable photon beam. The beamline is providing ALBA users with a modern infrared microspectroscopy facility covering a wavelength range from 0.4 to 100 μm . The design of the beamline optimizes performance in the mid-IR range and will give significantly enhanced efficiency, compared to a conventional source, in both far-IR and mid-IR regions¹.

On April 2016, after successful installation of all BL optical components, MIRAS started commissioning with synchrotron light. The transport mirrors were aligned until the first focus of synchrotron light was obtained outside the tunnel². During May 2016, all the transport mirrors of the beamline were aligned until the coupling of the synchrotron light with the Beamline endstation. The first infrared spectrum was obtained which was followed by the full commissioning and performance testing. MIRAS started operation with friendly users in July 2016; three different groups (working on Material science, archaeology and biomedicine) have performed successful measurements. The beamline is currently running with official users since October 2016, two months earlier than originally foreseen.

This contribution will present the new infrared beamline MIRAS at the ALBA Synchrotron light facility. Details of the beamline commissioning results, performances tests and preliminary results arising from a variety of experiments already carried out at the beamline will be reported.

Acknowledgements. The authors would like to thank all collaborators from inside and outside ALBA synchrotron light source. I.Y. acknowledges the advice and assistance received from Dr. Gary Ellis (CSIC, Institute of Polymer Science), Dr. Ulrich Shade (BESSYII) and from Dr. Gianfelice Cinque (Diamond).

¹ I. Yousef et al., Nuclear Instruments and Methods A, 673(1): 73–81 [2012].

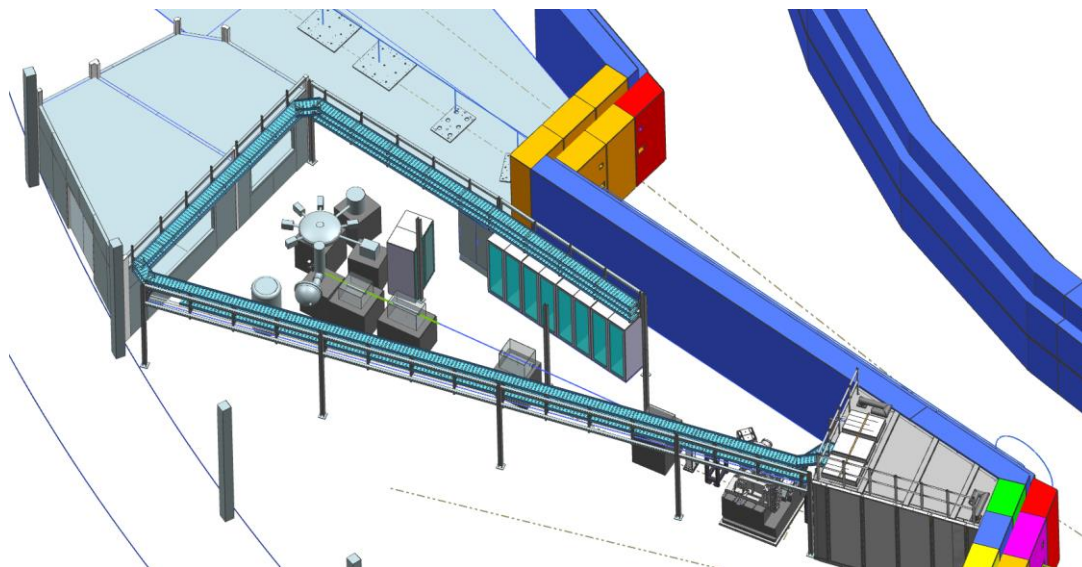
² MIRAS, www.albasynchrotron.es/en/beamlines/bl01-miras

THE LOREA ARPES BEAMLINE AT THE ALBA SYNCHROTRON

F. Bisti, D. Pierucci, M. Tallarida, E. Pellegrin, L. Aballe, S. Ferrer and J. Nicolas

Alba Synchrotron Light Facility, CELLS, Carrer de la llum 2-26, 08290, Cerdanyola del Vallès, Barcelona, Spain; fbisti@cells.es

In the present work, we report the design and construction status of LOREA, the ALBA synchrotron beamline devoted to electronic structure investigation by means of Angle Resolved Photo-Emission Spectroscopy (ARPES).



LOREA is the ninth beamline of the **ALBA synchrotron radiation source**, it is under construction and will be in operation in 2019.

The beamline is designed to cover **the photon energy range of 10-1000 eV**, with continuously variable polarization, resolving power of more than 10^4 in the whole range, and spot size of about $10 \times 10 \mu\text{m}^2$. The photon flux is expected to be of the order of 10^{13} (ph/s/0.1%BW) for photon energies up to 350 eV, and above 10^{12} (ph/s/0.1%BW) in the 350-1000 eV. Thanks to the wide energy range and high photon flux, LOREA will be suitable for high resolution **VUV ARPES** investigation in the range of 10-200 eV, with the possibility to extend the ARPES measurements in the 200-600 eV energy range (**Soft X-ray ARPES**). In addition, core level spectroscopy, resonant photoemission and X-ray absorption spectroscopy will be accessible in the whole energy range.

The end station of LOREA will be composed by a central radial distribution chamber to which all other vessels are connected, including chambers for ARPES investigation, **in situ UHV deposition and characterization**, high pressure deposition (**Chemical Vapor Deposition, CVD**, and **Atomic Layer Deposition, ALD**), **organic molecule** deposition; sample storage, docking of **vacuum suitcases**, docking of **STM**, and fast entry load lock.

Update and Recent Developments at XALOC and MISTRAL Beamlines

J. Andreu, X. Carpena, J.J. Conesa, F. Gil, B. Machado, J. Otón, A.J. Pérez-Berná, M. Rosanes, A. Sorrentino, R. Valcárcel, R. Boer, E. Pereiro, and J. Juanhuix

Experiments Division, Alba Synchrotron. Carrer de la Llum 2-26, 08290 Cerdanyola del Vallès, Barcelona (Spain); juanhuix@cells.es

MISTRAL and XALOC, two operating beamlines mostly dedicated to life sciences at the Alba synchrotron are continuously being updated and upgraded to follow the pace of the rapid evolution of the field. Here we report these upgrades and recent developments.

MISTRAL beamline¹ is one of the very few beamlines worldwide dedicated to transmission soft X-ray microscopy and, in particular, to cryo soft X-ray tomography of whole unstained cells at 30 nm resolution. A newly installed on-line fluorescence microscope inside the vacuum chamber of the TXM is routinely used to facilitate correlative microscopy approaches, which are essential in structural cell biology. A new grating is expected to increase the energy resolution at the high energy end (700-800 eV). Concerning the end-station, a near-future important upgrade at the beamline is the implementation of a dual axis tomography system inside the microscope chamber, which will result in a more isotropic resolution of the 3D tomographs. Finally, to further extend the depth of field of 3D tomographs, a variable multi-foci approach is currently routinely used and pending for further improvement. The scientific outcome of the MISTRAL beamline will be illustrated by recent examples of 3D cell imaging and material science hot topics such as magnetic nanodomains or electrical batteries.

XALOC² is the only operating beamline at the Alba synchrotron dedicated to Macromolecular Crystallography. Implemented upgrades involve both user experience, efficiency of the beamline and X-ray beam characteristics. The range of routine experiments has been increased by the implementation of the robot raster scans, full rotation of the mini-kappa goniometer, and easier and faster connection in remote experiments. Automatic data processing, which is essential in time-effective MX experiments, has been fully integrated in the experiment pipeline. The data processing is using a high speed processing cluster and includes a semi-automated crystal phasing with Phaser³ and Arcimboldo⁴ suites. Planned upgrades of the XALOC beamline include the upgrade of the moveable beamstop, the implementation of a humidity control system, and the modification of the robot to ensure the compatibility with the Unipuck system. A few examples of the structural biology projects currently being carried out at the beamline will be given.

¹ A. Sorrentino, J. Nicolás, R. Valcárcel, F.J. Chichón, M. Rosanes, J. Ávila, A. Tkachuk, J. Irwin, S. Ferrer and E. Pereiro, *J. Synchrotron. Rad.*, **2015**, 22, 1112–1117.

² J. Juanhuix, F. Gil-Ortiz, G. Cumi, C. Colldelram, J. Nicolas, J. Lidon, E. Boter, C. Ruget, S. Ferrer and J. Benach, *J. Synchrotron Rad.*, **2014**, 21, 679–689.

³ A.J. McCoy, R.W. Grosse-Kunstleve, P.D. Adams, M.D. Winn, L.C. Storoni, and R.J. Read, *J. Appl. Cryst.*, **2007**, 40, 658-674.

⁴ C. Millán, M. Sammito, I. Usón, *IUCrJ*, **2015**, 2, 95-105.

Update and recent developments at MSPD and CLÆSS BLs

**F. Fauth, L. Simonelli, C. Popescu, C. Marini,
O Vallcorba, W Olszewski, A Missyul, N. Ramanan, D. Heinis**

*CELLS-ALBA Synchrotron, Carrers de la Llum 2-26,
E-08290 Cerdanyola del Vallès, Barcelona, (Spain) ffauth@cells.es*

The BL04-MSPD and BL22-CLÆSS beamlines are ALBA high energy beamlines dedicated to chemistry and material science, using powder diffraction (PD) and X-ray absorption/X-ray emission spectroscopy (XAS/XES) techniques, respectively.

The Material Science and Powder Diffraction beamline BL04-MSPD has two fully operational end-stations. The first station, with its small 15 x 15 μm FWHM beam spot within 20-50 keV energy range, is devoted to High Pressure and Micro diffraction studies. The second station, owing to its dual detection setup, is dedicated to either high-angular resolution and/or high-throughput powder diffraction^{1 2}. The most significant recent upgrades on BL04-MSPD concern sample environments. For standard powder diffraction experiments in transmission mode using capillaries, it is now possible to measure in temperature range 5K to 1273K. In High Pressure experiments, non ambient conditions of temperature (10K to 600K) and pressure (up to 60 GPa) are standardly accessible using proper Diamond Anvil cells. More challenging conditions (1.2 Mbar and 1300K) could be achieved using special equipments.

Following last year intense commissioning of the X-Ray emission spectrometer (so-called CLEAR spectrometer), the BL22-CLÆSS beamlines appears now fully operational according to its initial specifications. Standard EXAFS and XANES data collection were already routinely available for many years from S-Kedge up to Lanthanides K-edge. XAS measurements had recently speeded up reaching a limit of ~ 0.02 seconds per point, giving access to a high quality full EXAFS (XANES) spectrum within a total of 1.5-2 minutes (30-45 seconds). Here as well considerable development on sample environments have been continuously pursued³. XAS experiments can now be performed in solid state material within 10K-1000K temperature range. Specific solid-gas and liquid cells have been developed, whereas safety environment for experiments involving gases has been reinforced. The latest procurement of a multichannel Si-drift detector will ensure faster XAS data acquisition in fluorescence mode.

For both BL04-MSPD and BL22-CLÆSS beamlines, the actual available techniques and environments, as well as selected key experiments, will be presented.

¹Francois Fauth, Inma Peral, Catalin Popescu, Michael Knapp *The new Material Science Powder Diffraction beamline at ALBA Synchrotron Powder Diffraction* **2013** 28, pp S360-S370

²Francois Fauth, Roeland Boer, Fernando Gil-Ortiz, Catalin Popescu, Oriol Vallcorba, Inma Peral, Daniel Fulla, Jordi Benach, Jordi Juanhuix, *The crystallography stations at the ALBA synchrotron*, Eur. Phys. J. Plus **2015** 130: 160

³Laura Simonelli, Carlo Marini, Wojciech Olszewski, Marta Àvila, Nitya Ramanan, Gemma Guilera, Vera Cuartero, Konstantin Klementiev, *CLÆSS: The hard x-ray absorption beamline of the ALBA CELLS synchrotron Cogent Physics* **2016** 3, 1231987.

DISCHARGE PRODUCTS ON METAL/O₂ CATHODES MAPPED BY X-RAY TRANSMISSION MICROSCOPY AT THE O-K EDGE

Dino Tonti^a, Mara Olivares-Marín^{a,b}, Imanol Landa-Medrano^{a,c}, Alvaro Yamil Tesio^a, Andrea Sorrentino^d, Lorenzo Stievano^e, Rung-Chuan Lee^f, Eva Pereiro^d, Idoia Ruiz de Larramendi^e, Nae-Lih Wu^g, Teófilo Rojo^{c,g}

^a Institut de Ciència de Materials de Barcelona (ICMAB-CSIC), Campus UAB Bellaterra, Cerdanyola del Vallès (Spain); dino.t@csic.es

^b Dep. de Ingeniería Mecánica, Energética y de los Materiales, Universidad de Extremadura, Mérida (Spain)

^c Dep. Química Inorgánica, Fac. Ciencia y Tecnología, Univ. del País Vasco (UPV/EHU) Leioa-Bizkaia (Spain)

^d ALBA Synchrotron Light Source, MISTRAL Beamline, Cerdanyola d. Vallès, Barcelona (Spain)

^e Institut Charles Gerhardt Montpellier UMR CNRS 5253, Univ. Montpellier, 34095 Montpellier cedex 5; RS2E, FR CNRS 3459, 33 rue Saint Leu, 80039 Amiens (France)

^f Department of Chemical Engineering, National Taiwan University, Taipei 10617 (Taiwan)

^g CIC EnergiGUNE, Albert Einstein 48, 0150, Miñano (Spain)

The search for the next-generation batteries has recently focused on rechargeable aprotic metal-oxygen batteries, considered very attractive as room-temperature devices with high theoretical energy densities (5x compared to Li-ion) for application in electrical vehicles. Na and Li/O₂ batteries form solid peroxides and superoxides during the discharging process, which then –ideally– decompose into the metal ions and oxygen when charging. In practice, the discharged compounds partially react with the electrolyte forming solid products that are difficult to remove and hinder its decomposition. As a consequence, the electrode remains passivated and the battery capacity fades within a few cycles. The composition and distribution of the compounds on the electrode is a critical information to understand the discharge process and mitigate its irreversible behavior.

With this goal we used energy-dependent transmission soft X-ray microscopy (TXM), providing pixel-by-pixel absorption spectra with high spatial and energy resolution. By scanning energy at the oxygen K edge it is possible to discriminate and quantify different oxygen-containing chemical species, regardless of their crystalline state.¹

With Li/O₂ we unambiguously demonstrated the presence of significant amounts of superoxide forming a composite with peroxide,² and secondary products such as carbonates or hydroxide using ether- or ionic liquid-based electrolytes,³ respectively. Conversely, in the case of Na/O₂ cells we detected significant peroxide amounts accompanying the superoxide main product.⁴ The use of ether based electrolytes produces in both cells a carbonate-rich shell wrapping the discharged peroxide/superoxide composites.

Acknowledgements. The X-ray microscopy experiments were performed at MISTRAL beamline at ALBA Synchrotron with the collaboration of ALBA staff. Work funded by the Spanish Government, the Generalitat de Catalunya, Eusko Jauriaritza/Gobierno Vasco, Universidad del País Vasco, and FEDER fund.

¹ D. Tonti, M. Olivares-Marín, A. Sorrentino, and E. Pereiro, *Studies of Lithium-Oxygen Battery Electrodes by Energy-Dependent Full-Field Transmission Soft X-Ray Microscopy*, in “X-ray Characterization of Nanostructured Energy Materials by Synchrotron Radiation”, M. Khodaei and L. Petaccia (Eds.), InTech, 2017.

² M. Olivares-Marín, A. Sorrentino, R. C. Lee, E. Pereiro, N. L. Wu, and D. Tonti, *Nano Lett.* 15, 6932, 2015

³ M. Olivares-Marín, A. Sorrentino, E. Pereiro, and D. Tonti, *J. Power Sources*, accepted

⁴ I. Landa-Medrano, A. Sorrentino, L. Stievano, I. Ruiz de Larramendi, E. Pereiro, L. Lezama, T. Rojo and D. Tonti *Nano Energy* 37, 224, 2017

Electronic Structure Investigation of a Layered-Oxide Cathode Material by a Multi-technique Approach

L. Simonelli^a, A. Sorrentino^a, S. Passerini^{b,c}, M. Giorgetti^d, Angelo Mullaliu^d, A. Birrozzi^c, N. Laszczynski^c, W. Olszewski^{a,e}, C. Marini^a, N. Ramanan^a, D. Heinis^a, D. Tonti^f

^a CELLS - ALBA Synchrotron Radiation Facility,

Carrer de la Llum 2-26 08290 Cerdanyola del Valles, Barcelona, Spain

^b MEET Battery Research Centre, Institute of Physical Chemistry University of Muenster, Corrensstr. 46, 48149 Muenster (Germany)

^c Helmholtz Institute Ulm (HIU), Electrochemistry I Helmholtzstraße 11, 89081 Ulm, and Karlsruhe Institute of Technology (KIT) PO Box 3640, 76021 Karlsruhe (Germany)

^d Department of Industrial Chemistry "Toso Montanari" University of Bologna, Viale del Risorgimento 4, 40136 Bologna (Italy)

^e Faculty of Physics, University of Bialystok, 1L K. Ciolkowskiego Str., 15-245 Bialystok, Poland

^f Institut de Ciència de Materials de Barcelona, Consejo Superior de Investigaciones Científicas (ICMAB-CSIC), Campus UAB Bellaterra, Barcelona, Spain

We present an ex-situ X-ray absorption and emission spectroscopy investigation into the lithiation/delithiation mechanism of the lithium-rich and cobalt-poor, cathode material, $\text{Li}[\text{Li}_{0.2}\text{Ni}_{0.16}\text{Mn}_{0.56}\text{Co}_{0.08}]\text{O}_2$, as such and after V-coating^{1,2}. The main focus of this work is to fully understand the role of manganese in the electrochemical redox process, focusing on the evolution of its electronic properties as a function of cycling and coating. A multi technique approach has been used to disentangle the several degrees of freedom involved. Soft and hard X-ray absorption and emission experiments were performed at the MISTRAL³ and CLAESS⁴ beamlines on the same set of samples. The soft and hard X-ray absorption pre-peak depend on the highly correlated structural, electronic, and magnetic properties. Soft X-ray absorption spectroscopy at the O K-edge permit to investigate the 3d levels of transition metals through their hybridization with oxygen. Hard X-ray absorption spectroscopy at the Mn K-edge allows isolating the Mn contribution. Finally hard X-ray emission spectroscopy gives complementary information that allows building a self-consistent picture by accessing to the local magnetic moment on the Mn site. By combining all the complementary results we reveal the role of Mn on the charge/discharge cycles, and the V coating effect on it. Moreover the results indicate the not completely reversible $\text{Ni}^{2+}/\text{Ni}^{4+}$ redox process as a function of charging and its different evolution as a function of coating.

¹Daniel Buchholz, Jie Li, Stefano Passerini, Giuliana Aquilanti, Diandian Wang, and Marco Giorgetti, ChemElectroChem 2015, 2, 85 – 97

²Nina Laszczynski, Jan von Zamory, Julian Kalhoff, Nicholas Loeffler, Venkata Sai Kiran Chakravadhanula, and Stefano Passerini, ChemElectroChem 2015, 2, 1768-1773

³A. Sorrentino, J. Nicolas, R Valcarcel, F. J. Chichon, M. Rosanes, J. Avila, A. Tkachuk, J. Irwin, S. Ferrer and Eva Pereiro, J. Synchrotron Rad. 22, (2015) 1112.

⁴L. Simonelli, C. Marini, W. Olszewski, M. Avila Perez, N. Ramanan, G. Guilera, V. Cuartero, and K. Klementiev, Cogent Physics, (2016), 3: 1231987

ADVANCES IN TTS- μ XRD METHODOLOGY AND APPLICATIONS

O. Vallcorba^a, J. Rius^b

^a ALBA Synchrotron Light Source, carrer de la Llum 2-26, Cerdanyola del Vallès, Barcelona, Spain; ovallcorba@cells.es

^b Institut de Ciència de Materials de Barcelona, CSIC, Campus de la UAB, 08193 Bellaterra, Catalonia, Spain; jordi.rius@icmab.es

Synchrotron through-the-substrate microdiffraction (tts- μ XRD) allows the direct measurement of X-ray diffraction data of samples on substrates, e.g. polished thin sections on glass. With the help of a coaxial visualization system, specific areas of interest of the sample are selected and measured in transmission, so that the irradiated sample microvolume mainly depends on the beam size (Figure 1). Diffraction from the microvolume may come from multiple grains¹ (powder pattern), or from one or few grains² (single crystal pattern). In both cases, the extracted intensities can be used to solve the crystal structure. However, for the single crystal case, the restricted rotation interval of the sample limits the accessible reciprocal space volume, so that data completeness becomes an important issue.

To increase data completeness different experimental solutions have been studied.³ One is the reduction of the sample substrate thickness. In this way the signal to noise ratio is greatly improved thus enabling a wider rotation range during measurement. This procedure allowed the crystal structure refinement of the complex phosphate Chladniite [R-3, $a=15.0133(3)$, $c=42.887(2)$ Å] from a single microvolume⁴ (96.8% completeness up to 1.05Å resolution). Since substrate thickness reduction is not always possible, a second solution for improving completeness is to collect an additional dataset at the same target point but with χ rotated by 90° (Figure 1). For the triclinic case, this represents an increase of ~20% when compared to the single χ measurement. Finally, the application of the tts methodology to follow the unit cell parameters of a single-crystal in a diamond anvil cell under pressure will be also shown.

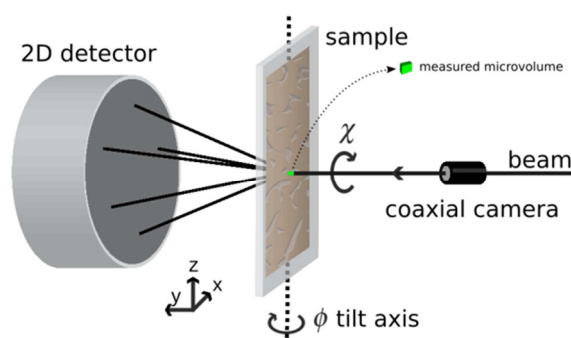


Figure 1. Experimental setup for tts- μ XRD. Diffraction data are collected by rotating the sample around the ϕ axis

Acknowledgements. The financial support from the Spanish ‘Ministerio de Economía, Industria y Competitividad’ (Project MAT2015-67593-P) and from the ALBA synchrotron (in-house project IH15-BL04) is gratefully acknowledged.

¹ J. Rius, A. Labrador, A. Crespi, C. Frontera, O. Vallcorba, J.C. Melgarejo, *Synchrotron Rad.* **2011**, *18*, 891-898.

² J. Rius, O. Vallcorba, C. Frontera, I. Peral, A. Crespi, C. Miravittles, *IUCrJ.* **2015**, *2*, 452-463.

³ J. Rius, O. Vallcorba, A. Crespi, F. Colombo, *Z. Kristallogr.* **2017**, accepted.

⁴ O. Vallcorba, Ll. Casas, F. Colombo, C. Frontera, J. Rius, *Eur. J. Mineral.* **2017**, *29*, 287-293.

AN IN-SITU NEAR AMBIENT PRESSURE PHOTOEMISSION ANALYSIS OF THE ELECTROCHEMICAL ACTIVATION OF A CATALYST SURFACE.

**J.P. Espinós,^a V.J. Rico,^a J. González-Cobos,^b J.R. Sánchez-Valencia,^a
V. Pérez-Dieste,^c C. Escudero,^c A. de Lucas-Consuegra,^d A.R. González-Elipe^a**

^aInstituto de Ciencia de Materiales de Sevilla, Universidad de Sevilla-CSIC. Avenida Americo Vespuccio 49, 41092. Sevilla, Spain. jpespinos@icmse.csic.es

^bInstitute of Chemical Research of Catalonia (ICIQ), Ave. Paisos Catalans 16, 43007 Tarragona, Spain.. jesus.gonzalez.cobos@gmail.com

^cALBA Synchrotron Light Source. Carres de la Llum, 2-26. 08290 Cerdanyola del Vallés, Barcelona, Spain. vperezdieste@cells.es

^dDepartamento de Ingeniería Química, Universidad de Castilla-La Mancha. Avenida Camilo José Cela 12, 13005 Ciudad Real, Spain. Antonio.LConsuegra@uclm.es

Electrochemical promotion of catalysis entails the enhancement of the catalytic activity of metal catalysts through their surface decoration by promoting atoms injected from a solid electrolyte^(1,2). In this work, we have used Near Ambient Pressure Photoemission to study in operando the surface composition of a K-doped Ni/ β -Al₂O₃ electrocatalyst, at 280°C and under different atmospheres (UHV, up to 1mbar H₂O, up to 1mbar HOCH₃) and electrochemical states (injected current, polarization voltage, open circuit, etc.). To this aim, Ni2p, Ni3p, O1s, K2p, C1s, K3p and Ni3d (VB) photoemission signals have been recorded in operando by excitation of the sample with photons of several energies (100 eV, 460 eV and 1170 eV).

We have shown that by galvanostatic and potentiostatic activation, potassium ions are reversibly reduced (oxydized) to metallic potassium at the Ni/Al₂O₃ interphase, from where they diffuse to the grain boundaries and outer surface of the nickel electrode. The evolution of the intensity of the K2p photoemission signal has been correlated with the current/voltage curves measured simultaneously, as a function of applied voltage, injected current and time.

Experiments carried out in vacuum or in the presence of water and methanol vapours show differences in the amount of potassium atoms at the surface and in their chemical state, that are attributed to electronic modifications induced by chemical interaction with adsorbed OH⁻ and CH₃O⁻ groups.

In addition, under methanol atmosphere, a thin film formed by carbon and metallic potassium is deposited on the surface of the nickel electrode. The kinetic of the growth of this film was study by following the intensity of Ni3p, C1s, K2p, K3p and Ni3d photoemission signals. Eventually, the thickness of this film rose in such an extent that the nickel electrode was fully buried. The binding energy and shape analysis of K2p and C1s signals and the K/C atomic ratio derived from them suggest that a KC₆-like compound is formed. The valence band structure and the work function of this film under methanol vapour have also been determined.

Acknowledgements. We thank the Junta de Andalucía (TEP8067, FQM-6900 and P12-FQM-2265), the Spanish Ministry of Economy and Competitiveness (Projects MAT2013-40852-R, 201560E055 and MAT2016-79866-R), the European Regional Development Funds program (EU-FEDER) and ALBA-CELLS for financial support.

¹ C.G. Vayenas, S. Bebelis, C. Pliangos, S. Brosda, Tsiplakides D. Electrochemical Activation of Catalysis: Promotion, Electrochemical Promotion and Metal-Support Interactions. New York: Kluwer Academic Publishers/Plenum Press; 2001.

² Lambert RM, Palermo A, Williams FJ, Tikhov MS. Electrochemical promotion of catalytic reactions using alkali ion conductors. Solid State Ionics. 2000;136-137:677-85

Spatial variation of the active phases during the catalytic oxidation of CO measured on a curved Pd(111) surface

F. Schiller^a, M. Ilyn^a, V. Pérez-Dieste^b, C. Escudero^b, C. Huck-Iriart^b, N. Ruiz del Arbol^c, B. Hagman^d, J. Gustafson^d, E. Lundgren^d, and J. E. Ortega^{a,e,f}

^a Centro de Física de Materiales CSIC, San Sebastian (Spain) (frederikmichael.schiller@ehu.es)

^b ALBA Synchrotron, Barcelona (Spain)

^c Instituto de Ciencia de Materiales CSIC, Madrid (Spain)

^d Department of Physics, Lund University (Sweden)

^e Departamento Física Aplicada I, Universidad del País Vasco, San Sebastian (Spain)

^f Donostia International Physics Centre DIPC, San Sebastian (Spain)

For decades, the study of chemical reactions on single metal surfaces has been aimed at identifying those active sites and crystal planes that feature nanoparticles.¹ However, nanocrystal facets coexist in a reduced space, and are expected to simultaneously undergo chemical and structural transformations during catalytic reactions.² At ALBA we explore chemical-structural interplays among crystal planes using curved crystals and near-ambient X-ray photoemission spectroscopy (XPS) experiments at CIRCE. As a test case for the approach, we used a curved Pd(111) surface, on which we freeze the CO oxidation reaction at the ignition temperature. By scanning the photon beam across the curved surface, we observe a smooth spatial variation of chemisorbed phases, demonstrating a different reaction stage at each crystallographic plane. As shown in the Figure, the XPS signal from chemisorbed CO reveals the linearly decreasing fraction of CO-poisoned areas, from the (111) direction up to a 10° critical angle, and at various temperatures around the onset of the reaction (light-off temperature). This behavior is explained as a collective structural response of the surface at the start of the reaction, consisting in the weighted segregation of less-active (111) phase and highly-active (223) and (332) facets in A-type and B-type vicinal planes, respectively.

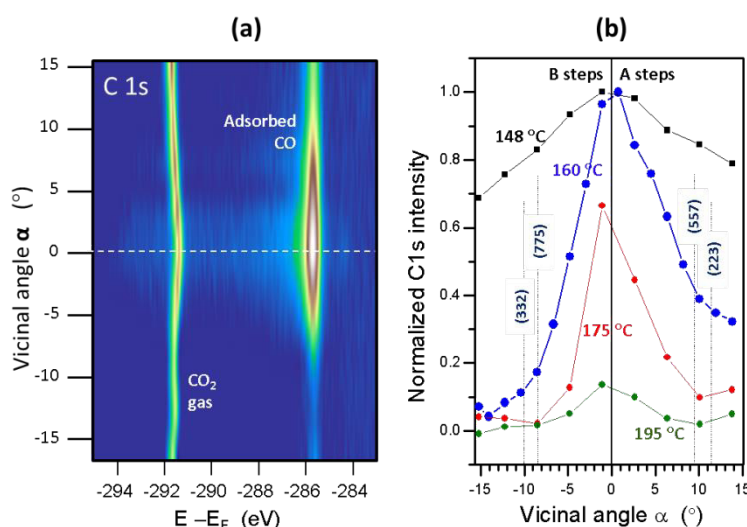


Figure: (a) C1s intensity (color scale) across a curved Pd(111) surface exposed to a 1 mbar CO, 1 mbar O₂ gas mixture at 160 °C, when cooling off the CO oxidation reaction. (b) Normalized C 1s intensity of the adsorbed CO peak of (a), at different temperatures around light-off, and across the curved surface. The linear drop from the (111) center toward 10° miscut planes suggests segregation of vicinal planes into active [(332) and (223) at A and B sides, respectively] and less-active (111) facets upon reaction light-off.

Acknowledgements. We acknowledge financial support from the Spanish Ministry of Economy (Grant MAT2013-46593-C6-4-P) and Basque Government (Grant IT621-13)

¹ Introduction to Surface Chemistry and Catalysis, edit. Somorjai, G.A. and Li, Y. John Wiley & Sons (2010).

² Vendelbo, S. B et al. Nat Mater 13, 884–890 (2014).

THE EFFECT OF OXIDIZING ATMOSPHERE ON CYSTINE/PYRITE(100) INTERACTION: PREBIOTIC CHEMISTRY IMPLICATIONS.

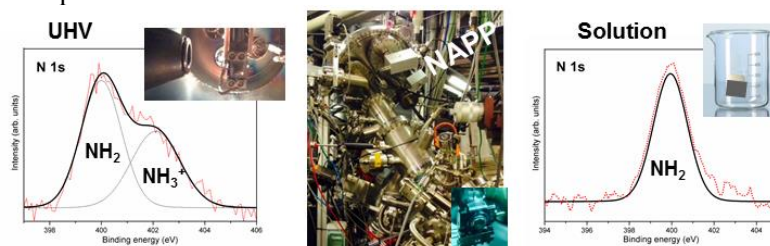
M. Sanchez-Arenillas^a, S. Galvez-Martinez^a, C. Escudero^b, V. Pérez-Dieste^b and E. Mateo-Marti^a

^a Centro de Astrobiología (CSIC-INTA), Torrejón de Ardoz, 28850 Madrid (Spain); mateome@cab.inta-csic.es.

^b ALBA Synchrotron Light Source, Carretera BP 1413 Km. 3.3, 08290 Cerdanyola del Vallès, Barcelona (Spain).

Prebiotic chemistry studies the formation of complex organic molecules from simpler organic and inorganic molecules through the chemical reactions in the Earth's early history¹. The identifications of the relevant types of environments and the organic molecules contributing to the origin of life remains an open question. Consideration of the contribution of solid surfaces is relevant for the study of the prebiotic Earth, Wächtershäuser² proposed that the first reactions that led to the formation of amino acids did occur on the surface of minerals (such as pyrite) because such surfaces have the potential to facilitate prebiotic polymerization. In fact, the role of mineral surfaces could be relevant to the origin of life, minerals may adsorb and concentrate these biomolecules, such as amino acids, and catalyse reactions, among them, the study of pyrite's physical properties and reactivity is crucial to the "iron-sulfur world"².

The aim of our studies is to get information about surface chemistry evolution of pyrite under well controlled oxidizing conditions³⁻⁴. Furthermore, to gather knowledge about how oxidizing environmental conditions affect molecular adsorption (cystine) and pyrite surface reactivity. APXPS studies have helped us to identify how pyrite surfaces and environmental conditions could favour the adsorption of specific amino acids chemical forms on mineral surfaces³⁻⁵ and to understand the influence of chemical and geophysical prebiotic conditions in the process. XPS analysis is employed to efficiently explore the molecular adsorption, to understand surface chemistry, and finally to describe critical influence of the presence of O₂ and CO₂ atmosphere in cystine-pyrite systems. We report the first oxidation studies of cystine/pyrite(100) system by APXPS (at ALBA), successful oxidation in-situ of the pyrite surface under well-controlled oxygen pressure atmospheres and then effective adsorption of the amino acid, in the anionic form, on this oxidised surface. A novel comparative analysis revealed remarkable differences with respect to molecular adsorption and surface chemistry induced under different gas atmospheres. Therefore, the system explored in this study holds interesting implications for supporting catalysed prebiotic chemistry reactions and the promising results confirm APXPS as innovative technique for these studies.



Acknowledgements. The APXPS experiments were performed at CIRCE beamline at ALBA Synchrotron Light Facility with the collaboration of ALBA staff. We acknowledge funding through Spanish research project ESP2014-55811 and M.S.A PhD grant BES-2011-044395.

¹ Miller, S.L. and Orgel, L.E. The origins of life on the earth, Prentice-Hall, 1974.

² Wächtershäuser, G. *Systematic and Applied Microbiology* **1988**, *10*, 207-210.

³ M. Sanchez-Arenillas, E. Mateo-Marti, *Chemical Physics*. **2015**, *458*, 92-98.

⁴ M. Sanchez-Arenillas, E. Mateo-Marti, *Phys.Chem.Chem.Phys.* **2016**, *18*, 27219-27225.

⁵ M. Sanchez-Arenillas, S. Galv ez-Martinez, E. Mateo-Marti, *Applied Surface Science* **2017**, *414*, 303-312.

Update and Recent Developments at the Circe and Boreas Beamlines

P. Gargiani^a, J. Herrero-Martin^a, H. B. Vasili^a,
S. M. Valvidares^a, M. Foerster^a, C. Escudero^a, A. Mandziak^b, D. Ruano^c, V. Pérez-Dieste^a, L. Aballe^a, and E. Pellegrin^a

^a ALBA Synchrotron Light Source, E-08290 Cerdanyola del Vallès (Spain); pgargiani@cells.es; jherrero@cells.es; hvasili@cells.es; mvalvidares@cells.es; mfoerster@cells.es; cescudero@cells.es; vperez@cells.es; laballe@cells.es; epellegrin@cells.es

^b Instituto de Química Física Rocasolano, CSIC, E-28006 Madrid (Spain); ania_mandziak@o2.pl

^c Instituto de Tecnología Química, CSIC, E-46022 Valencia (Spain); daruassan@itq.upv.es

In this contribution, we will give a concise overview on the recent technological and scientific highlights at the Boreas and the Circe soft x-ray beamlines of the ALBA synchrotron light source facility.

Regarding the Boreas beamline, results from the commissioning of the MARES end station will be presented, together with an updated technical description of the new capabilities for surface science preparation using a recently installed “satellite” surface science preparation chamber and an STM-AFM system (presently under installation). For the Circe PEEM end station, technical upgrades encompass, e.g., a gating electrode for time-resolved experiments and a new imaging technique based on the propagating surface acoustic waves (SAW). Scientific highlights include the observation of skyrmions in Pt/Co/MgO nanostructures. Last but not least, the recent implementation of a safe CO gas supply system at the Circe NAPP end station analysis chamber has made *in situ* XPS studies of, e.g., CO oxidation or Fischer-Tropsch processes possible.

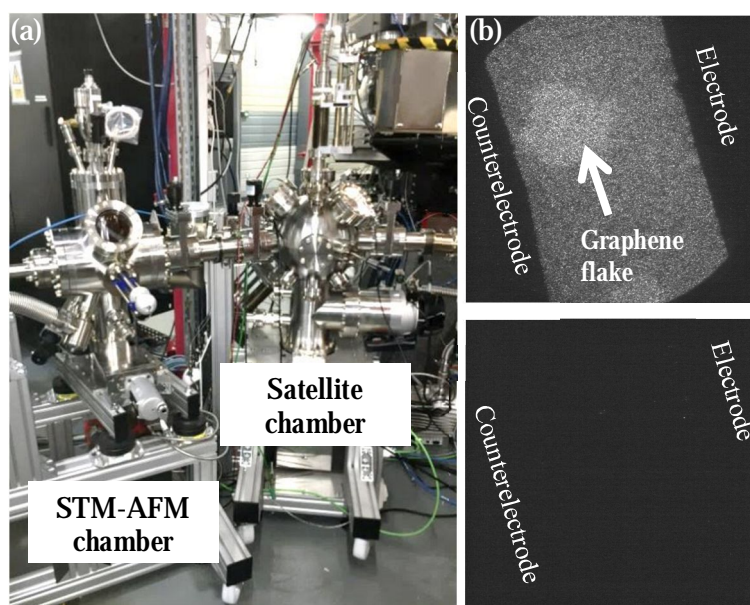


Fig 1: (a) Recently installed STM and surface preparation satellite chambers at Boreas (b) Effect of the PEEM gating electrode: “Off” mode (top) and “On” mode (bottom).

Magnetism catches the wave: Direct imaging of strain induced, sub-nanosecond magnetization dynamics

Michael Foerster^a, Ferran Macià^b, Joan Manel Hernández^c, Simone Finizio^{d,e}, Alberto Hernández-Mínguez^f, Nahuel Statuto^c, Sergi Lendínez^c, Paulo Santos^f, Josep Fontcuberta^b, Mathias Kläui^c, Lucia Aballe^a

^a ALBA Synchrotron Light Facility, 08290 Cerdanyola del Valles, Spain; mfoerster@cells.es

^b Institut de Ciència de Materials de Barcelona (ICMAB-CSIC), Campus UAB, 08193 Bellaterra, Spain

^c UBXLab, University of Barcelona, 08028 Barcelona, Spain

^d Swiss Light Source, Paul Scherrer Institut, CH-5232 Villigen PSI, Switzerland

^e Institute of Physics, Johannes Gutenberg-University Mainz, 55128 Mainz, Germany

^f Paul-Drude-Institut für Festkörperelektronik, Hausvogteiplatz 5-7, 10117 Berlin, Germany

The magnetoelastic effect or inverse magnetostriction (i.e. the change of magnetic properties by elastic deformation or strain) is a key mechanism in multiferroic coupling in heterostructures and nanocomposites. It has lately attracted considerable interest as a possible approach to control magnetization with electric fields (instead of currents) in future devices with low power consumption. However, so far most experiments addressing the magnetoelastic effect are either performed at slow speeds or lacking spatial resolution.

In this work, the dynamic magnetoelastic effect is measured for Ni microstructures under a time dependent elastic deformation produced by a surface acoustic wave (SAW) in a piezoelectric LiNbO₃ substrate. By synchronizing the SAW frequency with the repetition rate of the synchrotron x-ray light pulses (500 MHz in multibunch mode) which illuminate the sample in the photoemission electron microscope (PEEM), the magnetic domain configuration can be followed using X-ray magnetic circular dichroism contrast (XMCD) with a resolution of around 80 ps in time and 60 nm spatially.

Notably, different phase delays of the magnetic response with respect to the SAW piezoelectric strain are found: approx. 100 ps for coherent magnetization rotation and 300 ps for domain wall motion. These delays are mainly due to the intrinsic magnetization dynamics, and highlight the need for properly designing the magnetic system in order make use of the magnetoelastic effect on a fast time scale.

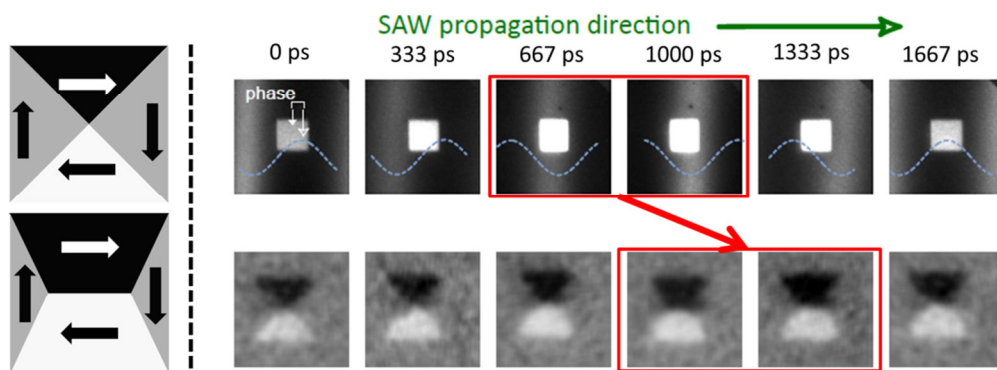


Figure 1. *left:* schematics of magnetic domains in a Nickel square without (top) or with (bottom) net anisotropy, forming a flux closure state (arrows indicate the magnetization directions and the gray color corresponds to the contrast in XMCD-PEEM). *right:* series of direct images (top) and XMCD magnetic images (bottom) taken with different relative positions of the strain wave (top, diffuse bright line) and the Ni square. The maximum deformation of the domains occurs around 300 ps after the wave has passed the squares (corresponding images highlighted by the red frames).

Combining vector XMCD-PEEM and micromagnetic simulations

J. de la Figuera¹, S. Ruiz-Gomez^{2,3}, L. Pérez^{2,3}, A. Mascaraque^{2,3}, A. Quesada⁴, A. Mandziak^{1,5}, C. Munuera⁷, L. Martín-García¹, P. Prieto⁶, I. Palacio⁷, M. Foerster⁵ and L. Aballe⁵

^a*Instituto de Química Física “Rocasolano”, E28006 Madrid (Spain);*

juan.delafiguera@iqfr.csic.es

^b*Dpto. de Física de Materiales, Universidad Complutense de Madrid, E28040 Madrid (Spain)*

^c*Unidad Asociada UMC-IQFR(CSIC), E28006 Madrid (Spain)*

^d*Instituto de Cerámica y Vidrio (CSIC), E28049 Madrid (Spain)*

^e*Alba Synchrotron Light Facility, CELLS, E08290 Barcelona (Spain)*

^f*Dpto. de Física Aplicada, Universidad Autónoma de Madrid, E28049 Madrid (Spain)*

^g*Instituto de Ciencia de Materiales de Madrid, CSIC, E28049 Madrid (Spain)*

X-ray magnetic circular dichroism (XMCD) in a photoemission microscope (PEEM) allows to acquire nanometer resolution maps of the magnetization from a surface or thin film. The full vector magnetization can be determined combining measurements at different azimuthal angles. It is possible then to use the experimental information as the initial configuration for micromagnetic simulations (MuMax3¹). Comparison between the experimental magnetization map and the calculated relaxed configuration is a useful source of information about the nanostructure under observation. Differences between both can point for example to deviations from bulk magnetic properties or to surface and interface effects. Even more details can be understood if the full atomic level topography of the structure is available, as can be obtained by combining XPEEM with ex-situ atomic and magnetic force microscopy (AFM/MFM) observations of the same nanostructures.

We will describe this approach and show its application to ferrite spinels grown in-situ in the PEEM. Ferrite spinels such as magnetite and cobalt ferrite have been proposed for spintronic devices such as spin valves. Despite their expected advantages, real nanostructures have disappointing properties, rather different from the properties of bulk spinels. The most likely explanation for these effects are growth defects, among which antiphase domain boundaries (APBs) are very common. In our case, flat single-crystal magnetite² and other mixed spinels³ are grown on Ru(0001) by oxygen-assisted molecular beam epitaxy at high temperature. The micro-crystals are virtually APB-free, since each one grows from a single nucleus, a fact that is reflected in their outstanding magnetic properties.

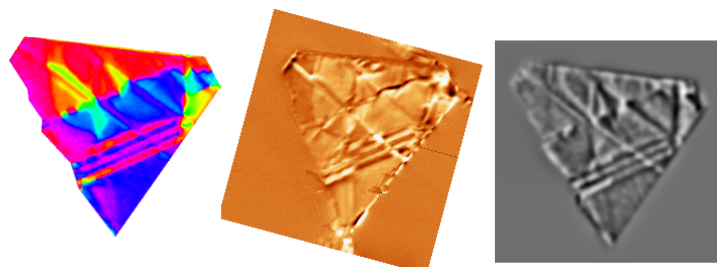


Figure 1. Left: magnetization pattern obtained in XMCD-PEEM for a cobalt ferrite island, Center: MFM image of the same island, Right: simulated MFM image using the XMCD-PEEM information as input

1 A. Vansteenkiste *et al.*, AIP Adv. **2014**, 4, 107133.

2 M. Monti *et al.* Phys. Rev. B. **2012**, 85, 020404.

3 L. Martín-García *et al.* Adv. Mat. **2015**, 27, 5955.

Magnetic anisotropy of 3d individual atoms on a surface with strong Rashba spin-orbit interaction

M. A. Valbuena^a, S. Schirone^a, R. Robles^a, S. Godey^a, A. Barla^b, C. Nistor^c, L. Persichetti^c, P. Gargiani^d, P. Gambardella^c and A. Mugarza^{a,e}.

^a Catalan Institute of Nanoscience and Nanotechnology (ICN2), CSIC and The Barcelona Institute of Science and Technology, Campus UAB, Bellaterra, 08193 Barcelona, Spain.; miguel.valbuena@icn2.cat

^b Istituto di Struttura della Materia (ISM), CNR, I-34149 Trieste, Italy.

^c Department of Materials, ETH Zurich, Hönggerberggring 64, CH-8093 Zurich, Switzerland.

^d ALBA Synchrotron Light Source, Carretera BP 1413 km 3.3, E-08290 Cerdanyola del Vallès, Spain..

^e ICREA, Institució Catalana de Recerca i Estudis Avançats, Lluís Companys 23, 08010 Barcelona, Spain.

The study of atomic-scale magnetic structures adsorbed on a non-magnetic substrate is a topic of fundamental interest with potential to realize single-atom magnets with long magnetic relaxation lifetimes^{1,2}. The Magnetic Anisotropy Energy (MAE) is a key parameter toward the ultimate limit of future data-storage memories based on single-atoms. Strategies to enhance the MAE require large orbital magnetic moments and strong spin orbit coupling (SOC). In this work we present a systematic experimental and theoretical investigation on the magnetic properties of the 3d transition metals single atoms deposited on the substitutional BiAg₂ alloy grown on Ag(111). The magnetic moments and the MAE have been investigated by combining X-ray Circular Magnetic Dichroism (XMCD) with density functional theory (DFT) calculations., and the theoretically predicted adsorption configuration confirmed by low temperature scanning tunneling microscopy (STM). The orbital to spin momentum ratios for all the studied elements (Co, Fe, Mn and V) are among the highest for 3d transition metal adatoms deposited on metallic substrates. Comparative studies on the bare Ag(111) and the isostructural and isoelectronic SbAg₂ surfaces, both with negligible SOC, indicate that the combination of the reduced adsorption symmetry and large SOC on BiAg₂ give rise to a significant enhancement of the MAE and determines its orientation.

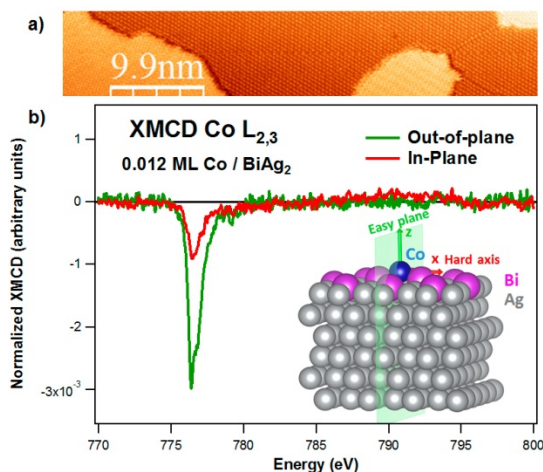


Figure 1. a) Atomically resolved STM image of BiAg₂ characterized before XMCD measurements. STM was connected to Boreas/Alba end-station. b) XMCD angular dependence of Co adatoms on BiAg₂

¹ Donati, F. *et al.* *Magnetic remanence in single atoms.* *Science.* **352**, 318–321 (2016).

² Rau, I. G. *et al.* *Reaching the magnetic anisotropy limit of a 3d metal atom.* *Science.* **344**, 988–992 (2014).

IDENTIFICATION OF A CUBIC RUTHENIUM CARBIDE NANO-CRYSTALLINE PHASE IN THE SYNTHESIS OF GRAPHENE ON RUTHENIUM ULTRATHIN FILMS

J. Bartolomé^a, F. Jiménez-Villacorta^a, L. Álvarez-Fraga^a, E. Climent-Pascual^{a,b}, E. Salas-Colera^{a,c}, M. X. Aguilar-Pujol^a, R. Ramírez-Jiménez^d, A. Cremades^e, C. Prieto^a and A. de Andrés^a

^a Instituto de Ciencia de Materiales de Madrid, CSIC, Cantoblanco 28049 Madrid, (Spain);

^b Escuela Técnica Superior de Ingeniería Industrial, Universidad Politécnica de Madrid, C/ José Gutiérrez Abascal 2, 28006 Madrid, (Spain);

^c Spanish CRG beamline at the ESRF, 71 Avenue des Martyrs, 38000 Grenoble, France;

^d Departamento de Física, Escuela Politécnica Superior, Universidad Carlos III de Madrid, Avenida Universidad 30, Leganés, 28911 Madrid, Spain;

^e Departamento de Física de Materiales, Universidad Complutense de Madrid, 28040 Madrid, Spain

Ruthenium is an adequate substrate for the synthesis of high quality graphene with large single crystal domains.¹ However, the mechanisms involved in the CVD growth of graphene on ruthenium are not well understood. In particular, the role of carbon incorporation into the Ru lattice during graphene growth is still unclear. The complex equilibrium between the different carbon sources, which comprise both adsorbed and dissolved C atoms as well as graphene itself, has been suggested to be a key factor in the growth of graphene on Ru (0001) crystals.² Nevertheless the formation of intermediate compounds such as ruthenium carbides and their influence in the growth process of graphene have not been considered so far. These carbides have been predicted to present outstanding mechanical properties of interest for protective coating applications³ and, similar to other transition metal carbides, high catalytic activities.

In this work we report on the identification of a novel RuC cubic phase obtained during CVD growth of graphene on nanostructured Ru ultrathin films (down to nominally 5 nm). The increased surface to volume ratio of the films facilitates the study of the graphene/Ru interface with particular attention to the incorporation of carbon atoms into the Ru lattice. Our results show that, while multilayer graphene films (MLG) are obtained at a growth temperature of 910 °C, single layer defective graphene is formed at 1000 °C. Synchrotron X-ray diffraction and X-ray absorption spectroscopy reveal the formation, further confirmed by electron backscattering diffraction, of a novel cubic RuC phase at or above 1000 °C, in opposition to the incorporation of interstitial carbon expected for the lower growth temperature. The obtained RuC:Ru volume ratio is found to depend on both the growth temperature and the Ru film thickness and texture, with a preferential transformation of Ru grains with a crystal orientation different to (0001). It is suggested that the formation of the carbide phase favors the synthesis of single layer graphene by hindering the segregation of C to the surface during cooling. This method allows obtaining nano-crystalline RuC and MLG covered Ru nanograins, which are expected to present interesting mechanical, catalytic and sensing properties.

Acknowledgements. We acknowledge funding from MINECO (MAT2015-65356-C3-1-R and provision of synchrotron facilities) and Comunidad de Madrid (S2013/MIT-2740). L.A.F. acknowledges a FPI grant (BES-2013-062759) from MINECO.

¹ P. W. Sutter, J.-I. Flege, E. A. Sutter, *Nat. Mater.* **2008**, *7*, 406–411.

² K. F. McCarty, P. J. Feibelman, E. Loginova, N. C. Bartelt, *Carbon* **2009**, *47*, 1806–1813.

³ Z. Zhao, M. Wang, L. Cui, J. He, D. Yu, Y. Tian, *J. Phys. Chem. C* **2010**, *114*, 9961–9964.

GRAPHENE-BASED SYNTHETIC ANTI-FERROMAGNETS AND FERRIMAGNETS WITH PERPENDICULAR MAGNETIC ANISOTROPY

P. Gargiani^a, R. Cuadrado^b, H.B. Vasili^a, M. Pruneda^b and M. Valvidares^a

^a ALBA Synchrotron Light Facility, Cerdanyola del Valles, 08290, Barcelona, Spain

^b ICN2 CSIC, Campus UAB, Bellaterra, 08193 Barcelona, Spain

Graphene-spaced magnetic systems provide the opportunity to combine the unique electronic and mechanical properties of graphene with ferromagnetic layers for the development of graphene-based spintronic applications.¹ The epitaxial growth of graphene together with the intercalation of magnetic-material layers,² allow the realization of layered graphene-spaced magnetic heterostructures with well-defined interfaces and with tunable magnetic properties depending on thickness, growth conditions and chosen substrates.³

Here we report on the realization of graphene-based synthetic antiferromagnets (SAF) and ferrimagnets (SFIM) layered systems of Fe/graphene/Co with strong perpendicular magnetic anisotropy, robust antiferromagnetic coupling above room temperature and tunable magnetic properties depending on layer thicknesses that may be suitable for future applications.⁴ Element-resolved soft X-ray absorption (XAS) and magnetic circular dichroism (XMCD) measurements indicate that sample growth can be engineered to realize fully compensated SAF or SFiM. Atomistic first-principle DFT calculations indicate that graphene mediated super-exchange type coupling is responsible for the observed strong perpendicular antiferromagnetic coupling. The experimental and theoretical results can booster the realization of novel graphene-based magnetic devices and spark the investigation on similar systems constituted by layered ferromagnetic films separated by 2D materials.

Acknowledgements. This work has been funded by Spanish MINECO/FEDER, grants no. FIS2013-45469-C4-3-R, FIS2015-64886-C5-3-P, Generalitat de Catalunya (2014SGR301), and EU Centre of Excellence MaX - Materials Design at the Exascale (H2020 Grant no. 676598) and ALBA IHR program.

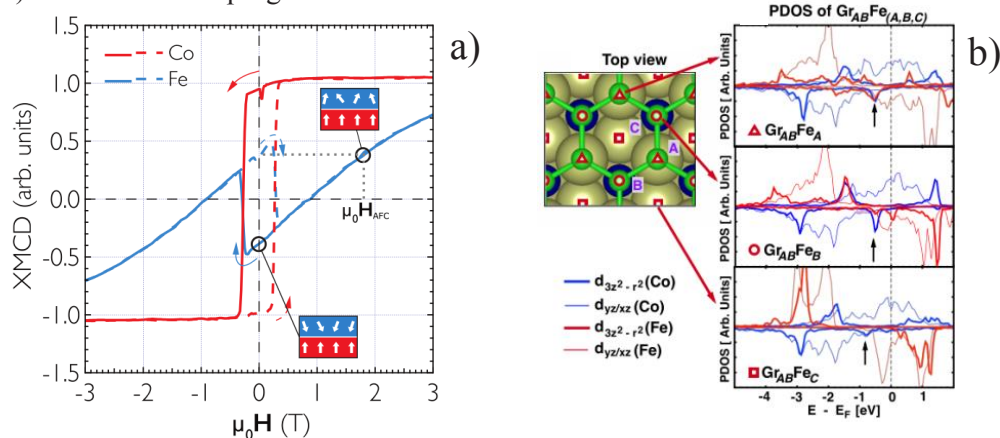


Figure 1: element specific hysteresis loop of Fe/Gr/Co/Ir(111) system; b) DFT projected DOS for Fe and Co and corresponding adsorption sites

¹ Roche, S. et al. Graphene spintronics: the European Flagship perspective. 2D Mater. 2, 30202 (2015).

² Coraux, J. et al. Air-Protected Epitaxial Graphene/Ferromagnet Hybrids Prepared by Chemical Vapor Deposition and Intercalation. J. Phys. Chem. Lett. 3, 2059–2063 (2012).

³ Yang, H. et al. Anatomy and Giant Enhancement of the Perpendicular Magnetic Anisotropy of Cobalt-Graphene Heterostructures. Nano Lett. 16, 145–151 (2016).

⁴ Gargiani, P., Cuadrado, R., Vasili, H. B., Pruneda, M. & Valvidares, M. Graphene-based synthetic antiferromagnets and ferrimagnets. arXiv:1609.07634 (2016).

Electronically highly cubic conditions for Ru in α -RuCl₃

S. Agrestini^a, C. Y. Kuo^a, K.-T. Ko^a, Z. Hu^a, D. Kasinathan^a, H. Babu Vasili^b, J. Herrero-Martin^b, S. M. Valvidares^b, E. Pellegrin^b, L.-Y. Jang^c, A. Henschel^a, M. Schmidt^a, A. Tanaka^d, and L. H. Tjeng^a

^a Max Planck Institute for Chemical Physics of Solids, Noethnitzerstr. 40, 01187 Dresden (Germany); stefano.agrestini@mpi.cpfs.de

^b ALBA Synchrotron Light Source, E-08290 Cerdanyola del Vallès, Barcelona (Spain);

^c National Synchrotron Radiation Research Center, 101 Hsin-Ann Road, Hsinchu 30076 (Taiwan);

^d Department of Quantum Matter, ADSM, Hiroshima University, Higashi-Hiroshima 739-8530 (Japan);

We studied the local Ru 4d electronic structure of α -RuCl₃ by means of polarization dependent x-ray absorption spectroscopy at the Ru-L_{2,3} edges. We observed a vanishingly small linear dichroism indicating that electronically the Ru 4d local symmetry is highly cubic. Using full multiplet cluster calculations we were able to reproduce the spectra excellently and to extract that the trigonal splitting of the t_{2g} orbitals is -12 ± 10 meV, i.e. negligible as compared to the Ru 4d spin-orbit coupling constant. Consistent with our magnetic circular dichroism measurements, we found that the ratio of the orbital and spin moments is 2.0, the value expected for a $J_{\text{eff}} = 1/2$ ground state¹. We thus show² that, as far as the Ru 4d local properties are concerned, α -RuCl₃ is an ideal candidate for the realization of Kitaev physics³.

Acknowledgements. We would like to thank the NSRRC and ALBA for providing us with beam time and for the support from the staff during the experiments. The research in Dresden was partially supported by the Deutsche Forschungsgemeinschaft through SFB 1143 and FOR1346. K.-T. Ko acknowledges support from the Max Planck-POSTECH Center for Complex Phase Materials (No. KR2011-0031558).

¹ B. J. Kim, H. Jin, S. J. Moon, J. Y. Kim, B. G. Park, C. S. Leem, J. Yu, T. W. Noh, C. Kim, S. J. Oh, J. H. Park, V. Durairaj, G. Cao, and E. Rotenberg, *Phys. Rev. Lett.* **2008**, *101*, 076402.

² S. Agrestini, C. Y. Kuo, K.-T. Ko, Z. Hu, D. Kasinathan, H. Babu Vasili, J. Herrero-Martin, S. M. Valvidares, E. Pellegrin, L.-Y. Jang, A. Henschel, M. Schmidt, A. Tanaka, and L. H. Tjeng, *preprint arXiv:1705.04550*.

³ G. Jackeli, and G. Khaliullin, *Phys. Rev. Lett.* **2009**, *102*, 017205.

Oral Contributions

Wednesday 11th October 16:30 - 17:00

Possibilities for collaboration with ALBA synchrotron

Miguel A. G. Aranda

ALBA Synchrotron, Carrer de la Llum 2-26, 08290, Cerdanyola del Vallès, Barcelona, Spain
migarcia@cells.es

The Experiments Division is one of the five divisions of ALBA and it is charged with the operation of the beamlines as well as complete interaction with our academic users. The structure of the division is shown in the attached figure and it is composed of three sections running the operating beamlines and another three support sections. Of course, ALBA is open to academic users based on the submission of proposals through our user office (<https://useroffice.cells.es/>). The academic proposals are evaluated by an international panel (Beamtime Review Panel) based on scientific excellence. The best proposals get beamtime and the Spanish teams get also funding for their travel expenses. I will not mention in this talk this approach neither the proprietary beamtime access and/or usage of our laboratories as this is covered by our industrial liaison office (<https://www.cells.es/en/industry/services>).

In addition to the usage of ALBA resources, beamtime and equipments, through the call for proposals for beamtime, there are other ways to scientifically collaborate with ALBA. In the talk, I will highlight the three most common ways for framing possible collaborations, enumerated just below, and I will also mention other ways to interact with ALBA synchrotron.

1. ALBA has a Ph.D. program where we co-fund half of the expenses after establishing the appropriate agreement(s). Normally, the selected applicant will be two years in the collaborating organization and another two years at ALBA.
2. We apply for MINECO (and another) research grants. In most cases, the applications are based on 'coordinated projects' where common interests allows the joint research grants.
3. ALBA has a program of 'continuous collaborators' that allows interested researchers to carry out a research stay up to 3 years.

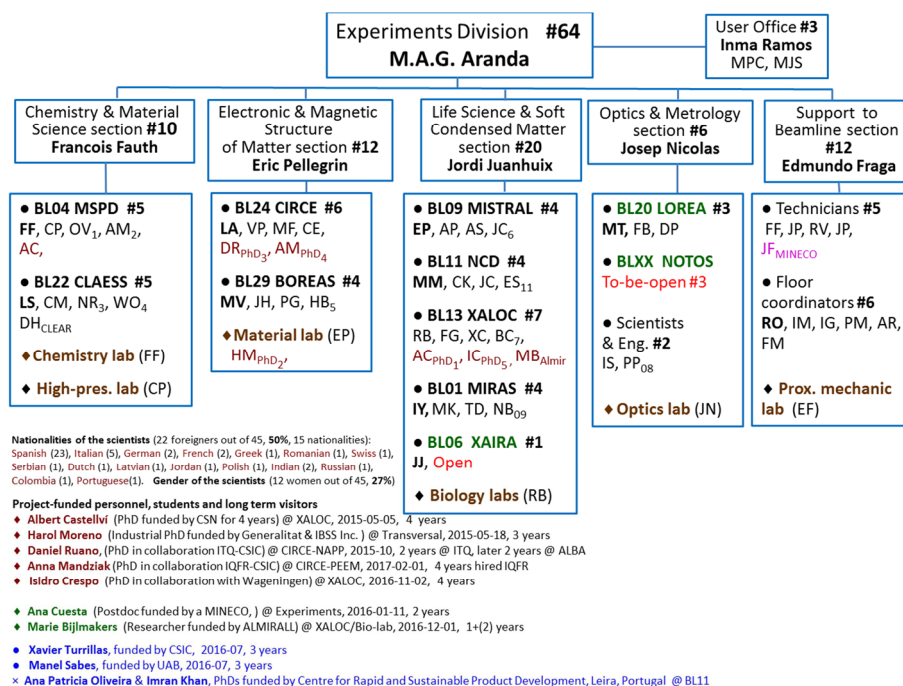


Figure 1. Structure of the Experiments Division of ALBA synchrotron as June-2017

CRYSTALLOGRAPHIC STUDIES ON PROTEIN MISFOLDING: THE c-SRC SH3 DOMAIN AS MODEL PROTEIN

A. Camara-Artigas^a, M. Plaza-Garrido^a and M^a C. Salinas-Garcia^a

^a Department of Chemistry and Physics. University of Almería, Agrifood Campus of International Excellence (ceiA3), Research Centre for Mediterranean Intensive Agriculture and Food Biotechnology (CIAMBITAL), Carretera de Sacramento s/n, Almería, 04120, Spain; acamara@ual.es

In the next few years, due to the increase in life expectancy, it is forecast that neurodegenerative diseases as Alzheimer's will be one major health issue. This disease belongs to the group of those caused by protein misfolding associated with the development of amyloid aggregates. It has not been yet elucidated the molecular determinants that result, at a given time, in changes in the folding of a specific protein. High-resolution structural information is necessary to rationalize the molecular features that produce the outbreak of these diseases. This will facilitate the study of the interactions responsible for both, the initiation of the process and its stabilization. For a long time, 3D domain-swapping (3D-DS), a special protein oligomerization process related to protein misfolding, has been related with the formation of amyloids. Unlike the amyloid, 3D-DS oligomers can crystallize and its structure can be solved by X-ray diffraction. Therefore, we propose the study of the first steps of the protein misfolding through a small modular domain that complies all the features to be used as a model for this purpose: the c-Src tyrosine kinase SH3 domain.¹ Our group has recently determined that this domain has both types of protein misfolding: 3D-DS and the formation of amyloid fibers. Besides, both processes are dependent on pH and the residues present in the folding nucleation site. Our purpose is to examine whether the determinants of the protein misfolding of these 3D-DS oligomers reside in the hinge-loop or it is related to residues in the folding nucleation site, or both. We have constructed several chimeric proteins based on this SH3 domain, where the characteristic β -turns of the protein at the RT- and n-Src-loops have been replaced for those present in the Fyn and c-Abl-SH3 domain. Preliminary results with a chimera Src-Abl SH3 domain, where both β -turns have been replaced for those in the c-Abl SH3 domain resulted in a dimer with two hinge loops opened at the same time.² To date, according to our knowledge, it is the first time that a double swapping has been reported for an intertwined dimer. Our previous results also showed that those factors that appear to affect the formation of amyloid fibers also affect to 3D-DS. As an example, the formation of salt bridges and π - π interactions between aromatic residues. Besides, we have also reported a dependency with the pH in the formation of these oligomers, which can be attributed to the protonation of specific residues. Here we present our preliminary results with these chimeric proteins.

Acknowledgements. This research was funded by the Spanish Ministry of Economy and Competitiveness (Spain) and FEDER (EU) [BIO2016-78020-R].

¹ Camara-Artigas, A., 2016. *Crystallographic studies on protein misfolding: Domain swapping and amyloid formation in the SH3 domain*. Archives of Biochemistry and Biophysics 602, 116-126.

² Camara-Artigas, A., Martínez-Rodríguez, S., Ortiz-Salmeron, E., Martín-García, J.M., 2014. *3D domain swapping in a chimeric c-Src SH3 domain takes place through two hinge loops*. Journal of Structural Biology 186, 195-203.

Li₃[Al(C₂O₄)₃] AND ITS HYDRATES: CRYSTAL STRUCTURE AND TRANSFORMATIONS

A. Missiul^a, M. Chislov^b

^a ALBA Synchrotron Light Source, Carrer de la Llum 2-26, 08290, Cerdanyola del Vallès, Barcelona, Spain; amissiul@cells.es

^b Saint Petersburg State University, 7/9 Universitetskaya emb., 199034, St. Petersburg, Russia; mikhail.chislov@spbu.ru

The double oxalates M^I[M^{III}(C₂O₄)₃] attract constant interest during last decades both due to their intrinsic physical and chemical properties and as precursors for the synthesis of the complex metal oxides. These salts are usually obtained in form of crystallohydrates with 0-6 water molecules per formula unit. The decomposition pathway of these hydrates is of special interest due to its multistage and often irreversible nature. Among possible compositions belonging to this group Li₃[Al(C₂O₄)₃] was never described before.

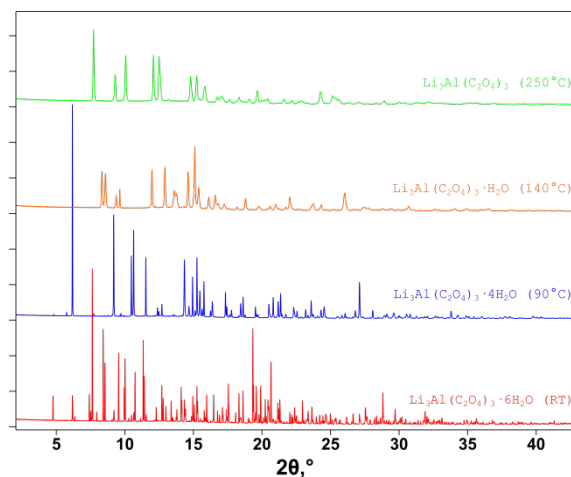


Figure 1. Diffraction patterns of the Li[Al(C₂O₄)₃]*xH₂O phases

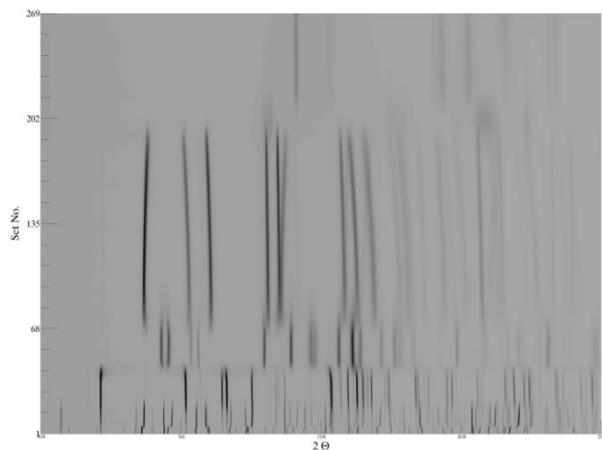


Figure 2. In situ diffraction investigation of Li₃[Al(C₂O₄)₃]·6H₂O decomposition.

The current work summarizes the results of the investigation of the crystal structure and stability of the different Li₃[Al(C₂O₄)₃] hydrates. The powder diffraction data were collected at the MSPD beamline of the ALBA synchrotron light source. The structure transformations were investigated using *in situ* powder diffraction and thermal analysis.

The freshly precipitated phase appeared to have a composition Li₃[Al(C₂O₄)₃]·6H₂O while the most stable one at the ambient conditions is Li₃[Al(C₂O₄)₃]·4H₂O. Heating of this phase leads to the sequential formation of Li₃[Al(C₂O₄)₃]·H₂O and anhydrous Li₃[Al(C₂O₄)₃]. All phases share the common building block consisting of the AlO₆ and LiO₆ octahedra bridged by the C₂O₄²⁻ anion. However, the formation of Li₃[Al(C₂O₄)₃]·H₂O includes the reorientation of these blocks. This reorientation results in the change of the space group from Pbcn to Pnna and is accompanied by the strong decrease of crystallinity.

The multistage decomposition of Li₃[Al(C₂O₄)₃] begins above 350°C and includes sequential formation of Li₂C₂O₄, Li₂CO₃ and, finally, γ-LiAlO₂. This provides a way to prepare highly reactive precursors of the aluminates which usually require extremely high temperatures for the solid state synthesis.

DETECTOR SYSTEMS FOR ADVANCED X-RAY STUDIES

A. Förster on behalf of the DECTRIS team

DECTRIS Ltd., Täferweg 1, 5405 Baden-Dättwil (Switzerland); andreas.foerster@dectris.com

Hybrid Photon Counting (HPC) X-ray detectors^{1,2} have transformed synchrotron research in the last decade by enabling noise-free detection and novel data acquisition modes. Two new HPC detector families promise to make even more ambitious science possible. First, PILATUS3 X CdTe detectors combine the advantages of HPC technology with the superior quantum efficiency of cadmium telluride (CdTe) at energies from about 10 keV to above 80 keV (ref. 3). All other detector properties are identical to those of the successful PILATUS3 X series, e.g. a pixel size of $172\ \mu\text{m} \times 172\ \mu\text{m}$ and frame rates of up to 500 Hz. Second, EIGER detectors⁴ offer smaller pixels of $75\ \mu\text{m} \times 75\ \mu\text{m}$, a frame rate of up to 9 kHz, and continuous read-out with 3 μs dead time between exposures.

The superior performance of EIGER in coherent diffraction applications, macromolecular crystallography and X-ray photon correlation spectroscopy will be demonstrated. Moreover, results from different synchrotron experiments highlight characteristics and capabilities of both EIGER and PILATUS3 CdTe detector systems: high count-rate capability, the absence of readout noise, and high spatial resolution. Additionally, we will present other characteristics of the CdTe sensors, such as energy resolution, long-term stability, quantum efficiency, and point-spread function. Diffraction tomography⁵, powder diffraction, and inelastic scattering at higher energies strongly benefit from the PILATUS3 CdTe detector characteristics. These applications show how better detectors empower new fields of X-ray photon research.

¹ C. Brönnimann, E. F. Eikenberry, B. Henrich, R. Horisberger, G. Huelsen, E. Pohl, B. Schmitt, C. Schulze-Briese, M. Suzuki, T. Tomizaki, H. Toyokawa, A. Wagner, *J. Synchrotron Rad.* **2006**, 13, 120-130.

² T. Loeliger, C. Broennimann, T. Donath, M. Schneebeli, R. Schnyder and P. Trueb, *IEEE Nucl. Sci. Symp. Conf. Rec.* **2012**, 610.

³ T. Donath, S. Brandstetter, L. Cibik, S. Commichau, P. Hofer, M. Krumrey, B. Lüthi, S. Marggraf, P. Müller, M. Schneebeli, C. Schulze-Briese, J. Wernecke, *J. Phys. Conf. Ser.* **2013**, 425, 062001.

⁴ R. Dinapoli, A. Bergamaschi, B. Henrich, R. Horisberger, I. Johnson, A. Mozzanica, E. Schmid, B. Schmitt, A. Schreiber, X. Shi, G. Theidel, *Nucl. Instrum. Meth. Phys. Res. A* **2011**, 650, 79-83.

⁵ S. D. M. Jacques, M. Di Michiel, A. M. Beale, T. Sochi, M. G. O'Brien, L. Espinosa-Alonso, B M. Weckhuysen, P. Barnes, *Angew. Chem. Int. Ed.* **2011**, 50, 10148-10152.

Initial stages of mixed nickel-iron oxides growth on Ru(0001)

A. Mandziak^{1,6}, J. de la Figuera¹, S. Ruiz-Gomez^{2,3}, L. Pérez^{2,3}, P. Prieto⁴, A. Quesada⁵, L. Martín-García¹, M. Foerster⁶ and L. Aballe⁶

¹*Instituto de Química Física “Rocasolano”, Madrid, 28006, Spain*

²*Dpto. De Física de Materiales, Universidad Complutense de Madrid, Madrid 28040, Spain*

³*Unidad Asociada UCM-IQFR(CSIC), Madrid 28006, Spain*

⁴*Dpto. De Física Aplicada, Universidad Autónoma de Madrid, Madrid 28049, Spain*

⁵*Instituto de Cerámica y Vidrio (CSIC), Madrid 28049, Spain*

⁶*Alba Synchrotron Light Facility, CELLS, Barcelona E-08290, Spain*

Transition metal oxides (TMO) are promising candidate materials for future spintronic devices. Their properties arise from the interaction between transition metal and oxygen ions in a given structure which are very sensitive to different bond length and angles, as well as to their particular cationic distribution. Among them, the spinel family comprises a large number of compounds. Spinel has an fcc anion lattice with cations occupying tetrahedral and octahedral sites. Spinel can be half-metallic (like Fe_3O_4 ^[1]), ferrimagnetic insulators, superconductors (LiTi_2O_4 ^[2]) or heavy fermion materials. However, their properties in thin film growth, as necessary for devices, are often disappointing, dictated by the defect density.

Here we demonstrate a method for preparing high quality ultrathin TMO films on a metallic substrate. Mixed nickel-iron oxides have been grown on Ru(0001) by oxygen-assisted molecular beam epitaxy at elevated temperatures (800 - 900K). The nucleation and growth process are observed *in situ* by means of Low Energy Electron Microscopy (LEEM). A comprehensive characterization is performed combining LEEM for structural characterization and PEEM (PhotoEmission Electron Microscopy) with synchrotron radiation for chemical and magnetic analysis via X-ray Absorption Spectroscopy and X-ray Magnetic Circular Dichroism (XAS-PEEM and XMCD-PEEM, respectively). The latter permits imaging the element specific magnetic domain structure.

The combination of in-situ experiments and micromagnetic characterization allowed us to determine magnetic domain configuration at microscopic level (fig. 1).

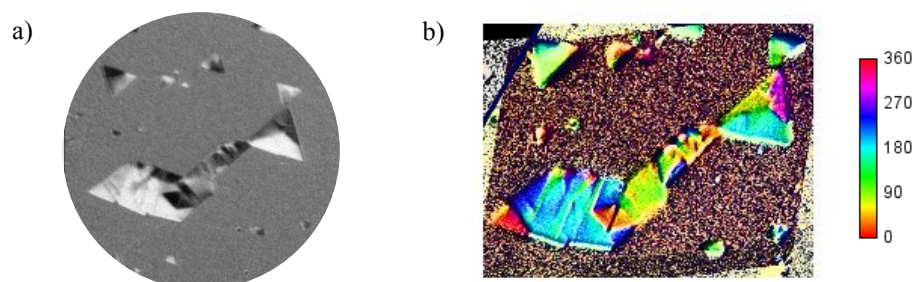


Fig.1: (a) XMCD-PEEM image and (b) the distribution of the magnetization of the island.

¹ K. Siratori *et al.* J. Phys. Soc. Jpn. **53**, 312 (1984)

² D. C. Johnston *et al.* Mater. Res. Bull. **8**, 777 (1973)

FTIR-microspectroscopy reveals changes in major cellular components of *Chlamydomonas* under metal(loid) stress

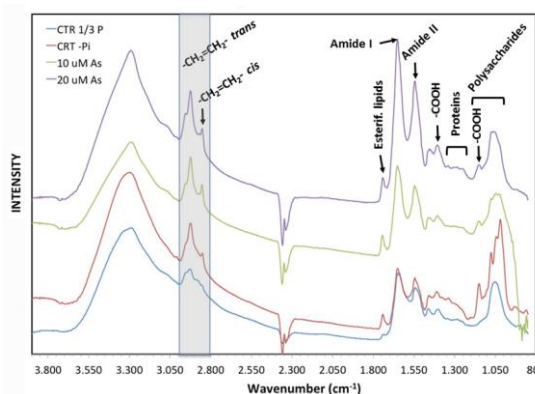
A. Barón^a, M. Arana^a, C. Conesa^a, R. Pastor^a, C. Ortega-Villasante^a, T. Ducic^b, I. Yousef^b, F. Martínez^a and L.E. Hernández^a

^a Laboratory of Plant Physiology, Department of Biology, Univesidad Autónoma de Madrid ES28049 Madrid (Spain); luise.hernandez@uam.es

^b MIRAS-BL, ALBA Synchrotron Light Source, ES08290 Cerdanyola del Vallès, Barcelona (Spain); iyousef@cells.es

Toxic metals, such as cadmium (Cd) and mercury (Hg), and metalloids, like arsenic (As), constitute a major threat to humans and the environment, as they can bioaccumulate and biomagnify in the trophic chain and different ecosystem components. Photosynthetic organisms are primary producers in most ecosystems and may represent the entry of those contaminants. We are studying the microalgae *Chlamydomonas reinhardtii* as a model unicellular eukaryotic organism, important not only for understanding the toxicity of these substances in aquatic environments, but also as a potent tool to characterize cellular mechanisms occurring in photosynthetic organisms upon toxic metal(loid) exposure. Among other symptoms, accumulation of As, Cd and Hg led to over production of reactive oxygen species (ROS), appearance of an oxidative burst and inhibition of photosynthesis, which were followed by strong alterations in major cellular components¹. To investigate the degree of changes occurring in biomolecules composition after 72 h exposure of *Chlamydomonas* to different concentrations of As, Cd and Hg (10 to 50 μM) we used the newly developed BL01 – MIRAS beamline at ALBA synchrotron, Barcelona to perform Synchrotron Fourier Transform Infrared FTIR-microspectroscopy of single cells. Cells were placed in CaF_2 windows (13 mm diameter x 0.5 mm), dried at room temperature and monitored by visible microscopy to check for homogeneous distribution. S-FTIR spectra were obtained in transmission mode using a Hyperion 3000 microscope coupled to Vertex 70 spectrometer at 4 cm^{-1} resolution with 256 co-added scans per spectrum. The microscope is equipped with a liquid nitrogen-cooled mercury cadmium telluride 50 mm MCT A detector ($4000\text{-}600\text{ cm}^{-1}$). The microscope uses a 36x Schwarzschild objective ($\text{NA}=0.52$) and a matching 32x condenser. All spectra were obtained using a single masking aperture size of $8\text{ }\mu\text{m} \times 8\text{ }\mu\text{m}$. More than 50 spectra per specimen were collected in the $4000\text{ to }800\text{ cm}^{-1}$ wavenumber range, to elaborate the profile shown in Fig. 1. We will present our data of microalgae treated with other toxic metals and discuss the differences observed.

Fig. 1. FTIR spectra of *Chlamydomonas* grown in control nutrient medium (CTR 1/3P), without H_2PO_4^- (CTR -Pi), without H_2PO_4^- and supplemented with H_2AsO_4^- 10 or 20 μM (As). Major functional groups are marked, and the grey bar highlights relevant changes in fatty acids occurring under As induced stress.



Acknowledgements. This research was funded by the Spanish Ministry of Economy and Competitiveness (AGL2014-53771-R)

¹ L.E. Hernández et al. *J. Exp. Bot.* **2015**, *66*, 2901-2911

VISUALIZING BATTERIES DISCHARGE PRODUCTS AT MISTRAL

A. Sorrentino^a, Mara Olivares-Marín^{b,c}, Imanol Landa-Medrano^{c,d,e}, E. Pereiro^a, A. Ponrouch^c, D. Tonti^c

^a ALBA Synchrotron Light Source, MISTRAL Beamline, Cerdanyola del Vallès, Barcelona (Spain); asorrentino@cells.es; epereiro@cells.es;

^b Dep. de Ingeniería Mecánica, Energética y de los Materiales, Universidad de Extremadura, Mérida (Spain); maraoom@unex.es;

^c Institut de Ciència de Materials de Barcelona (ICMAB-CSIC), Campus UAB Bellaterra, Barcelona (Spain); molivares@icmab.es; aponrouch@icmab.es; dino.t@csic.es;

^d Dep. Química Inorgánica, Fac. Ciencia y Tecnología, Univ. del País Vasco (UPV/EHU) Leioa -Bizkaia (Spain); imanol.landa@ehu.es;

^e Present address: BCMaterials, Parque Científico y Tecnológico de Bizkaia, 48160 Derio – Bizkaia (Spain);

In many applications the precise knowledge of composition and morphology of materials is a key information to control performance and reliability. This is especially true for battery materials: detailed information of the complex morphology and composition of the discharge products on the cathode as a function of their charging state are crucial for the identification and the understanding of the involved processes. Energy resolved full field transmission soft X-ray microscopy (TXM), is able to give a full picture at the nanometer scale of the chemical state and spatial distribution of many interesting elements, providing pixel-by-pixel absorption spectrum. This technique can be successfully performed at the Mistral beamline of the ALBA light source¹ where tomography complements the 2D chemical information with a 3D morphological description of the discharged products. In this work, after a description of the beamline and of the method of application of the technique to electrode materials, we will present the results from the studies we performed on discharge products of Li/O₂ and Na/O₂ batteries²⁻⁵. Also some new recent measurements performed on Ca^{-ion} batteries will be briefly discussed.

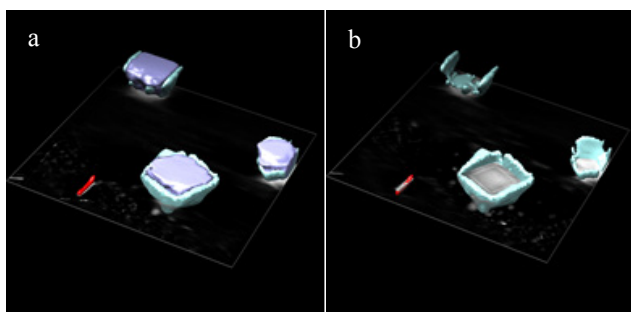


Figure: Three-dimensional reconstruction of some discharged particles of Na/O₂ battery. The images stress the carbonate distribution (green) with respect to the main discharged species (NaO₂ and Na₂O₂, violet). (a) with and (b) without the oxydes “nucleous”. The 2D field of view is about 10 μm x 10 μm. From I. Landa-Medrano *et. al.*⁴.

¹ A. Sorrentino, J. Nicolas, R. Valcarcel, F. J. Chichon, M. Rosanes, J. Avila, A. Tkachuk, J. Irwin, S. Ferrer and Eva Pereiro, *J. Synchrotron Rad.* **2015**, 22, 1112.

² M. Olivares-Marín, A. Sorrentino, R. C. Lee, E. Pereiro, N. L. Wu, and D. Tonti, *Nano Lett.* **2015**, 15, 6932.

³ Landa-Medrano, I.; Olivares-Marín, M.; Bergner, B. J.; Pinedo, R.; Sorrentino, A.; Pereiro, E.; Ruiz de Larramendi, I.; Janek, J.; Rojo, T.; Tonti, D. *J. Phys. Chem. C*, **2017**, 121 (7), 3822–3829.

⁴ I. Landa-Medrano, A. Sorrentino, L. Stievano, I. Ruiz de Larramendi, E. Pereiro, L. Lezama, T. Rojo and D. Tonti, *Nano Energy*, accepted.

⁵ M. Olivares-Marín; A. Sorrentino; E. Pereiro; D. Tonti, *Journal of Power Sources* **2017**, 359, 234-241.

Effect of cold Ar plasma treatment on the catalytic performance of Pt/CeO₂ in Water-Gas Shift reaction (WGS)

Laura Pastor-Pérez,^a Victor Belda-Alcazar,^a Carlo Marini^b, Antonio Sepúlveda-Escribano,^a Enrique V. Ramos-Fernandez^a

^a *Laboratorio de Materiales Avanzados, Departamento de Química Inorgánica-Instituto Universitario de Materiales, Universidad de Alicante, Ctra. San Vicente-Alicante s/n, 03690 San Vicente de Raspeig, Spain*

^b *ALBA Synchrotron, Cerdanyola del Vallès, 08290 Barcelona, Spain.*

Herein, we have studied the effect of Ar plasma treatment in the catalytic performance of Pt/CeO₂. We have prepared a catalyst that has been treated using different activation procedures. Thus, the catalysts have been activated by calcination, reduction in pure H₂, plasma treatment and the combination of them. The resulting materials have been characterized by X-ray photoelectron spectroscopy, X-ray adsorption near edge structure, temperature-programmed reduction with H₂. The resulting materials were then tested in water-gas shift reaction. We have found that the combination of calcination, plasma and reduction treatment leads to a very active catalyst for WGS. Furthermore, we have correlated the structure – performance relationship. Our work demonstrates that the electronic density generated by the cold Ar plasma treatment could help to overcome water dissociation and CO activation over the Pt/CeO₂ catalysts in the water-gas shift reaction. In any case, cold plasma seems to be a promising pre-treatment for metal-supported catalysts to be used in the WGS reaction

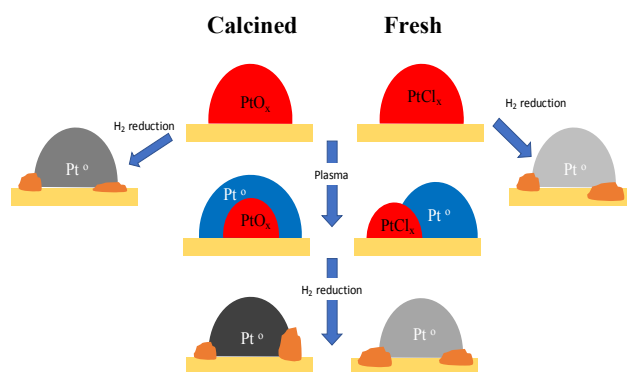


Figure 1. Scheme of the different type of particles formed.

LEEM-PEEM study of magnetic nanowires with chemical notches

S. Ruiz-Gómez^{a,b}, M. Foerster^c, L. Aballe^c, M. Proenca^d, I. Lucas^e, J. L. Prieto^f, A. Mascaraque^{a,b}, A. Quesada^g, J. de la Figuera^g and L. Pérez^{a,b,h}

^a Dept. Física de Materiales, Universidad Complutense de Madrid, Madrid, Spain

^b Unidad Asociada UCM-IQFR

^c Alba Synchrotron Light Facility, CELLS

^d Instituto de Sistemas Optoelectrónicos y Microtecnología, Universidad Politécnica de Madrid

^e Instituto de Nanociencia de Aragón, Universidad de Zaragoza, Zaragoza, Spain.

^f Instituto de Cerámica y Vidrio. CSIC.

^g Instituto de Química Física Rocasolano. CSIC.

^h IMDEA Nanociencia..

Future magnetic storage technology might rely on the movement of magnetic domain walls using spin polarized currents¹. In this technology, the magnetic domain walls that define the bits should be pinned in artificially created notches along magnetic wires². But the depinning of a domain wall from these notches has an intrinsic stochastic component which complicates the application of the proposed scheme in real devices³. To overcome those limits, new types of notches are needed. In this work we have introduced local changes in composition along permalloy nanowires. These chemical boundaries (chemical notches) may act as local well-reliable pinning sites.

To understand the behavior of magnetic domain walls, it is mandatory to use a technique that combines magnetic and chemical information at submicrometer spatial resolution. The LEEM-PEEM microscope in the CIRCE beamline at ALBA synchrotron fulfils all these requirements. We have used spatial resolution of the LEEM microscope to search for the individual nanowires in the substrate. Then, we have used XAS-PEEM to obtain images with chemical contrast (see Fig. 1a) and XMCD-PEEM to get magnetic contrast (Fig 1b). From these figures we correlate composition and magnetic properties of the nanowires. We have proven that chemical notches act as pinning sites for the domain walls. After applying a magnetic field, the domain walls move. These results open the possibility of using these chemically modulated nanowires as storage elements in race-track memories.

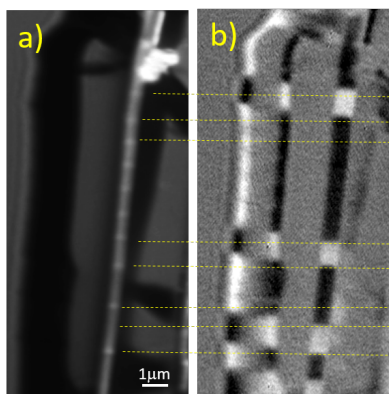


Image 1. (a) Image with chemical contrast (b) XMCD image at Fe K-edge.

¹ S. S. P. Parkin, M. Hayashi, and L. Thomas. *Science*, 2008, 320, 194

² M. Hayashi, L. Thomas, C. Rettner, R. Moriya and S. S. P. Parkin. *Nature Physics* 2007, 3, 21 - 25

³ M. Muñoz and J. L. Prieto. *Nat. Commun.*, 2 (2012) 562

Magnetic proximity effects of Pt/CoFe₂O₄ interface probed by x-ray magnetic circular dichroism

H. B. Vasili,¹ M. Gamino,² P. Gargiani,¹ M. Valvidares,¹ E. Pellegrin,¹
F. Sánchez,² and J. Fontcuberta²

¹ CELLS-Divisió Experiments, ALBA Synchrotron Light Source, E-08290 Cerdanyola del Vallès, Barcelona, Spain; hvasili@cells.es

² Institut de Ciència de Materials de Barcelona (ICMAB-CSIC), UAB Campus, E-08193 Bellaterra, Barcelona, Spain; fontcuberta@icmab.cat

Abstract:

Pure spin currents, which transport only (spin) angular momentum but no electrical charge, represent a new paradigm for spintronics.¹ For this purpose, a typical structure consists on a ferromagnetic insulator (FMI) covered by non-magnetic metal (NM) with large spin-orbit coupling, such as Pt, that is forming the new NM/FMI device structures. Cobalt ferrites, CoFe₂O₄ (CFO) and Y₃Fe₅O₁₂ (YIG), are the recent FMI materials within the focus of scientific endeavor. Indeed, spin magnetoresistance (SMR), related to interfacial spin mixing conductance, has been observed in Pt/CFO and Pt/YIG bilayers.² Yet, the observed SMR effects in Pt/FMI are not unambiguous because the observed SMR could be associated to a proximity effect, inducing magnetism in Pt rather than being a spin current signature. In Pt/YIG, there have been some attempts to address this issue by using XMCD at Pt absorption edges, with controversial results.^{3,4} In this context, we have addressed the problem from a different perspective, by simultaneously exploring electronic and magnetic reconfigurations potentially occurring at each layer in a Pt/CFO device. We have employed x-ray magnetic circular dichroism (XMCD) technique to unravel the magnetic moments of Pt atoms as well as Fe/Co ions at the selected Pt/CFO interfaces as described below.

We have fabricated two epitaxial CFO thin films of 24 nm thickness on (001)-oriented MgAl₂O₄ (MAO) substrates by PLD under the same growth condition (450°C, 0.1 mbar oxygen pressure). The two CFO//MAO samples, prepared in a same run, were further capped by dc-sputtered Pt (4 nm thick) layer grown either at room temperature (sample RT) or at a high temperature of 400°C (sample HT). Two main conclusions emerge from our study: (i) the absence of magnetic moment in Pt for the RT grown Pt/CFO//MAO sample (see Fig. 1(a)) rules out the proximity effects in the measured SMR and (ii) the HT growth results in a Pt magnetic moment (see Fig. 1(b)) and a concomitant reduction of the Fe/Co cations at the neighboring interfacial CFO strongly pointing to (Fe,Co)-Pt alloying. Our results provide a clear picture for the two distinct Pt/CFO interfaces grown under different conditions, thus allowing the understanding of differences related to either proximity effects or intermixing effects, and their impact on the observed SMR, which was never demonstrated before.

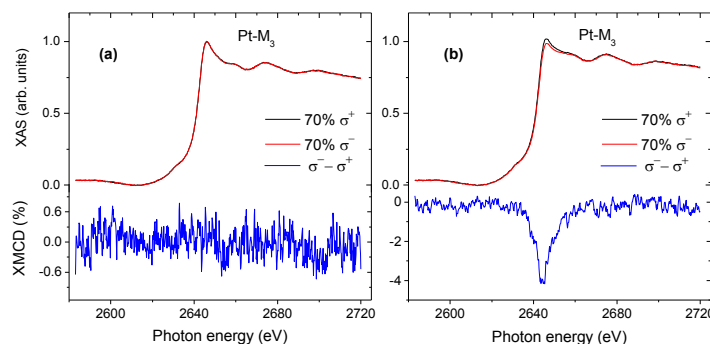


Fig. 1. The Pt-M₃ XAS and XMCD of (a) RT (b) HT grown Pt/CFO//MAO samples.

Acknowledgements:

This work has been supported by Spanish Government, Mineco Project no. MAT2014-56063-C2-1-R.

1. M. Althammer, *et al.* Physical Review B **87** (22), 224401 (2013).
2. M. Isasa, *et al.* Physical Review Applied **6** (3), 034007 (2016).
3. Y. M. Lu, *et al.* Physical Review Letters **110** (14), 147207 (2013).
4. S. Geprägs, *et al.* Applied Physics Letters **101** (26), 262407 (2012).

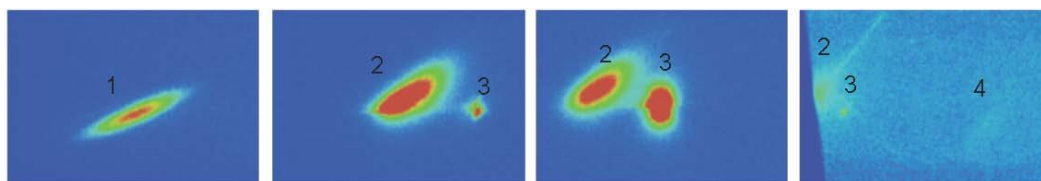
SURFACES WITH SWITCHABLE CATALYTIC ACTIVITY IN FILMS BY INVERSION OF THE FERROELECTRIC POLARIZATION OF THE SUBSTRATE

C. Hernández^a, J. Santiso^b, A. Quesada^c and X. Torrelles^a

^a Institute of Materials Science of Barcelona (ICMAB-CSIC), Universidad Autònoma de Barcelona, E08193 Cerdanyola del Vallès (Spain); chernandez@icmab.es, torrelles@icmab.es ^b Catalan Institute of Nanoscience and Nanotechnology (ICMAB-CSIC), Universidad Autònoma de Barcelona, E08193 Cerdanyola del Vallès (Spain); jose.santiso@icn2.cat ^c Institute of Ceramic and Glass (ICV-CSIC), Universidad Autònoma de Madrid, E28049 Madrid (Spain); a.quesada@icv.csic.es

Hydrogen with its unique properties of high-energy efficiency, easy storage, and freedom from pollution has been considered as a promising alternative to the conventional sources of energy. One of the most promising technologies capable of providing high energy yield without pollutant byproducts is the photocatalytic water splitting (PWS) using sunlight. Titania is of interest among others for the photovoltaic conversion of light to electricity^{1,2}. However, TiO₂ materials suffer from two major drawbacks. One of them is the fast charge carrier recombination (electron-hole pairs), which results in the release of unproductive energy. Another one is the inability to harvest visible light, since TiO₂ can only be excited by UV light due to its wide band gap of 3.0–3.2 eV, which only covers 5% of the solar spectrum^{3,4}. A promising strategy to increase the visible light activity of titania, as proposed in this project, takes into account that titania supported on a visible light absorbing core of a ferroelectric material shows enhanced visible light photoactivity⁵. This is due to the dipolar field of the ferroelectric that can influence the motion of charge carriers in the catalytic coating.

In this work we focus on the preparation of TiO₂ thin films grown on BaTiO₃(001) films oriented on SrTiO₃(001) by PLD. Under our conditions, BaTiO₃ grows in a layer-by-layer growth mode. In order to investigate the surface morphology, crystalline orientation, microstructure, and film/substrate interface of the films, different characterization techniques, i.e.: x-ray diffraction (XRD), atomic force microscopy (AFM) and



high-resolution transmission electron microscopy (HRTEM) were applied. Ferroelectricity of the BaTiO₃ films was proved by electrical measurements performed on Ag/BaTiO₃/SRO heterostructures.

Figure 1. Reciprocal space images at different L-values corresponding to the (1,0,L) reflection. Peak numbers 1, 2, 3 and 4 correspond to TiO₂ (101), BTO (101), STO (101) and TiO₂ (103) reflections.

¹O'Regan, B. & Grätzel, M. A low-cost, high efficiency solar cell based on dye-sensitized colloidal TiO₂ films. *Nature* **353**, 737–740 (1991). ²Hussain, H. *et al.* Structure of a model TiO₂ photocatalytic interface. *Nat. Mater.* (2016). doi:10.1038/NMAT4793 ³Breckenridge, R. G. & Hosler, W. R. Electrical Properties of Titanium Dioxide Semiconductors. *Phys. Rev.* **91**, 793–802 (1953). ⁴Pascual, J., Camassel, J. & Mathieu, H. Fine structure in the intrinsic absorption edge of TiO₂. *Phys. Rev. B* **18**, 5606–5614 (1978). ⁵Gao, B., Kim, Y. J., Chakraborty, A. K. & Lee, W. I. Efficient decomposition of organic compounds with FeTiO₃/TiO₂ heterojunction under visible light irradiation. *Appl. Catal. B Environ.* **83**, 202–207 (2008).

AP-XPS study of Methanol Steam Reforming catalysts

D. Ruano^a, V. Pérez-Dieste^a, C. Mateos-Pedrero^b, A. Mendez^b, CSR. Azenha^b and P. Concepción^c

^a ALBA Synchrotron, E08290 Cerdanyola del Vallés (Spain); vperez@cells.es

^b Department of Chemical Engineering, E4200, University of Porto (Portugal);

cmpedrero@fe.up.pt

^c Institute of Chemical Tecnology, E46022, Universidad Politécnica de Valencia (Spain);

pconcepc@upvnet.upv.es

H₂-based energy has long been regarded as a promising alternative to conventional fuels. Low temperature methanol steam reforming (MSR) is an attractive source for nearly CO free H₂ production. Cu-based catalysts are the most commonly used for MSR, due to their high activity and low CO production, but they present pyrophoricity, easy deactivation and poor thermal stability. Moreover, Pd-based catalysts have also been considered due to the fact that they have excellent thermal stability¹. ZrO₂ has been reported to present some interesting catalytic properties (redox and chemical properties) in this reaction, which make it a good support².

Regarding the active species in copper based catalysts for MSR, there is still ambiguity about their nature. Indeed, Cu⁰ and/or Cu⁺ species have been proposed to be involved in the catalytic process³. In the present work two PdCu based catalysts, supported on monoclinic and cubic ZrO₂, with different CO/H₂ selectivities, have been investigated. In order to determine the nature of copper species under reaction conditions, an in-situ X-ray Photoelectron Spectroscopy study under conditions close to the ones of the MSR process has been performed. The AP-XPS results indicate that copper is partially oxidized to Cu²⁺ under reaction conditions in the less H₂ selective catalyst (CuPd/ZrO₂-c), while it remains as Cu⁰ in the most selective catalyst (CuPd/ZrO₂-m) (Fig. 1).

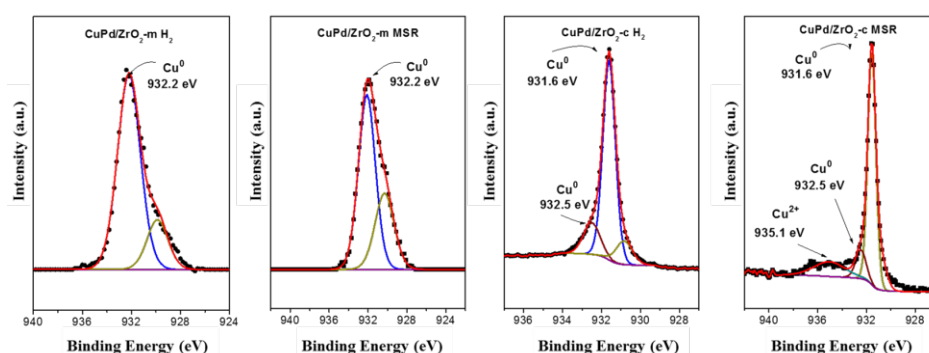


Fig. 1. Cu2p_{3/2} AP-XPS of the catalysts CuPd/ZrO₂-m and -c in H₂ and in MSR at 1150 eV.

Acknowledgements. The research leading to these results has received funding from the European Project: MATching zeolites SYNthesis with CATalytic activity (Project ID: 671093). Part of this work was financially supported by European Union's Seventh Framework Programme (FP/2007-2013) for the Fuel Cells and Hydrogen Joint Technology Initiative under grant agreement no. [303476]. The APXPS experiments were performed at the CIRCE beamline of the ALBA synchrotron light facility with the collaboration of ALBA staff.

¹Takezawa, T., Iwasa, N. *Catal. Today*. **1997**, 36, 45-56.

²C. Chang, J. Wang, C. Chang, B. Liaw, Y. Chen. *Chem. Eng. J.* **2012**, 192, 350-356.

³GS. Wu, DS. Mao, GZ. Lu, Y. Cao, KN. Fan. *Catal. Lett.* **2009**, 130, 177-184.

CHAIN ORIENTATION IN BULK HETEROJUNCTION PHOTOVOLTAIC THIN FILMS AS REVEALED BY NEAR EDGE X-RAY ABSORPTION FINE STRUCTURE

E. Gutiérrez^a, A. Rodríguez-Rodríguez^a, T.A. Ezquerra^a, E. Rebollar^b, M. Valvidares^c, P. Gargiani^c and M.C. García-Gutiérrez^a

^a Instituto de Estructura de la Materia (IEM-CSIC), Serrano 121 Madrid, Spain;

edgar.gutierrez@iem.cfmac.csic.es

^b Instituto de Química-Física Rocasolano (IQFR-CSIC), Serrano 119, Madrid, Spain

^c ALBA Synchrotron, Carrer de la Llum 2-26, E-08290 Cerdanyola del Vallès, Barcelona, Spain

Organic photovoltaics (OPVs) are one class of solar energy conversion devices, offering the advantages of low cost, light weight, solution processability and mechanical flexibility over existing photovoltaic technologies. Efficient organic solar cells typically employ a bulk heterojunction (BHJ) photoactive layer, where an electron-donating (p-type) material and an electron-accepting (n-type) material form a nanosized phase-separated interpenetrating network¹. Due to the macromolecular nature of conjugated polymers, the orientation and assembly of molecular chains in these materials affect their charge transport properties. Therefore, investigation of chain orientation and π -stacking in homopolymer and polymer blend thin films is highly important. Near Edge X-Ray Absorption Fine Structure (NEXAFS) is very sensitive to the detailed chemical structure of the sample and to the molecular orientation when using a polarized X-Ray beam. Polymers as organic components are widely studied in the carbon K-edge. NEXAFS in the Total Electron Yield mode (TEY) is surface sensitive with a depth resolution of about 10 nanometers. We have measured TEY at the carbon K-edge (280-320 eV) of semiconducting polymers (poly(3-hexylthiophene-2,5-diyl) (P3HT) and poly[N-9'-heptadecanyl-2,7-carbazole-alt-5,5-(4',7'-di-2-thienyl-2',1',3'-benzothiadiazole)] (PCDTBT)), the fullerene derivative ([6,6]-phenyl C71 butyric acid methyl ester (PC₇₀BM)) and blends of them. The preliminary TEY results indicate that both homopolymer and blend thin films show linear dichroism (Fig.1), indicating a preferential orientation of molecular chains. The experiments were performed in the BOREAS beamline at ALBA synchrotron.

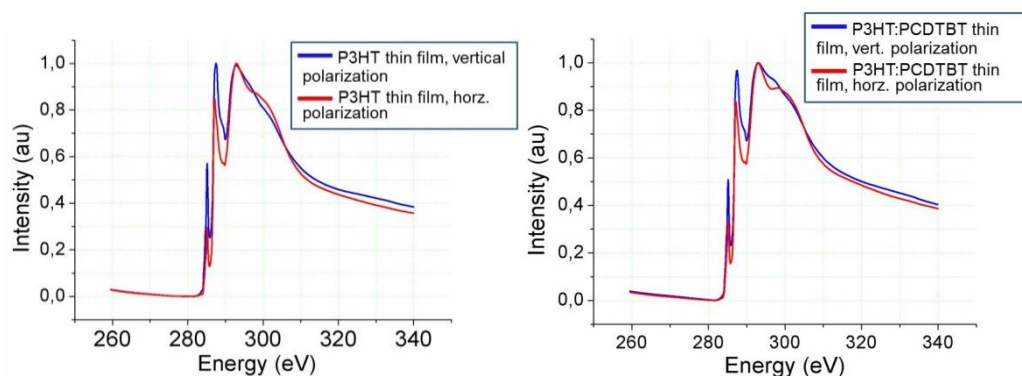


Figure 1. TEY NEXAFS of a) P3HT thin film and b) P3HT:PCDTBT (1:1) thin film.

Acknowledgements. This work has been supported by MINECO (Projects: MAT2014-59187-R, MAT2015-66443-C02-1-R, CTQ 2013- 43086-P).

¹ A. Rodríguez-Rodríguez et al, "Competition between phase separation and structure confinement in P3HT/PCDTBT heterojunctions: Influence on nanoscale charge transport", *Polymer*, **2015**, *77*, 70-78.

Substrate binding and catalysis in *Oceanobacillus iheyensis* macrodomain: A bacterial macrodomain capable of reversing protein mono-ADP-ribosylation

F. Gil-Ortiz^a, R. Zapata-Pérez^b, A.B. Martínez-Moñino^b, A.G. García-Saura^b, J. Juanhuix^a, A. Sánchez-Ferrer^b

^aCELLS-ALBA Synchrotron Light Source, 08290 Barcelona (Spain); fgil@cells.es

^bDepartment of Biochemistry and Molecular Biology-A, Faculty of Biology, University of Murcia, Campus Espinardo, 30100 Murcia (Spain); alvaro@um.es

ADP-ribosylation is a post-translational protein modification that plays a key role in many cell processes¹. Macrodomains are ubiquitous and evolutionarily conserved domains that recognize or transform ADP-ribose derivatives². In humans, they are involved in transcription, X-chromosome inactivation, neurodegeneration and modulating PARP1 signaling, making them potential targets for therapeutic agents. Unfortunately, some aspects related with the substrate binding and catalysis of MacroD-like macrodomains still remain unclear. The proposed catalytic mechanism for MacroD-like proteins requires the presence of three conserved residues³. However, mutation of the proposed catalytic aspartate does not completely abolish enzyme activity, thus only the existence of a different pool of catalytic residues or an alternative mechanism may clarify the dilemma. Here, we present a functional and structural characterization of a macrodomain from the extremely halotolerant and alkaliphilic bacterium *Oceanobacillus iheyensis* (OiMacroD), related to hMacroD1/hMacroD2, shedding light on substrate binding and catalysis. The crystal structures of D40A, N30A and G37V mutants, and those with MES, ADPr and ADP bound were determined at the MX beamline XALOC (ALBA Synchrotron), allowing us to identify five fixed water molecules that play a significant role in substrate binding. Another key element, involved not just in substrate binding but also in catalysis, is the $\beta 6$ - $\alpha 4$ loop. The substrate-induced rigid body closure of this element acts as a clamp over the pyrophosphate, stacking the distal ribose in the right orientation for catalysis. In addition, D40A mutant revealed an additional structural role for this catalytic residue: to organize the $\beta 3$ - $\alpha 1$ loop maintaining the proper architecture of the active site. Besides, this study supports the existence of two catalytic mechanisms. Under normal conditions, the conserved aspartate deprotonates a nearby water molecule, facilitating the O-acetyl-ADP-ribose (OAADPr) hydrolysis. However, when this aspartate is absent, they could carry out 1'-OAADPr deacetylation through a nucleophilic attack on the C1'' atom by activating a water molecule bound to OAADPr molecule. This fact may be favoured by the rapid equilibrium reached between the different OAADPr isomers. Furthermore, it is revealed that OiMacroD not only catalyzes OAADPr hydrolysis but as found in human, archaeal and viral macrodomains, bacterial macrodomains are able to reverse mono-ADP-ribosylation from target proteins. Finally, a substrate-coordinated water molecule seems to be involved in catalysis, being indispensable to reach the proper conformation of the OAADPr, as revealed by the G37V mutant.

Acknowledgements. This study was partially supported by Spanish grants from MINECO-FEDER (BIO2013-45336-R) and from Ayudas a los Grupos y Unidades de Excelencia Científica de la Región de Murcia, Fundación Séneca-Agencia de Ciencia y Tecnología de la Región de Murcia (19893/GERM/15, Programa de Apoyo a la Investigación 2014).

¹ Barkauskaite, E., Jankevicius, G., Ahe, I. I. (2015). *Mol. Cell* **58**, 935–946.

² Karras, G.I., Kustatscher, G., Buhecha, H.R., Allen, M.D., Pugieux, C., et al. (2005) *EMBO J.* **24**, 1911–1920.

³ Chen, D. et al. (2011) *J. Biol. Chem.* **286**, 13 261–13 271.

APPLICATION OF SYNCHROTRON INFRARED MICRO-REFLECTANCE FOR THE STUDY OF DIVERSE MATERIALS

E.I. González-Castillo^a, P.S. Shuttleworth^a, S. Quiles-Díaz^a, P. Enrique-Jiménez^b,
A. Flores^b, F. Ania^b, H.J. Salvagione^a, M.A. Gómez-Fatou^b, I. Yousef^c,
M. Kreuzer^c and G. Ellis^a.

^a Institute of Polymer Science & Technology, ICTP-CSIC, c/ Juan de la Cierva 3, 28006 Madrid (Spain) gary.ellis@csic.es

^b Institute of the Structure of Matter, IEM-CSIC, c/ Serrano 119, 28006 Madrid (Spain)

^c MIRAS Beamline, ALBA Light Source, Carrer de la Llum 2-26, 08290 Cerdanyola del Vallès, Barcelona (Spain)

Infrared microspectroscopy with a synchrotron source has experienced sustained growth since it was first introduced in the mid 1990's,¹ and has developed into a very powerful tool for diffraction-limited spatial differentiation of heterogeneous materials in a wide range of areas² including, amongst others, polymer science.³ In the latter case, whilst most of the research undertaken has been on thin polymer films in transmission mode, using confocal or non-confocal aperture arrangements. From a sampling perspective, reflectance techniques are undoubtedly the most versatile, especially when reflection-absorption or attenuated total reflectance, ATR, can be successfully employed. The high brightness of the synchrotron source provides a considerable signal-to-noise (S/N) advantage that translates into increased versatility with respect to both spatial contrast (via smaller apertures and oversampling methods) and measurement time, which translates into faster point-imaging or larger map sizes over the same timescale.

In this work the advantages of the synchrotron source are discussed for the case of less-exploited micro-reflectance approaches, in particular specular reflectance (SR) and grazing angle (GA) microspectroscopy. In the former case, we show that the numerical aperture of Schwartzchild objectives used in commercial IR microscopes allow the near-normal incidence approximation⁴ to be effectively employed. We demonstrate that from highly-polished surfaces of low-reflectance materials, e.g. polypropylene (PP), excellent S/N ratios can be achieved through apertures down to $1 \times 1 \mu\text{m}^2$, Figure 1. This has been exploited to study various materials including epoxy/thermoplastic/CNT nanocomposites, PP/carbon fibre composites, PEEK/glass fibre composites, and PP/graphene nanocomposites, and both advantages and limitations of the approach will be discussed.

Acknowledgements. EIGC acknowledges a PhD grant from the CONACYT (Mexico). SQD and PEJ acknowledge FPI Fellowships, and PSS a Ramón y Cajal PostDoc Fellowship, from the MINECO (Spain). MINECO also provided financial support through Grants MAT2014-54231-C4-4P, MAT2014-59674-JIN, MAT2013-47898-C2-1R and MAT2013-47898-C2-2R.

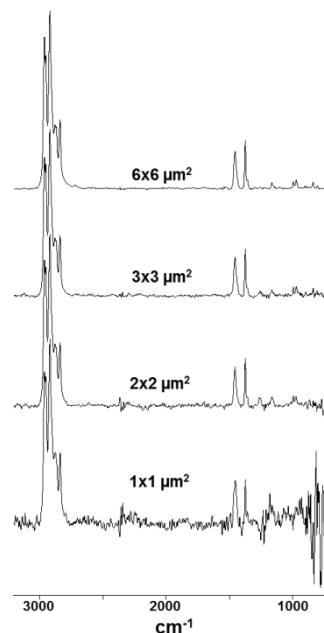


Figure 1. Micro-SR spectra of iPP at various apertures (30s acquisition, 4 cm^{-1} resolution).

¹ G.L.Carr, J.A. Reffner, G.P. Williams, *Rev. Sci. Instrum.* **1995**, *66*, 1490-1492

² M.C. Martin, U. Schade, P. Lerch, P. Dumas, *TrAC Trends Anal. Chem.* **2010**, *29*, 453-463

³ G.J. Ellis, M.C. Martin, *Eur. Polym. J.* **2016**, *81*, 505-531.

⁴ M. Claybourn, "Infrared Reflectance Spectroscopy of Polymers", Global Press **1998**

SPIN AND ORBITAL ORDERINGS IN $\text{La}_{1.5}\text{Ca}_{0.5}\text{CoO}_4$ STUDIED BY RESONANT SOFT X-RAY SCATTERING

G. Subías¹, J. García¹, J. Blasco¹, M. C. Sánchez¹, J. Herrero-Martín² and S. M. Valvidares²

¹Instituto de Ciencia de Materiales de Aragón, Departamento de Física de la Materia Condensada, CSIC-Univ. Zaragoza, 50009 Zaragoza (Spain); gloria@unizar.es

²ALBA synchrotron, Ctra.BP1413 Km 3.3, 08290 Cerdanyola del Vallès, Barcelona (Spain)

In the layered perovskite Co oxides $\text{La}_{2-x}\text{Ca}_x\text{CoO}_4$, the magnetic and electronic phases have been shown¹ to change depending on the hole concentration x with the spin and charge ordered phases coexisting in a wide hole carrier range around $x=0.5$. The half-doped material exhibits charge-order characterized by the super-lattice reflections at $q=(1/2,1/2,l)$ (l =integer) observed by neutron scattering and resonant x-ray scattering experiments¹⁻³. The magnetic structure changes approximately at $x=0.5$ from an antiferromagnetic structure with a modulation vector $q=(1/4,1/4,1/2)$ to another one with $q=(1/4,1/4,1)$ with increasing x , both antiferromagnetic structures¹ ($T_N \sim 55$ K) were only observed in $\text{La}_{1.5}\text{Ca}_{0.5}\text{CoO}_4$. However, the underlying Co spin states remain unclear and, in addition to the spin state, the orbital moment is also a key parameter for the physical properties of Co oxides.

Resonant Soft X-ray Scattering (RSXS) has been developed in recent years and become a powerful technique for determining not only the magnetically ordered structure but also the local electronic structure at an element-selective level in spin-charge-orbital ordered 3d oxides⁴. Very recently, we have been successful in measuring the $(1/4,1/4,0)$, $(1/4,1/4,1)$ and $(1/4,1/4,1/2)$ reflections of $\text{La}_{1.5}\text{Ca}_{0.5}\text{CoO}_4$ at low temperature below ~ 55 K in the MARES UHV-reflectometer at the BOREAS beamline (ALBA synchrotron). Each resonant reflection was measured on a separate single crystal so the correspondent reflections are the specular ones. The RSXS intensities only appear at the Co L_3 edge region of energies, which indicates a large orbital magnetic moment at Co ions. The RSXS measurements show similar spectra and a dependence on both the azimuth angle and the linear polarization of the incident beam (Fig. 1). The resonant spectral shape closely resembles that of a Co^{2+} -based system⁵, which suggests that the magnetic structures are composed of the Co^{2+} high spin state.

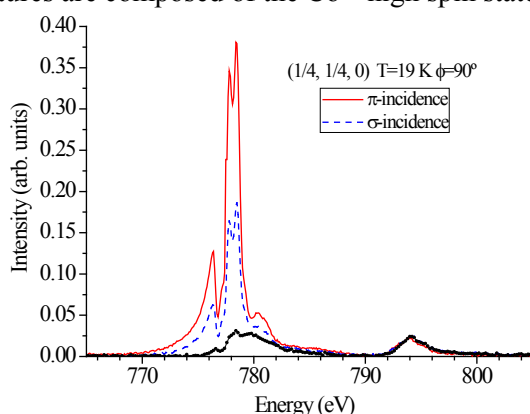


Fig. 1. Co $L_{2,3}$ RSXS energy scans at the $(1/4, 1/4, 0)$ reflection with different incident polarization compared with the fluorescence background scan at $\phi=90^\circ$.

¹ K. Horigane *et al.*, *J. Phys. Soc. Jpn.* 76, 114715, 2007.

² K. Horigane *et al.*, *J. Phys. Soc. Jpn.* 77, 044601, 2008.

³ ESRF experimental report on proposal HC1954, 2015.

⁴ U. Staub *et al.*, *J. Sync. Rad.* 15, 469, 2008.

⁵ J. Herrero-Martín *et al.*, *Phys. Rev. B* 91, 220403, 2015.

Chemically Selective Cleaning of Contaminated B₄C-Coated Optics by RF remote O₂ and H₂ plasma

H. Moreno Fernández^a, M. Thomasset^b, G. Sauthier^c,
D. Rogler^d, R. Dietsch^d, V. Carlino^e, E. Pellegrin^a

^aCELLS-ALBA, Carrer de la Llum 2-26, E-08290 Cerdanyola del Valles, Spain; hmoreno@cells.es, epellegrin@cells.es

^bSOLEIL Synchrotron, L'Orme des Merisiers, F-91192 Gif-sur-Yvette, France; muriel.thomasset@synchrotron-soleil.fr

^cICN2, UAB Campus, E-08193 Bellaterra, Spain; guillaume.sauthier@icn2.cat

^dAXO DRESDEN GmbH, D-01237 Dresden, Germany; daniela.rogler@axo-dresden.de

^eibss Group Inc., Burlingame, CA 94010, USA; vince.carlino@ibssgroup.com

Boron carbide (B₄C) - due to its exceptional mechanical properties - is one of the few existing materials that can withstand the extremely high brilliance of the photon beam from free electron lasers (FELs) and is thus of considerable interest for optical applications in this field. However, as in the case of many other optics operated at modern accelerator-, plasma-, or laser-based light source facilities, B₄C-coated optics are subject to ubiquitous contaminations. These contaminations - that are carbon atoms deposited on the surface when residual hydrocarbons dissociate during the interaction with photons or by secondary electrons - represent a serious issue for the operation of the pertinent high performance beamlines due to a severe reduction of photon flux, beam coherence, creation of destructive interference and scattering losses, not necessarily restricted to the photon energy range of the carbon K-edge. Thus, a variety of B₄C cleaning technologies have been developed at different laboratories with varying success¹. Here, we present a study regarding the low-pressure RF plasma cleaning of a series of carbon-contaminated B₄C test samples by using an inductively coupled remote O₂/Ar and Ar/H₂ RF plasma, produced by an IBSS GV10x plasma source following previous studies using the same RF plasma source^{2,3}. Results regarding the chemistry, morphology as well as other aspects of the B₄C optical coatings and surfaces before and after the plasma cleaning process are reported.

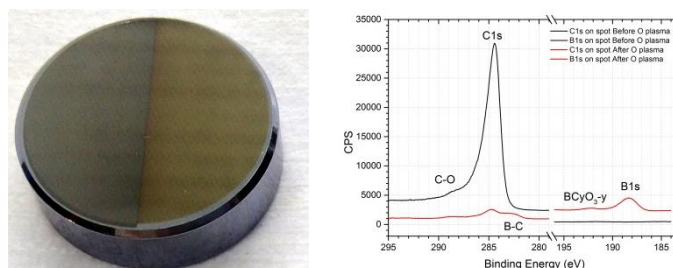


Figure 1. To the left, a B₄C-coated mirror with half a-C contaminated surface; to the right a XPS spectra for an O₂ plasma-cleaned sample.

¹ Graham, S., Steinhaus, C., Clift, M., Klebanoff, L., and Bajt, S., "Atomic hydrogen cleaning of EUV multilayer optics," Proceedings of SPIE 5037, 460-469 (2003).

²Gonzales, M., Reyes, J., Šics, I., Goñi, A. R., Moreno, H., Carlino, V., and Pellegrin, E., "Remote plasma cleaning of optical surfaces: Cleaning rates of different carbon allotropes as a function of RF powers and distances," Applied Surface Science **362**, 448-458 (2016).

³Pellegrin, E., Šics, I., Reyes, J., Perez, C., Lopez, J., Langlois, M., Fernandez, J., and Carlino, V., "Characterization, optimization and surface physics aspects of in situ plasma mirror cleaning," J. Synchrotron Rad. **21**, 1-15 (2014).

Ion energy distributions within RF inductive coupled plasmas as used for the cleaning of optical surfaces.

H. Moreno Fernández^a, J. Cotrino^b, I. Crespo^a, V. Carlino^c, E. Pellegrin^a

^aCELLS-ALBA, Carrer de la Llum 2-26, E-08290 Cerdanyola del Valles, Spain;

hmoreno@cells.es, icrespo@cells.es, epellegrin@cells.es

^bInstituto de Ciencia de Materiales de Sevilla, C./ Américo Vespucio49, E-41092 Sevilla;

cotrino@us.es

^cibss Group Inc., Burlingame, CA 94010, USA; vince.carlino@ibssgroup.com

Reactive plasma treatments have become a sustainable option for the cleaning of ubiquitous carbon contaminations on synchrotron and free electron laser (FEL) beamline optics,^{1,2} and so do provide a solution that beamline scientists seek for when carbon atoms are deposited on beamline optics by the dissociation of residual hydrocarbons while interacting with photons. Nevertheless, the non-equilibrium character of these plasmas and their rich plasma chemistry make them very complex and thus hard to understand. In particular, these plasmas are valued for their capability of producing large amount of radicals and ions that cannot be understood without the help of plasma diagnostics.³ Here, we present a study regarding low-pressure RF Ar, O₂/Ar, and Ar/H₂ feedstock gas plasmas produced by an IBSS model GV10x downstream plasma source as used for cleaning of carbon-contaminated optics. The spatial ion energy distribution was measured using a quadrupole mass spectrometer (M.S.) at different RF powers as well as different distances from the plasma source. It was found that neutral plasma species don't play an important role in the cleaning process, as cations are the main species occurring within the plasma. In more detail, the dominant cation in Ar/O₂ plasma is found to be O₂⁺, while for Ar/H₂ plasma Ar⁺, H₂⁺ and H₃⁺ are prevailing. For mass 40 (Ar⁺) using different plasma feedstock gases such as Ar, H₂/Ar, and O₂/Ar differences in kinetic energy were found, with the H₂/Ar plasma configuration having the highest cation energy for this atomic species.

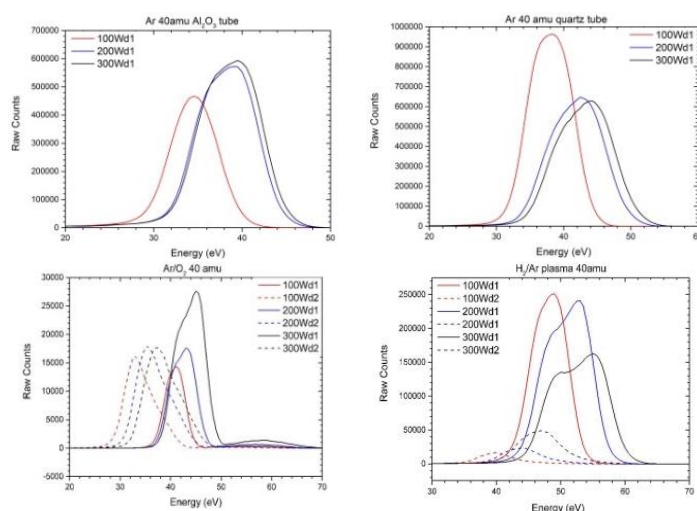


Figure 1. Top panel: Ion energy distribution functions (IEDF) for two different Ar plasma source configurations at different RF powers. Bottom panel: IEDF for mass 40 (Ar⁺) in Ar/O₂ plasma (left) and Ar/H₂ plasma (right) at different RF powers and source distances.

¹ Gonzales, M., Reyes, J., Šics, I., Goñi, A. R., Moreno, H., Carlino, V., and Pellegrin, E., "Remote plasma cleaning of optical surfaces: Cleaning rates of different carbon allotropes as a function of RF powers and distances," *Applied Surface Science* **362**, 448-458 (2016).

² Pellegrin, E., Šics, I., Reyes, J., Perez, C., Lopez, J., Langlois, M., Fernandez, J., and Carlino, V., "Characterization, optimization and surface physics aspects of in situ plasma mirror cleaning," *J. Synchrotron Rad*

³ Benedikt, J., Hecimovic, A., Ellerweg, D., Keudell, A., "Quadrupole mass spectrometry of reactive plasmas" *Journal of Physics D: Applied physics* **45**, 1-23 (2012).

STRUCTURE SOLUTION FROM A SINGLE MICROVOLUME BY SYNCHROTRON TTS-MICRODIFFRACTION

J.Rius^a, O. Vallcorba^b, A. Crespi^a and C. Miravittles^a

^a *Institut de Ciència de Materials de Barcelona-CSIC, Campus de la UAB, Bellaterra, Catalonia (Spain); jordi.rius@icmab.es*

^b *ALBA Synchrotron Facility-CELLS, Experiments Division (MSPD beamline), Barcelona, (Spain); ovallcorba@cells.es*

Solving crystal structures by δ -recycling¹ direct methods from synchrotron through-the-substrate-microdiffraction (*tts*- μ D) data² can be more or less difficult depending on the amount of missing intensities. This is especially true in the case of triclinic crystalline phases that are only present in one point (μ volume) of the polished thin-section. To understand the dependence of the δ -recycling success rate on the Ewald sphere completeness, some simulations were performed which showed that a minimum completeness of 60% is required for getting a significant number of successful δ -recycling trials. To increase the completeness per μ volume, a new data collection strategy was tested which is based on the measurement of two series of orthogonal ϕ -scans. The corresponding results show that the crystal structure of axinite can be solved from the merged datasets provided that the ϕ -scan limits are at least $\pm 30^\circ$.

For high-symmetry phases, due to the Laue symmetry redundancy, a single series of ϕ -scans normally suffices for the application of δ -recycling direct methods. However, when for experimental causes this series is incomplete, the orthogonal χ strategy also provides a simple way to increase the completeness. This study also proves that the inclusion in the δ -recycling approach of non-detected reflections (with zero intensity) slightly improves the quality and efficiency of the phase refinement.

All measurements were performed at the HP-microdiffraction station (MSPD beamline) of ALBA Synchrotron (Barcelona) and the calculations with slightly modified versions of XLENS for δ -recycling and of TTS_software for the rest (Both available at departments.icmab.es/crystallography/software).

Acknowledgements. Financial support of the Ministerio de Economía y Competitividad (MAT2015-67593-P and Severo Ochoa: SEV-2015-0496) is acknowledged.

¹ J. Rius, *IUCrJ*, **2014**, *1*, 291-304.

² J. Rius, O. Vallcorba, C. Frontera, I. Peral, A. Crespi. & C. Miravittles, *IUCrJ*, **2015**, *2*, 452-463.

ELEMENT-SPECIFIC RESONANT MAGNETIC X-RAY SCATTERING STUDIES OF SPIN ORDER IN THE SINGLE MAGNETIC SITE OF MULTIFERROIC $\text{Mn}_{0.85}\text{Co}_{0.15}\text{WO}_4$

J. Herrero-Martin^a, C. Mazzoli^b, S. Francoual^c, J. Stempfer^c, F. Fabrizi^d, P. Bencok^d, P. Steadman^d, A. N. Dobrynin^d, A. Bombardi^d, A. A. Mukhin^e, V. Skumryev^f and J. L. García-Muñoz^g

^aALBA Synchrotron Light Source, Cerdanyola del Vallès, Spain;

^bBrookhaven Natl. Lab., Natl. Synchrotron Light Source 2, Upton, NY 11973 USA;

^cDeutsch Elektronen Synchrotron, Notkestr. 85, Hamburg, Germany;

^dDiamond Light Source, Didcot, Oxfordshire, United Kingdom;

^eProbkhorov General Physics Institute, Russian Academy of Science, Moscow, Russia;

^fDpt. Física, Universitat Autònoma de Barcelona, Bellaterra, Spain;

^gInstitut de Ciència de Materials de Barcelona, ICMA-B-CSIC, Bellaterra, Spain;

garcia.munoz@icmab.es

Tuning synthesis towards the induction of magnetic frustration and complex magnetic orders breaking the spatial inversion symmetry is regarded as an effective way of producing multiferroic (MF) and magnetoelectric (ME) materials. MnWO_4 and the $(\text{Mn},\text{Co})\text{WO}_4$ extended family are reference models for the study of the mutual interaction between spins and polar orders. The introduction of Co favors a strong competition between its large magnetocrystalline anisotropy (McA) and dominant Mn-Mn exchange interactions. As a result it stabilises the characteristic ferroelectric (FE) behavior of MnWO_4 at low temperatures (T), and uplifts the T-x phase diagram richness with the appearance of new FE phases and magnetic structures. Moreover, this family of MFs is intrinsically inhomogeneous since the two different magnetic ions (Mn and Co) occupy the same crystallographic position.¹⁻³

Employing resonant magnetic soft x-ray scattering (RMSXS) we investigated the magnetic order in a MF crystal with the $\text{Mn}_{0.85}\text{Co}_{0.15}\text{WO}_4$ critical composition above its FE transition, focusing on its well-known collinear AF4 phase. Thanks to RMSXS' chemical selectivity we have demonstrated that Co moments in AF4 arrange antiferromagnetically following their own strong uniaxial McA, the collinear order of Mn spins pointing to a different direction.⁴ This implies intrinsic remarkable deviations of the spins arrangement at the local scale from the average description provided by neutron diffraction.

These element-resolved magnetic results call for reexamining the phase diagram of this family of MFs. The relevance of similar non-collinearity effects (stimulated by competing magnetocrystalline anisotropy terms) in ordered Mn and Co spins at a single crystallographic position is being investigated in the spiral ferroelectric phases of the same crystal. RMSXS measurements under the application of an E-field were also used to study the ME effect on the ordered magnetic domains distribution and the electric coercivity.

Acknowledgements. MINECO (and ERDF) project MAT2015-68760-C2-2, and “Severo Ochoa” Programme for Centres of Excellence in R&D (SEV- 2015-0496). Beamtime granted by Diamond, DESY and ALBA.

¹ K. Taniguchi *et al*, *Phys. Rev. Lett.* **2008**, *101*, 207205.

² Y.-S. Song *et al*, *Phys. Rev. B.* **2010**, *82*, 214418.

³ I. Urcelay-Olabarria *et al*, *Phys. Rev. B.* **2015**, *91*, 104429; also, *J. Applied Cryst.* **2016**, *49*, 520.

⁴ J. Herrero-Martin *et al*, *Phys. Rev. B.* **2015**, *91*, 220403(R)

Mössbauer and EXAFS studies of bulk and thin film CoFe_2O_4 : cation distribution at room and low temperatures

J. de la Figuera^a, P. Prieto^b, A. Serrano^c, J.F. Marco^a

^aInstituto de Química Física «Rocasolano», CSIC, 28006 Madrid (Spain) (jfmarco@iqfr.csic.es)

^bUniversidad Autónoma de Madrid, 28049 Madrid (Spain)

^cSpLine, Spanish CRG BM25 Beamline, ESRF, 38000 Grenoble (France)

Cobalt ferrite, CoFe_2O_4 (CFO) is a remarkable oxide with the highest magnetocrystalline anisotropy of any spinel ferrite¹. It has a spinel structure, an fcc anion lattice with Co and Fe cations in tetrahedral (A) and octahedral (B) sites. Formally, it is expected to have a formula of $(\text{Fe}^{3+})_A(\text{Co}^{2+}\text{Fe}^{3+})_B\text{O}_4$. But the particular cation distribution can differ from the canonical one in real samples. In turn, the electronic and magnetic properties depend strongly on the cation distribution. The Fe cationic distribution has been probed by Mössbauer spectroscopy. Experiments have been reported indicating that thermal treatments of a given sample can affect the distribution².

But one issue with variable temperature Mössbauer experiments of CFO^{3,4} is that the spectra evolve strongly in the temperature range from 100 K to 300 K. In fact, the two sextets corresponding to Fe^{3+} in tetrahedral and octahedral positions change their relative areas by a factor of 3. This evolution can be interpreted in terms of a different Debye characteristic temperature for Fe^{3+} in each site, or by a change of the cation population with temperature. Although at low temperature it is more natural to ascribe it to the former, it is still unusual. For example, in magnetite (iron spinel), there is nearly no difference between the Debye characteristic temperatures of both sites. In order to determine the origin of the observed changes we will compare Mössbauer spectra and extended x-ray absorption fine structure spectra acquired in single crystals and power samples.

¹ Handbook of Magnetism and Advanced Magnetic Materials. (Wiley-Blackwell, 2007).

² M. Takahashi and M.E. Fine, J. Appl. Phys. **1972**, *43*, 4205.

³ S.J. Kim, S. W. Lee and C.S. Kim, Jap. J. Appl. Phys. **2001**, *40*, 4897.

⁴ J. de la Figuera et al., Croatica Chemica Acta **2015**, *88*, 453.

REVERSIBLE STORAGE OF CH₄/CO₂ AS GAS HYDRATES IN CONFINED NANOSPACE

José L. Jordá^a, Mirian E. Casco^b, Fernando Rey^a, François Fauth^c, Manuel Martínez-Escandell^b, Francisco Rodríguez-Reinoso^b, Enrique V. Ramos-Fernández^b and Joaquín Silvestre-Albero^b

^a *Instituto de Tecnología Química (UPV-CSIC) Universitat Politècnica de València-CSIC, Avda. de los Naranjos s/n, 46022 Valencia (Spain) jjorda@itq.upv.es*

^b *Laboratorio de Materiales Avanzados, Instituto Universitario de Materiales-Departamento de Química Inorgánica, Universidad de Alicante, Ctra. San Vicente-Alicante s/n, 03690 San Vicente del Raspeig (Spain)*

^c *ALBA Light Source, 08290 Cerdanyola del Vallés, Barcelona (Spain)*

Methane hydrates constitute the largest known reserve of fossil hydrocarbons.¹ However, the exploitation of those reserves using conventional methods is extremely complex from a technical point of view, due to the location of the reservoirs and the potential risks of destabilization and massive release of the confined gas to the atmosphere. So, new methods for the use of these hydrates for gas storage and release have been studied in the last years. It has been found that the formation of methane hydrates takes place at relatively mild conditions (around -3°C and 5 MPa of pressure), providing a high storage capacity per mass and volume unit. Also, it was found that methane can be substituted by other small molecules, as CO₂.²

Our research focused on the study of different materials that could provide an appropriate support for the formation of those hydrates under mild conditions.^{3,4,5} Those materials could facilitate not only the formation of the methane hydrate but also the replacement of CH₄ with CO₂, and its subsequent storage, allowing the transport of the methane from the deposits to the power plant, its controlled release, and the removal of the formed carbon dioxide as a new hydrate. In the present work, a high surface activated carbon was used as the support, and the process was followed using *in situ* synchrotron powder X-ray diffraction at the beamline MSPD at the Spanish synchrotron ALBA.

Our results indicate that the selected support is an excellent material to promote the nucleation and growth of methane and carbon dioxide hydrates. This process is very fast and highly reversible, being the CO₂ hydrate more stable than the CH₄ hydrate. Changes in the gas atmosphere composition and pressure gives rise to the exchange of these two molecules. This is attributed to the ability of the ice-like water molecules to adapt to the gas phase environment. These results open the possibility of using these materials not only for the CH₄/CO₂ hydrate conversion but also for short and long-term gas storage, gas separation, sensors, and so on.

Acknowledgements. Authors thank financial support from MINECO projects MAT2013-45008-p, MAT2015-71842-P (MINECO/FEDER), Consolider Ingenio 2010-Multicat CSD-2009-00050, Severo Ochoa SEV-2012-0267, Strategic Japanese-Spanish Cooperation Program (PLE2009-0052) and Concert Project-NASEMS (PCIN-2013-057), as well as PROMETEO projects from the Generalitat Valenciana. E.V.R.F. thanks for his Ramon y Cajal grant (RyC-2012-11427). Authors thank synchrotron ALBA for beamtime availability at beamline MSPD.

¹ T. S. Collet, *Aapg. Bull.* **2002**, 86, 1971-1992.

² E. D. Sloan Jr., C. A. Koh, *Clathrate Hydrates of Natural Gases*, 3rd ed., CRC Press, Boca Raton, FL, USA, **2007**.

³ M. E. Casco et al., *Nature Commun.* **2015**, 6:6432, 1-8

⁴ M. E. Casco et al., *Chem. Eur. J.* **2016**, 22, 10028-10035

⁵ M. E. Casco et al., *Chem. Sci.* **2016**, 7, 3658-3666

Potential antiparasitic DNA minor groove binding drugs against *Trypanosoma brucei*, causative agent of Sleeping sickness.

C.R. Millán^a, F.J. Acosta-Reyes^{ab}, N. Saperas^a, C. Dardonville^c, H. DeKoning^d & J.L. Campos^a

^aDepartment of Chemical Engineering, Universitat Politècnica de Catalunya, E08019 Barcelona (Spain); Lourdes.campos@upc.edu

^bHoward Hughes Medical Institute, Columbia University, New York, NY 10032, USA

^cInstituto de Química Médica, IQM-CSIC, 28006 Madrid, Spain; dardonville@iqm.csic.es

^dInstitute of Infection, Immunity and Inflammation, College of Medical, Veterinary and Life Sciences, University of Glasgow, Glasgow G12 8TA, UK; Harry.De-Koning@glasgow.ac.uk

Approximately 70 million people distributed over a surface of 1.55 million km² are estimated to be at different levels of risk of contracting **sleeping sickness**. *Trypanosoma brucei* accounts for 82.2% of the population at risk. About 6 million to 7 million people worldwide, mostly in Latin America, are estimated to be infected with *Trypanosoma cruzi*, the parasite that causes **Chagas disease**. We study drugs interacting with minor groove DNA, such as the N-phenylbenzamide bis(2-aminoimidazoline) derivatives¹. The main objective was to identify their cellular target inside the parasite. We were able to demonstrate that the drugs have a clear effect on the S-phase of *T. brucei* cell cycle by inflicting specific damage on the kinetoplast. The Kinetoplast has more than 70% of AT-DNA.



Figure 1. Structure of the DNA duplex d(AAATTT)2 with the compound FR60 at 1.25 Å resolution

The crystal structure of the complex of the oligonucleotide d[AAATTT]2 with FR60 was solved at 1.25 Å (PDB-ID: 5LIT) it shows that the drug covers the minor groove of DNA. We conclude that FR60 is a powerful trypanocides that act directly on the kinetoplast.

Acknowledgements. We thank all the Staff for valuable assistance at the ALBA BL13-Xaloc beamline.

Spatially localized molecular orientation in polymer films by synchrotron FTIR imaging

M Kreuzer^a, M. Impéror-Clerc^b, S. Rouziere^b, R. Pfaendner^c, B. Laycock^d, M. Stec^c and C. J. Garvey^d

^a *Alba Synchrotron Light Source, Cerdanyola del Vallès, Barcelona, (Spain);*

mkreuzer@cells.es

^b *Laboratoire de Physique des Solides, Université Paris-Sud, Orsay, (France);*

marianne.imperor@u-psud.fr, stephan.rouziere@u-psud.fr

^c *Fraunhofer Institute of Structural Durability and System Reliability LB, Darmstadt,*

(Germany); Rudolf.Pfaendner@lbf.fraunhofer.de, m.stec@uq.edu.au

^d *School of Chemical Engineering and the Dow Centre for Sustainable Engineering Innovation, The University of Queensland, St Lucia QLD 4072 (Australia);* b.laycock@uq.edu.au

^e *Australian Centre for Neutron Scattering, ANSTO, Locked Bag 2001, Kirrawee DC NSW 2232, (Australia);* cjg@ansto.gov.au

Poly(lactic) acid (PLA) is a biopolymer which suffers from poor mechanical properties and high cost. The addition of polyethylene (PE) introduces a toughening effect which dramatically improves these material properties. However, while PE is a low cost semi-crystalline thermoplastic, it is difficult to blend with PLA. Here we report on static characterization of films produced by blown film extrusion and initial measurements using the polarized FTIR microscopy capability of the MIRAS beamline at ALBA. Our aim is to understand the reorientation of polymer chains during extension and to provide a molecular understanding of the enhancement of properties of PLA films by the addition of PE. Two-dimensional wide-angle x-ray scattering (WAXS) patterns from the films as prepared are typical of a semi-crystalline polymer blend, consisting of isotropic and size broadened Bragg peaks superimposed over a broad amorphous and isotropic halo, revealing that the PE is at least partially crystalline and there is no preferential orientation of the PE crystallites. The fractional crystallinity of the film and dimensions of the crystalline regions of PE are estimated by deconvolution of the amorphous halo and Bragg peaks from the 1-dimensional radial average and applying the Scherrer equation to the broadening of diffraction peaks¹. By contrast small angle x-ray scattering (SAXS) from the films is anisotropic: at the lowest angles around the beam stop there is a marked anisotropy; and at wider solid angles there is a broad anisotropic feature typical of the poorly ordered lamella of semi-crystalline polymers. This feature exhibits two different characteristic repeat spacing in directions orthogonal to each other. We apply the linear correlation function (LCF)² to the sector averages of the SAXS from both directions to extract repeat spacing and the fractional crystallinity of these lamellae. ATR-FTIR measurements on the static films were consistent with the perspectives of both SAXS and WAXS as a semi-crystalline blend. To understand and provide chemically selective visualization of the orientation of polymer chains during extension we performed polarized FTIR microscopy. Additionally the visual appearance of the films was homogeneous. Spatially resolve FTIR microscopy in transmission mode revealed no resolvable chemical heterogeneity before stretching. As the films were stretched visually dark bands appeared in the films. These bands were associated with chemical and orientational heterogeneity.

¹ Garvey, C.J., I.H. Parker, and G.P. Simon, On the interpretation of X-ray diffraction powder patterns in terms of the nanostructure of cellulose I fibres. *Macromolecular Chemistry and Physics*, 2005. 206(15): p. 1568-1575.

² Hsu, Y.C., et al., A fundamental study on photo-oxidative degradation of linear low density polyethylene films at embrittlement. *Polymer*, 2012. 53(12): p. 2385-2393.

Poster Contributions

P-24

KYDNEY STONES STUDIES BY SYNCHROTRON RADIATION: APPLICATION OF IMAGING TECHNIQUES

I. H. Valido^a, A. Pell^a, A. M. Díaz-Rovira^a, M. Resina-Gallego^a, M. A. Subirana-Manzanares^a, C. Marini^b, L. Simonelli^b, M. Valiente^a, M. López-Mesas^a

^a Centre Grup de Tècniques de Separació en Química (GTS), Departament de Química, Universitat Autònoma de Barcelona, Facultat de Ciències. Edifici CN. 08193 Bellaterra (Spain); Montserrat.lopez.mesas@uab.cat

^b ALBA Synchrotron Light Facility, Carrer de la Llum 2-26, 08290 Cerdanyola del Vallès (Spain)

Renal Nephrolithiasis is a clinical condition that implies the formation of microcrystals aggregates on the kidney, commonly known as kidney stones. This disease affects approximately 12% of men and 6% of women, and has a recurrence rate around 40%. The 66% of the renal calculi are represented by calcium oxalate stones, considering both the mono (COM) and the dihydrate (COD) forms.¹ The studies on the formation of this kind of stones and the interaction between different phases are important in order to understand the pathophysiology, plan a therapy and prevent the recurrence.

The main objectives of this study are the understanding of the chemical distribution of calcium oxalate species in kidney stone, as well as the determination of the nucleation point and the phases that interact with it. Different non-destructive techniques have been used: μ -XRF (Micro X-Ray Fluorescence) imaging, μ -XAS (Micro X-Ray Absorption Spectroscopy) and μ -IR imaging. The data were collected at CLÆSS beamline (μ -XRF and μ -XAS) and at SMIS beamline (μ -IR) of ALBA and SOLEIL Synchrotron facilities respectively.

μ -XRF maps with around 150 μ m of spatial resolution have been acquired at different energies chosen around the Ca K-edge, where the expected representative species (COM, COD, hydroxyapatite -HAP- and CaCO₃) were showing the highest spectral contrast. The chemical distributions of the major species in the stone surface have been extracted by operating with the different images and have been confirmed by Ca K-edge XAS spectra collected in the different regions. In the case of the μ -IR experiment, it was possible to obtain the same information by introducing the profile of the references spectra. The advantage of the recently implemented μ -XRF imaging at CLÆSS lies in the fact that space resolved μ -XAS are directly accessing to the absorption spectra in different regions, permitting the identification of the corresponding species or their convolution. Instead, in the case of the μ -IR imaging it is possible to access similar information but the results are highly dependent on the approximations applied during the data treatment. To conclude, it is possible to determine the chemical distribution of the calcium oxalate species in the kidney stone by using μ -XRF, μ -XAS and μ -IR imaging techniques and to differentiate the HAP nucleation point (Randall's Plaque). From this work, the implementation of μ -XRF at CLÆSS beamline allows to achieve the marked objectives with a faster procedure that requires less data manipulation than the μ -IR imaging, usually applied for this kind of studies.

Acknowledgements. The authors thank the Spanish Ministry MINECO, project CTM 2015-65414-C2-1-R for financial support.

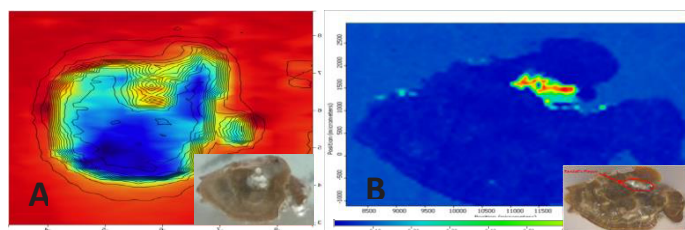


Figure 1: A) map performed in CLÆSS with XAS technique, and B) map performed in SMIS with μ -IR technique. Same stone in both cases, but re-polished in B in order to measure in reflectance, remarking the nucleation point, an hydroxyapatite concretion known as Randall's Plaque

¹ F. Blanco-Lucena, "Chemical speciation on urinary lithiasis. Image analysis and separation techniques for the study of lithogenesis". Universitat Autònoma de Barcelona, Doctoral thesis 2014. (<http://hdl.handle.net/10803/285557>)

Structural properties of β -metal(II) hydroxides: XAS and Raman combined spectroscopic studies on lattice stability

P-25

C. Marini^a, W. Olszewski^a, N. Ramanan^a, S. Caramazza^b, B. Joseph^c, L. Simonelli^a, P. Postorino^b

^a ALBA Synchrotron Light Source, Crta. BP 1413, Km. 3.3, 08290 Cerdanyola Del Vallès, Barcelona, Spain, cmarini@cells.es

^b Physics Department, Sapienza University of Rome, P.le Aldo Moro 5, 00185 Roma, Italy

^c Elettra Sincrotrone Trieste, SS14, Km 163.5, 34149 Basovizza TS, Italy

We present a combined temperature-dependent Ni and Co K-edge x-ray absorption and high pressure Raman spectroscopic investigation of β -Ni(OH)₂ and β -Co(OH)₂. Extended x-ray absorption fine structure analysis has made possible the characterization of the dynamics and strengths of the metal-oxygen and metal-metal bonds, leading to the determination of the associated Debye Temperature and distances. Debye Temperatures are then used to fully characterize the elastic constants and Einstein frequencies of the two systems. The Raman data show a continuous hardening of the phonon modes with increase in pressure, associated with the vibration of metal-oxygen sub-lattices, whereas a systematic frequency softening is displayed by the hydroxyl (OH) symmetric stretching mode in both compounds. These contrasting behaviors imply a gradual development of lattice instability with pressure mainly due to the displacement of H atoms around the metal-oxygen axis. The presented data allow a direct comparison of the two local-lattice instabilities.

ASSESSING GRAPHENE OXIDE TOXICITY IN CANCER CELLS BY FTIR MICROSPECTROSCOPY

M. Kreuzer^a, P. M. Costa^b and K. Al-Jamal^b

^a ALBA, MIRAS infrared spectroscopy beamline, E08290 Cerdanyola de Vallès (Spain);

mkreuzer@cells.es

^b Institute of Pharmaceutical Science, Faculty of Life Sciences & Medicine, King's College London, SE1 9NH London (UK)

Malignant glioma is the most common and lethal type of brain tumour, due to its high invasive capacity, therapy resistance and difficult early diagnosis. Current therapeutic options are largely unsatisfactory, with an average patient survival after diagnosis of 9 to 12 months. Malignant gliomas are fuelled by a small population of stem-like cells, designated glioma cancer stem cells (GSCs), that are extremely resistant to conventional therapies and promote tumour relapse. There is therefore a need to target not only the bulk of tumour cells but also GSCs, aiming at achieving complete glioma eradication.

Graphene-based composites have attracted significant interest in the area of biomedicine, due to their exceptional physicochemical properties and unique biocompatibility.¹ These materials have been successfully exploited as nanocarriers for delivery of a variety of chemotherapeutic drugs and nucleic acids. Moreover, graphene composites can potentially be used in radio-frequency therapy due to their tuneable and intrinsic electrical/optical properties, and for simultaneous therapeutic, sensing and bio-imaging purposes.

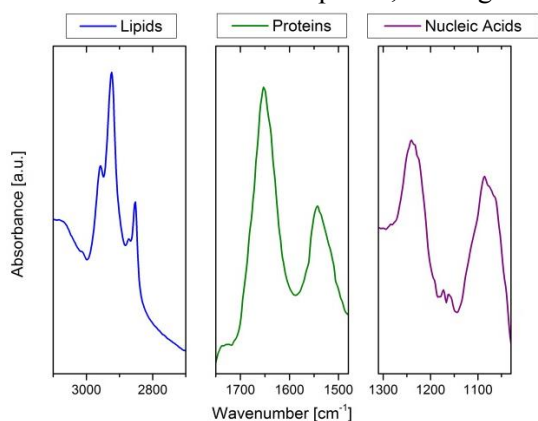


Figure 1. Typical spectral signatures of glioma cancer cells (GL261).

In this study we present Fourier transform infrared (FTIR) microspectroscopy experiments to obtain deeper insights into the biochemical mechanisms underlying the toxicity of functionalized and oxidised graphene (click2 GO) on stem (G26, G7, IENS) and non-stem (GL261) glioma cancer cells. The main intracellular biomolecules such as nucleic acids, proteins and lipids have characteristic infrared vibrational modes and thus, give distinct FTIR signals (Figure 1).² Multivariate analysis of the spectra recorded using principal component analysis (PCA) revealed clear differences in the DNA, protein and lipid regions in the presence of click2 GO

on the stem and non-stem like glioma cancer cells. This information is essential to better characterise the damage in the GSCs provoked by the interaction with click2 GO.

Acknowledgements. These experiments were performed at MIRAS beamline at ALBA.

¹ K.-C. Mei, N. Rubio, P. M. Costa, H. Kafa, V. Abbate, F. Festy, S. S. Bansal, R. C. Hider, and K. T. Al-Jamal, *Synthesis of double-clickable functionalised graphene oxide for biological applications*, Chem. Commun., vol. 51, no. 81, pp. 14981–14984, **2015**.

² M. J. Baker, J. Trevisan, P. Bassan, R. Bhargava, H. J. Butler, K. M. Dorling, P. R. Fielden, S. W. Fogarty, N. J. Fullwood, K. a Heys, C. Hughes, P. Lasch, P. L. Martin-Hirsch, B. Obinaju, G. D. Sockalingum, J. Sulé-Suso, R. J. Strong, M. J. Walsh, B. R. Wood, P. Gardner, and F. L. Martin, *Using Fourier transform IR spectroscopy to analyze biological materials*, Nat. Protoc., vol. 9, no. 8, pp. 1771–91, **2014**.

Surface relaxation and charge density: the case of Au(111)

M. A. Valbuena^{a,b}, C. Quirós^{c,d}, E. Salagre^a, A. Oliva^a, M. Plaza^a, J. Martínez-Blanco^a, J. Rubio-Zuazo^{e,f}, P. Segovia^{a,g}, E.G. Michel^{a,g}

^a Departamento de Física de la Materia Condensada, Universidad Autónoma de Madrid, 28049 Madrid, Spain.

^b Catalan Institute of Nanoscience and Nanotechnology (ICN2), CSIC and The Barcelona Institute of Science and Technology, Campus UAB, Bellaterra, 08193 Barcelona, Spain.; miguel.valbuena@icn2.cat.

^c Departamento de Física, Universidad de Oviedo, 33007 Oviedo, Spain.

^d Centro de Investigación en Nanomateriales y Nanotecnología (CINN)(CSIC-Universidad de Oviedo), 33940 El Entrego, Spain.

^e Instituto de Ciencia de Materiales de Madrid, Consejo Superior de Investigaciones Científicas, Cantoblanco, Madrid, 28049, Spain.

^f BM25-SpLine The Spanish CRG Beamline at the ESRF, Grenoble, 38043 Cedex 9, France

^g Condensed Matter Physics Center (IFIMAC), Universidad Autónoma de Madrid, 28049 Madrid, Spain.

The formation of a surface usually generates a spontaneous contraction of the surface plane to re-establish the equilibrium (surface relaxation)¹. There are many surfaces where the spontaneous contraction is very small or even it is an expansion instead of a contraction². Interestingly, there are several prominent cases of surfaces exhibiting an anomalous expansion that also present a surface electronic state with a significant density of states^{2,3,4,5}. Theoretical calculations have found that the sign and magnitude of the relaxation of the topmost atomic layers of Al(100) is mainly determined by the rearrangements of the surface state charge³. In short, the presence of a surface state increases the surface charge density, and this affects the surface relaxation. Analogous calculations show that Au(110) and Au(100) (without a high density of surface states) present a conventional surface relaxation (contraction), while Au(111) (with a prominent Shockley surface state) is characterized by an anomalous expansion⁶. These findings point towards a strong involvement of the density of surface states in the relaxation finally observed.

We report combined surface x-ray diffraction (SRXD) and Angle Resolved Photoemission Spectroscopy (ARPES) results, correlating the change in surface relaxation as the occupation of the electronic surface state is modified. To this end, we tune the Au(111) surface state filling in a controlled way, by depositing suitable acceptor or donor molecular species. Then, we measure the surface relaxation as a function of the surface state charge by SXRD. The SXRD analysis includes the measurement of several Crystal Truncation Rods as a function of coverage of the donor or acceptor species. The results are fitted using standard procedures and provide the surface relaxation. The charge contents in the Au(111) surface state is also experimentally determined as a function of coverage from ARPES measurements of the Fermi contour of the Au(111) surface state. Our results establish a direct relationship between surface relaxation and charge contents in the Au(111) surface state and shed light on the nature and deep origin of the surface relaxation process.

¹ S.Y. Tong "Surface Crystallography by LEED: Theory, Computation, and Structural Results", Springer.

² H.L. Davis et al, Phys. Rev. Lett. **68**, 2632 (1992).

³ V. Chis and B. Hellsing, Phys. Rev. Lett. **93**, 226103 (2004).

⁴ F. Reinert et al, Phys. Rev. B **63**, 115415 (2001).

⁵ J. Sun et al, New Journal of Phys. **12**, 063016 (2010).

⁶ Li Guan et al, Solid. State. Commun. **149**, 1561 (2009).

X-RAY DICHRISM AND CHIRALITY: SPIN FILTERING EFFECTS IN ORGANIC THIN FILMS

M.A. Niño^a, P. Gargiani^b, F.J. Luque^c, I.A. Kowalik^d, D.Arvanitis^e, J.J. de Miguel^c

^a Instituto Madrileño de Estudios Avanzados IMDEA Nanociencia, c/Faraday, 9 E-28049 Madrid (Spain); miguelangel.nino@imdea.org

^b ALBA-CELLS Synchrotron E, Barcelona (Spain) pgargiani@cells.es

^c Dpto. Física de la Materia Condensada C-III, Universidad Autónoma de Madrid, Campus de Cantoblanco E-28049 Madrid (Spain) juanjose.demiguel@uam.es

^d Institute of Physics, Polish Academy of Science, al. Lotników32/46, 02-668 Warsaw (Poland) ikowalik@ifpan.edu.pl

^e Dpt. of Physics and Astronomy, Uppsala University, P.O. Box 516, 751-20 Uppsala (Sweden) dimitri.arvanitis@physics.uu.se

Chiral structures, and in particular chiral molecules, are fascinating objects in many areas: in Physics the relationship between chirality and magnetism has puzzled researchers since the 19th century, and only in the 21st century we have learn to make use of this relationship, for example using the ability of chiral layers to scatter electrons differently depending on their spin. Chiral surfaces open the door, from a technological point of view, to use different properties like chiral selectivity, enantiospecific chemical reactions¹ or the possibility to use these materials as spin filters².

We have used synchrotron based spectroscopic techniques (XAS, XMCD, spin polarized UPS) to study the influence of the chirality on the magnetism. We have grown monolayer-thick films of 1,2-diphenyl-1,2-ethane diamine (DPEDA) and 1,2-diphenyl-1,2-ethane diol (DPED) on Cu(001) and on Co/Cu(100) surfaces in UHV by Molecular Beam Epitaxy (MBE). This molecule has two chiral centers and presents two enantiomers, which are designated according to their conformation and optical activity as (R,R)-(+)-DPED/A and (S,S)-(-)-DPED/A. We observe clearly dichroic features (natural circular dichroism) by measuring the absorption by the molecular film of circularly polarized X-rays (XAS) of opposite helicity, at the carbon K edge. This dichroic asymmetry depends on the chirality (opposite sign for the two enantiomers) showing the preservation of the chiral character of these molecular thin films in the electronic structure upon adsorption.

The effect of this chiral molecular film adsorbed on ferromagnetic cobalt has been measured though XMCD at the Co L-edges, showing a change in the magnetic moment in the cobalt atoms at the surface, with the implication of a charge transfer with spin polarization. More indeed, we have observed macroscopic spin polarizations in electron currents photoemitted from molecular films of DPED and DPEDA adsorbed on Co/Cu(100) surfaces, showing that chiral molecules in a non-spiral geometry can filter spin electrons. These measurements also show that the different enantiomers of the same molecule can produce spin polarizations oriented along different directions in space³.

Acknowledgements. This work was supported by MICCINN/MINECO (Spain) through the programme MAT2014-59315-R.

¹ A. Gellman et al. *J. Am. Chem. Soc.* **2013**, *135*, 19298.

² B. Göhler et al. *Science* **2011**, *331*, 894.

³ M. A. Niño et al *Adv. Mat.* **2014**, *26*, 7474.

STRUCTURAL STUDY OF THE LOCAL ORDER IN AMMONIA-MODULATED FE(II) HYDROXYPHOSPHONOACETATE PROTON CONDUCTORS

M. Bazaga-García^a, A. Cabeza^a, R.M.P. Colodrero^a, I.R. Salcedo^a, P. Olivera-Pastor^a and E.R. Losilla^a

^a *Departamento de Química Inorgánica, Cristalografía y Mineralogía, Facultad de Ciencias, Campus de Teatinos s/n, Universidad de Málaga, 29071 Málaga (Spain); m.bazaga@uma.es*

Layered Fe(II) carboxiphosphonate, Fe-HPAA·2H₂O¹, is a crystalline multifunctional coordination polymer exhibiting properties as photocatalyst² and proton conductor. Post-synthesis modification by ammonia/water adsorption³ strongly enhances its proton conductivity. However, this process entails a progressive amorphization but in no case intercalation of the guest species was detected. Understanding the mechanism involved in this increased conductivity is crucial to develop novel high performance proton conductors for PEMFCs. Thus, total scattering and PDF study has been carried out to explore the mechanism of ammonia adsorption and subsequent amorphization.

Different length scales have been investigated to characterize the average and local structure at variable ammonia loaded in order to ascertain possible structural modifications after gas/solid reactions. While significant short range order (from 1.4 to 10 Å) variations were observed even for low loadings, the average structure seems to be basically preserved except for the highest ammonia/water contents.

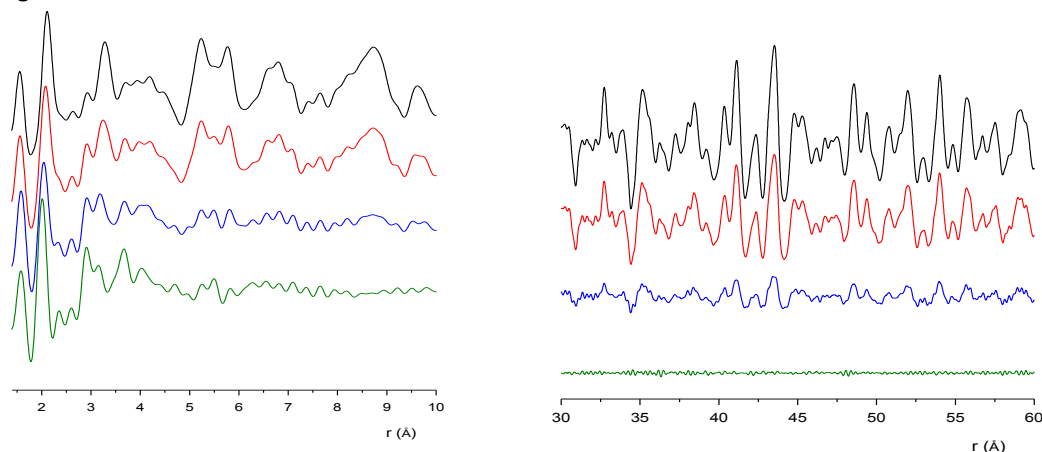


Figure 1. Radial distribution functions for FeHPAA exposed to NH₃ gas at several times (0h black, 36h red, 48h blue and 72h green)

Acknowledgements. The work at UMA was funded by MAT2016-77648-R, MAT2013-41836-R (MINECO, Spain) and FQM-1656 (Junta de Andalucía) research grants and CELLS-ALBA Synchrotron is thanked for the provision of synchrotron X-ray beamtime at BL04-MSPD.

¹ R. Fu, S. Xiang, H. Zhang, J. Zhang, and X. Wu, *Cryst. Growth Des.* **2005**, *5*, 1795-1799.

² M Bazaga-García, A. Cabeza, P. Olivera-Pastor, I. Santacruz, R. M. P. Colodrero, and M. A. G. Aranda, *J. Phys. Chem. C* **2012**, *116*, 14526–14533.

³ M. Bazaga-García, R. M. P. Colodrero, M. Papadaki, P. Garczarek, J. Zoń, P. Olivera-Pastor, E. R. Losilla, L. Le n-Reina, M. A. G. Aranda, D. Choquesillo-Lazarte, K. D. Demadis and A. Cabeza, *J. Am. Chem. Soc.* **2014**, *136*, 5731–5739.

REAL-TIME SAXS STUDIES AS A FUNCTION OF TEMPERATURE OF SEBS BLOCK COPOLYMER WITH GRAPHENE

P. Enrique-Jimenez^a, S. Quiles^b, H. J. Salavagione^b, M. A. Gómez-Fatou^b, F. Ania^a and A. Flores^a

^a *Departamento de Física Macromolecular, Instituto de Estructura de la Materia (IEM-CSIC), Serrano 119, 28006 Madrid, Spain (araceli.flores@csic.es)*

^b *Departamento de Física de Polímeros, Elastómeros y Aplicaciones Energéticas, Instituto de Ciencia y Tecnología de Polímeros (ICTP-CSIC), Juan de la Cierva 3, 28006 Madrid, Spain*

Block copolymers have been widely studied due to their tendency to self-assemble into a range of ordered structures such as spheres, cylinders and lamellae at a nanometer scale. Poly(styrene-*b*-ethylene-*co*-butylene-*b*-styrene), SEBS, is a triblock copolymer with physical properties similar to those of rubber but can be processed as a thermoplastic. The incorporation of graphene to SEBS using specific chemical approaches can impart electrical conductivity¹ and produce electromechanical materials with potential applications in flexible electronics or body motion sensing. The understanding of the influence of graphene on the structure of the SEBS matrix is of fundamental importance to optimize the final properties.

In this work, the nanostructure of SEBS/graphene nanocomposites, as a function of temperature and graphene content, has been investigated. SAXS measurements were carried out using synchrotron radiation in the BL11-NCD beamline at ALBA (Barcelona, Spain). Pristine SEBS and the nanocomposites containing graphene modified with polystyrene or polyethylene brushes have been studied. The modification of the graphene surface was expected to enhance the interaction with the styrene or the olefin blocks of SEBS. For both nanocomposites, graphene was incorporated in small quantities (0.8 and 1.5 vol.%). Portions of SEBS and SEBS/graphene films casted from solution were positioned perpendicularly and parallel to the incident beam inside a Linkam hot stage (THMS600) and the 2D patterns were analyzed using the fit2D software.

SAXS patterns in the perpendicular configuration have revealed that SEBS exhibits a planar oblique cell at room temperature (RT). Real time temperature scans have shown a transformation into hexagonal symmetry at ≈ 180 °C, well above the glass transition temperature of polystyrene. This transformation is irreversible and the hexagonal packing remains upon cooling. Results support the hypothesis that the oblique cell is associated to local lattice deformations arising from mechanical stresses during the solvent evaporation process. This should be most pronounced in the direction of the film thickness and, indeed, experiments in the parallel configuration have revealed a marked elliptical SAXS pattern. In contrast, SEBS/graphene materials in the perpendicular arrangement exhibit a hexagonal arrangement of cylinders at RT that remains up to ≈ 300 °C. Such behavior has been associated to graphene interfering in the affine lattice deformation. Results in the parallel arrangement are also in good agreement with this contention and the eccentricity of the elliptical traces have been found to decrease with increasing graphene content for both types of nanocomposites.

Financial support: MINECO (grants MAT2013-47898-C2-1-R and MAT2013-47898-C2-2-R). PEJ and SQ also acknowledge a FPI Fellowship.

¹ H. J. Salavagione, S. Quiles-Díaz, P. Enrique-Jiménez, G. Martínez, F. Ania, A. Flores and M. A. Gómez-Fatou, *Macromolecules* 2016, 49, 498-4956.

SYNCHROTRON X-RAY DIFFRACTION MEASUREMENTS ON BIODEGRADABLE FILMS OF PHBV/CELLULOSE NANOCRYSTALS

P-31

R. Bouza, L. Barral, S. Malmir and Y. Farrag

Universidade da Coruña, Grupo de Polímeros, Departamento de Física, Escuela Universitaria Politécnica, Serantes, Avda. 19 de Febrero s/n 15471, Ferrol, Spain rbouza@udc.es

The effect of CNC incorporation on crystalline structure of PHBV, small and wide-angle X-ray diffraction (SAXS/WAXS) was done simultaneously at the BL-11 non-crystalline diffraction beamline of the ALBA Synchrotron (Spain). ADSC (Quantum 210r CCD) and Rayonix (LX255-HS) were used as detectors. Considering WAXS diffractograms similar behavior was observed for both PHBV and PHBV/CNC6 samples, exhibiting the characteristics diffraction peaks of orthorhombic crystalline structure¹. Crystallization process occurred at higher temperature for the filled sample. This suggested evidence of nucleating agent effect of CNC particles. WAXS patterns in heating scan showed the existence of more perfect crystalline structures in PHBV/CNC6 sample. From SAXS patterns, the SAXS maxima position (s_{max}) shifted to smaller values as temperature increased. Using the position of mentioned parameter, summation of thickness of repeating crystalline (L_c) and amorphous (L_a) regions: long spacing (L) was calculated since $s_{max}=1/L^2$. The results are given in Fig 1. For both samples, a notable increment was seen at a border near 140 °C. In the temperature range before this, long spacing increased with slightly slower rate for the nanocomposite sample, which supposed to be in relation with the presence of CNC particles that restrict the free chain mobility. In addition, it was measurable up to around 164 °C for this sample, which was higher than that for neat PHBV (around 158 °C).

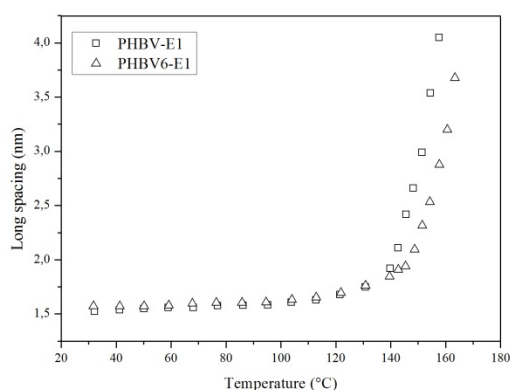


Fig. 1: Variation in long spacing as a function of temperature of PHBV and PHBV/CNC6 samples.

Acknowledgements. These experiments were performed at Non Crystalline Diffraction beamline at ALBA Synchrotron with the collaboration of ALBA staff.

¹ H. Sato, N. Suttiwijitpukdee, T. Hashimoto, Y. Ozaki, *Macromolecules* **2012**, 45, 2783–2795.

² A. Muñoz-Bomilla, M. L. Cerrada, M. Fernández-García, A. Kubaka, M. Ferrer, M. Fernández-García. *Int. J. Mol. Sci.* **2013**, 14, 9249-9266.

PXRD and PDF analysis of multifunctional lanthanide nitrilotris-methylphosphonate-based proton conductors

R.M.P. Colodrero^a, A. Cabeza^a, I. R. Salcedo^a, M. Bazaga-García^a, and P. Olivera-Pastor^a.

^a *Departamento de Química Inorgánica, Cristalografía y Mineralogía, Facultad de Ciencias, Campus de Teatinos s/n, Universidad de Málaga, 29071 Málaga (Spain); colodrero@uma.es*

Metal phosphonates are multifunctional solids which possess tunable properties, such as H-bond networks, while exhibiting high chemical and thermal stability¹.

Depending on the protonation of the ligand, different crystalline phases can be obtained. Here, we report three different families of proton conductors based on lanthanide nitrilotris-methylphosphonates. Compounds having cationic layers compensate by chloride or sulfate anions were isolated: $[\text{Ln}(\text{H}_4\text{NMP})(\text{H}_2\text{O})_2]\text{Cl}\cdot 2\text{H}_2\text{O}$ ² and $\text{Ln}(\text{H}_5\text{NMP})\cdot\text{SO}_4\cdot 4\text{H}_2\text{O}$ [H_6NMP = nitrilotris(methylphosphonic acid)]. The crystal structure of $\text{Gd}(\text{H}_5\text{NMP})\cdot\text{SO}_4\cdot 4\text{H}_2\text{O}$ was solved ab initio from synchrotron powder diffraction data ($\lambda=0.4124$ Å, beamline BL04-MSPD ALBA) and refined by the Rietveld method. Chloride containing phases show two irreversible solid state transformations take place: (1) a crystalline-to-crystalline phase transition, $\{\text{Ln}-\text{H}_4\text{NMP} \rightarrow [\text{Ln}_2(\text{H}_3\text{NMP})_2(\text{H}_2\text{O})_4]\cdot 4.5\text{H}_2\text{O}$ for $\text{Ln}=\text{La}, \text{Pr}\}$, and (2) crystalline-to-amorphous phase transition, $\{\text{LnH}_4\text{NMP} \rightarrow [\text{Ln}(\text{H}_3\text{NMP})]\cdot 1.5\text{H}_2\text{O}$ for $\text{Ln}=\text{Gd}-\text{Ho}\}$, both implies the loss of HCl and structural rearrangements of the frameworks. Variations in average and local structure have been monitored by high resolution powder diffraction and PDF analysis, upon exposure the samples at high relative humidity and temperature (95% RH and 80 °C), in order to understand their behavior as proton conductors.

Acknowledgements. The work at UMA was funded by MAT2016-77648-R, MAT2013-41836-R (MINECO, Spain) and FQM-1656 (Junta de Andalucía) research grants and CELLS-ALBA Synchrotron is thanked for the provision of synchrotron X-ray beamtime at BL04-MSPD.

¹ P. Ramaswamy, N. E. Wong and G. K. H. Shimizu, *Chem. Soc. Rev.* **2014**, *43*, 5913-5932.

² M. Bazaga-García, G. K. Angeli, K. E. Papathanasiou, I. R. Salcedo, P. Olivera-Pastor, E. R. Losilla, D. Choquesillo-Lazarte, G. B. Hix, A. Cabeza and K. D. Demadis. *Inorg. Chem.* **2016**, *55*, 7414-7424.

XAS study of Cu-Bi thin films and nanowires for spintronics applications

S. Ruiz-Gomez^a, L. Pérez^{a,b}, C. Gonzalez-Ruano^a, I. Lucas^c,
M. Plaza^d, A. Serrano^e, M. A. Gonzalez^a and A. Mascaraque^a

^a Dept. Física de Materiales, Universidad Complutense de Madrid, Madrid, Spain

^b IMDEA

^c Instituto de Nanociencia de Aragón, Universidad de Zaragoza, Zaragoza, Spain.

^d Dept. Física de la Materia Condensada, Universidad Autónoma de Madrid, Madrid, Spain.

^e European Synchrotron Radiation Facility, Grenoble, France..

Materials that may exhibit a giant Spin Hall Effect (SHE) have recently received attention due to the possibility of converting an electric current into a spin current without the need of ferromagnets¹. In addition to the small intrinsic SHE in pure metals, scattering on impurities with strong spin-orbit coupling can contribute to an enhanced SHE. In fact, there are calculations that predict that some combinations of noble metals and impurities could lead to a very large SHE. Recent theoretical papers have proposed that alloys of Bi diluted in a Cu matrix should show giant SHE^{2,3}. However, in order to attain large SHE values, two conditions are mandatory: (i) high quality samples and (ii) relatively large Bi concentrations⁴.

In almost all experimental papers appeared so far, Bi concentration is kept below 1%⁵ due to the difficulty of growing alloys with higher Bi content avoiding Bi clustering. In this work we report the increment of Bi doping well above 1% in BiCu alloys in two different geometries, thin films and nanowires, while keeping the quality of the samples. To elucidate if the Bismuth is homogeneously distributed in the sample or it is forming cluster we carried out XAS/XANES studies in the Cu and Bi edges.

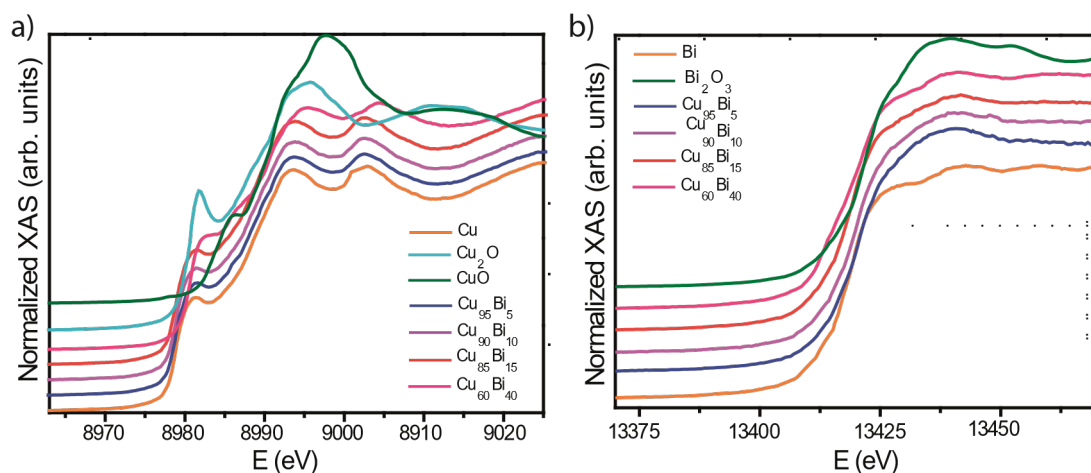


Image 1. (a) Normalized XANES spectra at Cu K-edge of the different CuBi thin films (b) Normalized XANES spectra at the Bi L3-edge of CuBi thin films.

¹ J. Sinova, S. O. Valenzuela, J. Wunderlich, C. H. Back, and T. Jungwirth *Rev. Mod. Phys.* 2015, 87, 1213

² B. Gu, Z. Xu, M. Mori, T. Ziman, and S. Maekawa. *J. Appl. Phys.* 2015, 117, 17D503.

³ P. M. Levy, H. Yang, M. Chshiev, and A. Fert. *Phys. Rev. B* 2013, 88, 214432.

⁴ D. V. Fedorov, C. Herschbach, A. Johansson, S. Ostanin, I. M., M. Gradhand, K. Chadova, D. Ködderitzsch, and H. Ebert. *Phys. Rev. B* 2013, 88, 085116.

⁵ Y. Niimi, Y. Kawanishi, D. H. Wei, C. Deranlot, H. X. Yang, M. Chshiev, T. Valet, A. Fert, Y. Otani. *Phys. Rev. Lett.* 2012, 109, 156602.

CORRELATION BETWEEN NANOSTRUCTURE AND ELECTRICAL PROPERTIES IN SEBS NANOCOMPOSITES INCORPORATING GRAPHENE MODIFIED WITH POLYETHYLENE BRUSHES

S. Quiles-Díaz^a, P. Enrique^b, H.J. Salavagione^a, A. Flores^b, F. Ania^b, and M.A. Gómez-Fatou^a

^a *Departamento de Física de Polímeros, Elastómeros y Aplicaciones Energéticas, Instituto de Ciencia y Tecnología de Polímeros (ICTP-CSIC), Juan de la Cierva 3, 28006 Madrid (Spain) magomez@ictp.csic.es.*

^b *Departamento de Física Macromolecular, Instituto de Estructura de la Materia (IEM-CSIC), Serrano 119, 28006 Madrid, Spain*

One of the main challenges in polymer/graphene nanocomposites is to obtain electrical conductivity at very low nanofiller content. This is especially attractive with elastomeric matrices since flexible conductors offer a great potential for applications in bodily motion sensors and actuators, among others. Poly(styrene-*b*-ethylene-co-butylene-*b*-styrene) (SEBS) triblock copolymer is a thermoplastic elastomer of industrial relevance and an ideal candidate to prepare electromechanical materials based on graphene. However, conductivity values in the range required for practical applications have not been achieved in this type of nanocomposites and only improvements in mechanical properties have been attained.

In this work, we have developed conductive nanocomposites of SEBS with a chemically modified graphene. Graphene has been functionalized with short polyethylene brushes by thiol-ene click chemistry in order to enhance the interactions of the filler with the ethylenic phase of the block copolymer.¹ This strategy is intended to promote the dispersion of graphene in the electron-poor domains and substantially increase the mobility of carriers with a direct impact on electrical conductivity. Special emphasis has been placed on investigating the influence of the modified nanofiller on the nanostructure and phase separated morphology of SEBS by SAXS, AFM and TEM. SAXS measurements have been carried out using synchrotron radiation in the BL11-NCD beamline at ALBA (Barcelona, Spain).

The nanocomposites present a percolation threshold for electrical conductivity slightly above 0.7 vol % and reach conductivity values of $\sim 10^{-3}$ S cm⁻¹ for ~ 2.5 vol % of graphene. The variation of the electrical conductivity with temperature has shown a different mechanism depending on filler content. While the conductivity at low filler loadings is dominated by a hopping mechanism, at the highest loadings a tunneling mechanism is suggested. SAXS experiments have demonstrated that the presence of graphene modifies the morphology of the SEBS domains, reducing their size and promoting an isotropic distribution of cylinders arranged in hexagonal packing as the filler content increases. In addition, the FWHM of the main SAXS peak at different temperatures for the conductive nanocomposites can be correlated with the different conductivity mechanisms.

Acknowledgements. Financial support from MINECO (MAT2013-47898-C2-1-R and MAT2013-47898-C2-2-R). S.Q.-D. and P.E.-J. acknowledge a FPI Fellowship. We also acknowledge the collaboration of ALBA staff (BL11), and especially to Dr. Eva Crosas for her dedication and availability.

¹ H. J. Salavagione, S. Quiles-Díaz, P. Enrique-Jiménez, G. Martínez, F. Ania, A. Flores and M. A. Gómez-Fatou, *Macromolecules* **2016**, *49*, 4948-4956.

X-RAY PHOTOELECTRON SPECTROSCOPY OF CERIA-SOOT UNDER OPERANDO CONDITIONS AT ALBA SYNCHROTRON

P-35

X. Garcia^a, L. Soler^a, A. Casanovas^a, C. Escudero^b, V. Pérez-Dieste^b and J. Llorca^a^a Institute of Energy Technologies, Department of Chemical Engineering and Barcelona Research Center in Multiscale Science and Engineering, Universitat Politècnica de Catalunya, EEBE, Eduard Maristany 10-14, 08019 Barcelona, (Spain); jordi.llorca@upc.edu^b ALBA Synchrotron Light Source, Carrer de la Llum 2-26, 08290 Cerdanyola del Vallès, Barcelona (Spain)

Soot particles constitute one of the main pollutants emitted by diesel engines and its removal has become an environmental and health requirement. Ceria-based catalysts appear to be suitable for diesel soot oxidation, since they can easily and reversibly be reduced to non-stoichiometric structures while retaining its fluorite crystal structure¹. It is generally assumed that soot oxidation over ceria conforms to the Mars-van Krevelen mechanism, in which lattice oxygen in the first few surface layers of ceria is transferred onto soot, and exposure to gaseous O₂ subsequently fills up the vacancies created on the oxide. This unique redox property, also named oxygen storage capacity (OSC), largely depends on the morphology of ceria nanoparticles, determined by different crystalline planes. It has been demonstrated that CeO₂ nanorods and nanocubes exhibit higher catalytic activity for soot oxidation than conventional polycrystalline ceria, due to the exposure of more reactive {110} and {100} planes rather than the less reactive {111} plane, prevalent among ceria nanoparticles².

We have recently studied by ambient-pressure X-ray photoelectron spectroscopy (AP-XPS) at the ALBA Synchrotron the surface of polycrystalline CeO₂ during soot oxidation under *operando* conditions, and our experiments demonstrated the capacity of ceria to oxidize soot owing to the formation of oxygen vacancies and the creation of active oxygen paramagnetic O₂⁻ superoxide species and diamagnetic O₂²⁻ peroxide species. Indeed, these active oxygen species are the main cause for soot abatement³. In this study we extend the use of *operando* AP-XPS to study the oxidation of soot by nanoshaped ceria (cubes and rods), and the results have allowed us to conclude that the exposed crystal planes by the different ceria nanoshapes have a strong influence on the formation of Ce(III) species, oxygen vacancies and active oxygen species.

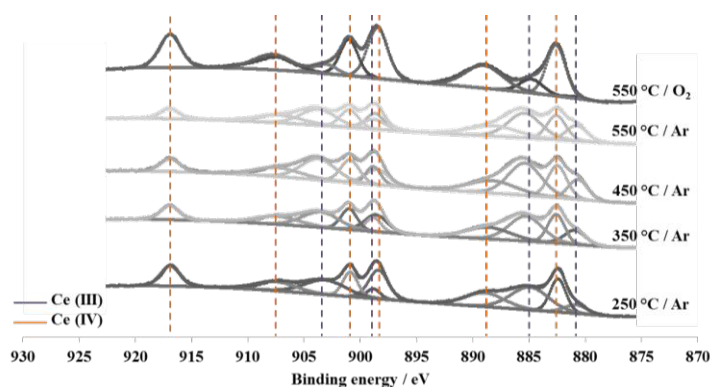


Figure 1. Ce 3d spectra recorded over CeO₂ nanorods under argon atmosphere at different temperatures and replacing argon with O₂ at 550 °C

Acknowledgements. We are grateful to MINECO/FEDER grant ENE2015-63969-R.

¹ A. Bueno-López, *Appl. Catal. B* **2014**, *146*, 1-11

² E. Aneggi, D. Water, C. De Leitenburg, J. Llorca, A. Trovarelli, *ACS Catal.* **2014**, *4*, 172-181

³ L. Soler, A. Casanovas, C. Escudero, V. Pérez-Dieste, E. Aneggi, A. Trovarelli, J. Llorca, *Chem. Cat. Chem.* **2014**, *8*, 2748-2751

ELECTRONIC AND SPIN-STATE INSTABILITIES IN COBALTITES INVESTIGATED BY X-RAY ABSORPTION, EMISSION AND DIFFRACTION TECHNIQUES

J. Herrero-Martin^a, J. Padilla-Pantoja^b, S. Lafuerza^c, A. Romaguera^b, F. Fauth^a
and J. L. García-Muñoz^b

^aALBA Synchrotron Light Source, Cerdanyola del Vallès, Spain;

^bInstitut de Ciència de Materials de Barcelona, ICMA-B-CSIC, Bellaterra, Spain;

^cB ESRF-The European Synchrotron, 71, Avenue des Martyrs, Grenoble, France;

garcia.munoz@icmab.es

The spin-state (SS) of trivalent cobalt is being examined in a variety of cobalt oxides due to its proven ability to condition their electric transport, magnetic and electronic properties. Metal-insulator transitions or conductivity changes are found in a wide variety of compounds with perovskite and related structures such as $LnCoO_3$,¹ $Ln_{1-x}A_xCoO_3$,^{2,3} the layered double perovskites $LnBaCo_2O_{5.50}$ ⁴ or more complex structures.⁵ A recently synthesized cobaltite is $Ba_2Co_9O_{14}$ (BCO), a charge-ordered Co^{2+}/Co^{3+} rhombohedral $R-3m$ system that contains five crystallographically independent Co sites (Co_i), with octahedral (Co_i , $i=1,2,4,5$) and tetrahedral (Co_3) coordination, and undergoes a conductivity (insulator-insulator) transition at $T_{SS} \sim 567$ K.⁵

In combination with a synchrotron diffraction study in the 300-773 K range, soft x-ray absorption (XAS), x-ray magnetic circular dichroism (XMCD) and $K\beta$ x-ray emission spectroscopies (XES) have been applied to probe the electronic and spin state of Co ions at the different crystallographic sites.⁶ Charge transfer multiplet (CTM) calculations were applied to generate theoretical XAS and XMCD spectra that were used to discern and crosscheck our hypothesis on the spin-state in divalent and trivalent Co sites of the structure.

The resistivity drop -on warming across T_{SS} - arises from a spin-state transition at trivalent cobalt sites. Neutron data confirmed P_5-1 magnetic symmetry of Co_3 and Co_5 divalent sites below $T_N \approx 41$ K. CTM calculations confirm that the divalent Co sites are both in an $S=3/2$ high spin state. However, ordered Co_5 moments are far lower than expected for a Co^{2+} ion in a high spin ($S=3/2$) configuration [$m(Co_5) = 1.8 \mu_B/Co$]. Our x-ray spectroscopic results also allow us to discard a reduced electronic localization at Co_5 sites due to an unusually large charge transfer to O ligands.

Independently, the analysis of measured Co $K\beta$ XES spectra agrees with this model. With the help of known reference compounds, the integrated absolute difference (IAD) method allows for a quantitative analysis of the emission lines: differences in the number of unpaired spins per photoabsorbing ion in the $3d$ shell (ΔS) are (empirically) linearly related to the IAD values. The strong moment reduction in Co_5 , confirmed by independent groups, is too large to be due to covalency effects.

Diffraction results reveal a marked expansion across T_{SS} in the Co-O bond lengths around Co_1 and Co_2 octahedral sites. This anomalous expansion was also detected but it is much weaker in the Co_4O_6 octahedra.⁶ At T_{SS} the spin blockade of electronic transport is partially removed at the octahedral trimers and also at the Co_4O_6 units.

¹ A. Podlesnyak *et al*, *Phys. Rev. Lett.* (2006) 97, 247208.

² J. Herrero-Martin *et al*, *Phys. Rev. B* (2012), 86, 125106.

³ J.L. García-Muñoz *et al*, *Phys. Rev. B* (2016), 94, 014411.

⁴ A. Maignan *et al*, *Phys. Rev. Lett.* (2004) 93, 026401.

⁵ J. M. Chen *et al*, *Phys. Rev. B* (2012) 85, 094424.

⁶ J.L. García-Muñoz *et al*, *Phys. Rev. B* (2017) 95, 235129.

First XPS Results from the Commissioning of the Liquid μ -Jet Setup at the Circe NAPP End Station

P-37

E. Pellegrin^a, C. Escudero^a, V. Pérez-Dieste^a, J. Prat^a, and S. Ferrer^a

^a CELLS-ALBA Synchrotron Light Source, Carrer de la Llum 2-26, E-08290 Cerdanyola del Vallès (Spain); epellegrin@cells.es; cescudero@cells.es; vperez@cells.es; ferrer@cells.es.

The advent of liquid μ -jet setups as proposed by Faubel and Winter¹ – in conjunction with X-ray Photoemission Spectroscopy (XPS) – has opened up a large variety of experimental possibilities in the field of atomic and molecular physics as well as for more general experiments requiring a continuous flow of fresh sample materials due to the inherent sensitivity of, e.g., biological specimen under investigation with respect to the high brilliance (synchrotron or FEL) photon beam. Starting in 2015, a liquid μ -jet setup (originally produced by MicroLiquids GmbH, Germany) has been adapted to the specific technical requirements of the Circe Near Ambient Pressure Photoemission (NAPP) end station and has been successfully commissioned in December 2016 (see Fig. 1). In this contribution, we will report on the NAPP results from this commissioning activity, encompassing XPS data from water (with 10^{-4} M NaCl, see, e.g., Fig. 2), aqueous halide salt solutions, and aqueous methanol solutions.

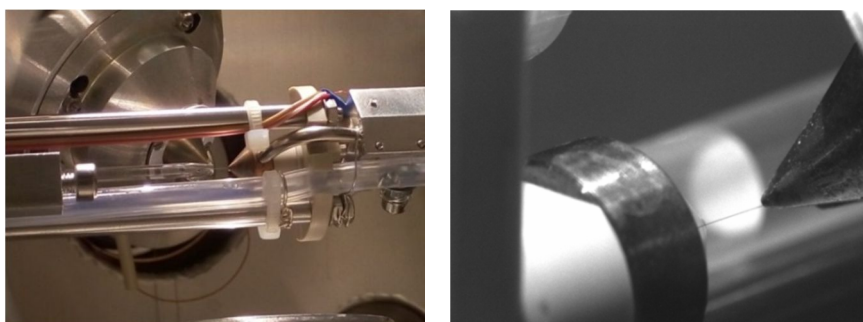


Fig. 1: The liquid μ -jet setup as installed in NAPP end station with the jet nozzle and catcher at the forefront and the electron analyzer nozzle on the back. The liquid μ -jet (thin dark grey line on the right hand side) has a diameter of 30 μ m.

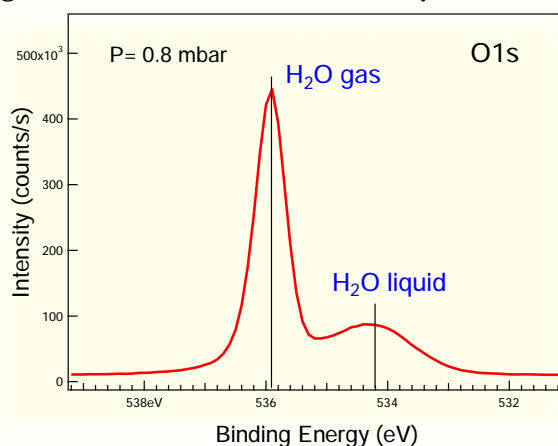


Fig. 2: Typical O1s XPS line taken from a water liquid μ -jet taken at a vacuum pressure of 0.8 mbar. The O1s line from water in the gas phase can be clearly distinguished from that of the liquid.

¹ B. Winter and M. Faubel, *Photoemission from Liquid Aqueous Solutions*, *Chem. Rev.* 2006, 106, 1176-1211

Recent advances at the CIRCE XPEEM

Michael Foerster, Lucia Aballe

ALBA Synchrotron Light Facility, 08290 Cerdanyola del Valles, Spain

The CIRCE beamline for electron spectroscopy and microscopy provides photons in the energy range 100 – 2000 eV with full polarization control, high resolution and intensity. One of its branches hosts a combined X-ray PhotoEmission Electron Microscope (XPEEM) and Low Energy Electron Microscope (LEEM) with energy analyzer, which permits imaging surfaces with chemical, structural, and magnetic sensitivity down to a lateral spatial resolution of 20 nm with photoelectrons and 10 nm in LEEM mode¹. It can be also used in microspot-LEED, -XPS and -ARPES working modes.

Since the beginning of user operation a variety of auxiliary equipment and custom-built sample holders have been added to offer a wide range of non-standard measurements in the fields of nanomagnetism, electronic devices, surface science, multiferroics, magnetization dynamics, etc².

Recent results of user and in house projects will be presented to illustrate the capabilities of the XPEEM experimental station and its custom sample environment at the present state. Future plans will be outlined as a basis for discussions with the user community.

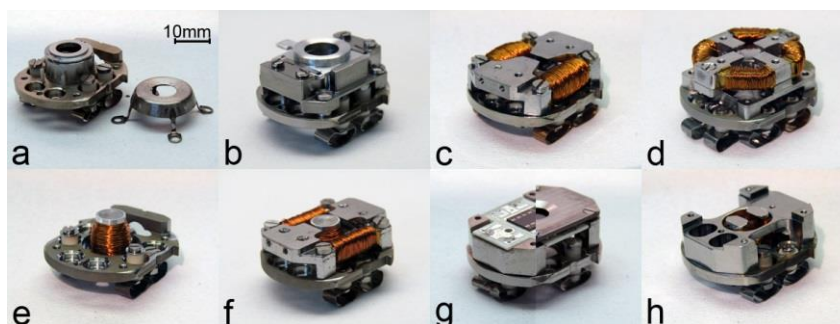


Figure 1: Photographs of some of the different sample holders in use at the ALBA PEEM: (a) Standard Elmitec sample holder for high temperature (cap on the side). (b) Sample holder with adapter piece for platelets as used in many deposition and characterization systems. Sample holders with (c) uniaxial in-plane electromagnet, (d) quadrupole in-plane electromagnet, (e) out-of-plane electromagnet, (f) combined out-of-plane and wide gap in-plane electromagnets. (g) Sample holder with adapter piece for a printed circuit board (PCB) for electrical contacts, e.g. by bonded wires. The cap is mounted floating, to avoid short-circuiting the contact wires. (h) Sample holder with adapter piece for PCB and a mini in-plane electromagnet (also out-of-plane magnets can be mounted in the central free space).

[1] Aballe et al., J. of Synch. Rad. 22 (3), 745 (2015)

[2] Foerster et al., Ultramicroscopy 171, 63 (2016)

STRUCTURAL BASIS OF THE ONCOGENIC INTERACTION OF PHOSPHATASE PRL-1 WITH THE MAGNESIUM TRANSPORTER CNNM2

Paula Giménez-Mascarell^{a1}, Iker Oyenarte^{a1}, Serge Hardy^{b2}, Tilman Breiderhoff^{cd3}, Marchel Stuiver^e, Elie Kostantin^{bf}, Tammo Diercks^a, Angel L. Pey^{g4}, June Ereño-Orbea^a, María Luz Martínez-Chantar^h, Reham Khalaf-Nazzalⁱ, Felix Claverie-Martin^{j5}, Dominik Müller^c, 6, Michel L. Tremblay^{b,f,k2,7} and Luis Alfonso Martínez-Cruz^{a8}

^a Structural Biology Unit, Center for Cooperative Research in Biosciences (CIC bioGUNE), Technology Park of Bizkaia, 48160 Derio, Bizkaia, Spain,

^b Rosalind and Morris Goodman Cancer Research Centre,

^c Department of Pediatric Nephrology, Charité Universitäts Medizin, Berlin, 13353 Berlin, Germany

^d Berlin Institute of Health, Berlin, Germany,

^e In-Cell NMR Laboratory, Department of NMR-supported Structural Biology, Leibniz Institute of Molecular Pharmacology (FMP Berlin), Robert-Rössle Strasse 10, 13125 Berlin, Germany,

^f Department of Biochemistry, and ^k Division of Experimental Medicine, Department of Medicine, McGill University, Montreal, Quebec H3A 1A3, Canada,

^g Department of Physical Chemistry, Faculty of Sciences, University of Granada, Av. Fuentenueva s/n, 18071 Granada, Spain,

^h Metabolomics Unit, Center for Cooperative Research in Biosciences (CIC bioGUNE), Technology Park of Bizkaia, 48160 Derio, Bizkaia, Spain,

ⁱ Department of Biomedical Sciences, An-Najah National University, P. O. Box 7, Nablus, Palestinian Territory,

^j Research Unit, Nuestra Señora de Candelaria University Hospital, 38010 Santa Cruz de Tenerife, Spain

Mg is an indispensable cation involved in many vital processes that include neurotransmission, enzyme activity, proliferation, differentiation, migration, and apoptosis. Its transport through the cellular membranes is mediated by specialized proteins among which are the four members of the Cyclin M (CNNM) family of transporters. In 2014 a breakthrough study (Hardy et al. *Oncogene*. 2014) showed that CNNMs are also involved in cancer development and progression via its association with a three member family of phosphatases called PRLs (Phosphatases of Regenerating Liver) (PRL1-3). PRLs are considered the most oncogenic of all tyrosine phosphatases as they are overexpressed in all kind of tumors, playing a critical role in metastatic progression. The association of CNNM with PRL causes an increase in the intracellular levels of magnesium in the tumor, thus promoting its proliferation and migration. Here we present the structural basis of the interaction between CNNM2 and PRL1, which involves the regulatory domain of the transporter and critical catalytic residues of the phosphatase. Our crystal structure shows a heterotetrameric complex that consist of a disc-like dimer of Bateman modules from CNNM2, bound to two independent PRL-1 molecules located at each side of the disk. The structure highlights the role of residue D558 from CNNM2 that, by entering the catalytic cavity of PRL-1, inhibits the phosphatase activity. These data put the flesh on the bones on the molecular mechanism by which the CNNM/PRL association increases the intracellular levels of magnesium in tumors, and sets the basis for the design of drugs that impede the association between these two families of proteins.

Synchrotron studies (x-ray absorption, photoemission, diffraction, μ) of hexagonal boron nitride thin films

D. Esteban, J. Cascales, I. Caretti, R. Gago and I. Jiménez

Instituto de Ciencia de Materiales de Madrid (ICMM-CSIC), Campus de Cantoblanco, E-28049 Madrid (Spain); david.esteban@csic.es

Hexagonal boron nitride (h-BN) is the preferred substrate for graphene growth, because of the similar structure and its electrical insulating behavior. Nowadays, the growth of ultrathin films is dominated by Chemical Vapor Deposition (CVD) techniques, due to the superior quality achieved hitherto. However, the growth by Physical Vapor Deposition (PVD) is desired due to the cleanliness of the process and the absence of nasty precursors.

In this work, a series of h-BN films with different thickness, texture, grain size and defect ratio were grown by Ion Beam Assisted Deposition (IBAD), by boron evaporation concurrent to the bombardment with nitrogen ions, using different ion energies and growth temperatures. In this way, we can control the order of the surface layer in the film.

Different synchrotron characterization techniques, including x-ray absorption near edge spectroscopy (XANES), photoemission (XPS) and x-ray diffraction (XRD) have been used to characterize the h-BN thin films. Some of the results will be presented and discussed.

XANES studies of MoBCN coatings: influence of Mo-doping in the BCN structure and film properties

I. Jiménez, I. Caretti, R. Gago, J. Cascales, and D. Esteban

Instituto de Ciencia de Materiales de Madrid (ICMM-CSIC), Campus de Cantoblanco, E-28049 Madrid (Spain); ijimenez@icmm.csic.es

The incorporation of refractory metals into ceramic protective coatings has been proposed as a way to increase the thermal resistance of such coatings and their tribological performance at high temperatures. Based on this premise, we are examining the effect of Mo incorporation into Boron-Carbon-Nitrogen (BCN).

In this work, a series of MoBCN coatings with Mo contents between 1- 10 at.% and a broad variation of B:C:N ratios, from carbon-rich to boron-rich, were grown by Ion Beam Assisted Deposition (IBAD), by using simultaneously two electron beam evaporators and a broad beam ion gun. The first e-beam evaporator was fed with different mixtures of C:Mo, the second one with the stoichiometric B₄C compound, and the ion gun with N₂ gas. In this way, the atomic and ionic fluxes of Mo, B, C and N condense as thin films of MoBCN with composition dependent on the substrate location. The method is optimized to produce up to 20 different coatings in a single run.

Characterization of the bonding structure was performed by XANES at BESSY synchrotron, and has been compared with FTIR and Raman data from laboratory measurements. A general discussion is presented on the growth method, the effect of Mo incorporation on the BCN structure and how the physical properties of BCN coatings are affected.

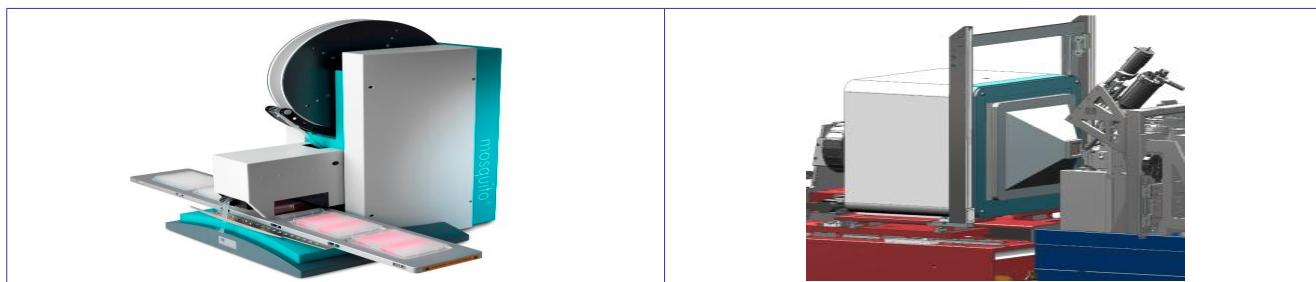
Poster Contributions

P-42

XALOC, the user-tailored beamline for all your scientific needs

Jordi S. Andreu, José Avila, Roeland Boer, Barbara M. Calisto, Xavi Carpena,
 Fernando Gil-Ortiz, Nahikari González, Ricardo Valcarcel, Jorge Villanueva
 Alba Synchrotron, c/ de la Llum 2, 08290 Cerdanyola del Vallès, Catalonia, Spain

Structural Biology is an area prone to constant innovation mostly motivated by improvements of the techniques in which it relies. Macromolecular crystallography (MX), the most powerful methodology for visualizing molecular structures at an atomic range, is now starting to share its worldwide hegemony with the latest advances in CryoEM or FELs, for instance. XALOC, the tunable MX beamline at the third generation 3-GeV ALBA synchrotron near Barcelona, doesn't want to lose pace and has pushed hard to match the experiment requirements of its users. The result is a highly stable and reliable X-Ray source (as an average ISa of ~20 illustrates) which can be remotely operated (more than 40% of academic proposals experiments in 2016/17) thoroughly used by a wide range of scientists working in so far related fields such as MOFs, membrane transport or DNA repair.



Insights of the newly acquired Mosquito LCP robot (left) and the projected He chamber (right)

As a matter of fact, recent upgrades have been performed (✓) or are under way (✓, to be operative during the actual 2017/2018 period) affecting all areas of a typical MX experiment, ranging from sample preparation up to final data processing:

Sample Preparation	-two new crystallization robots at the nearby BioLab: -Mosquito LCP ✓ -Dragonfly ✓ -miniKappa full omega range ✓	Data Collection	-6 KeV threefold flux increase -MxCUBE ✓ and ISPyB ✓ -EDNA Strategy at Cluster ✓ -faster detector readout (new LIMA) ✓ -remote DC ✓
Sample Mounting	-CATS: unipuck ✓ + gripper upgrade ✓ (60% sample storage increase; sample change achieved in just 10s) -plates (raster ✓, moveable beamstop ✓) -sample autofocus ✓	Data Processing	-XAMURAI (+ Phaser & Arcimboldo) ✓
	New experimental methodologies		-He Chamber for native phasing ✓ -high P/T for small molecule users ✓

- Abad, J. – 6, 29
Aballe, L. – 42, 51, 52, 53, 62, 66, 97
Acosta-Reyes, F.J. – 80
Agrestini, S. – 7, 57
Aguilar-Pujol, M.X. – 55
Alemán, B. – 27
Alén, B. – 25
Alfonso, E. – 14
Al-Jamal, K. – 84
Alonso, J. – 23, 24
Altarelli, M. – 6, 18
Álvarez-Fraga, L. – 30, 55
Amenitsch, H. – 11
Anastasi, P. A. F. – 17
Andrada-Chacón, A. – 6, 35
Andrés, A. de – 6, 30, 55
Andreu, J. – 43, 100
Ania, C.O. – 33
Ania, F. – 72, 88, 92
Arana, M. – 63
Aranda, M.A.G. – 7, 36, 41, 58
Artigués, M. – 20
Arvanitis, D. – 86
Ávila, J. – 100
Azenha, CSR. – 69
Balcells, L. – 16
Baonza, V.G. – 35
Barawi, M. – 14
Barla, A. – 54
Barón, A. – 63
Barral, L. – 89
Barranco-García, R. – 13
Bartolomé, J. – 7, 55
Bazaga-García, M. – 88, 90
Belda-Alcazar, V. – 65
Bencok, P. – 77
Benseny-Cases, N. – 41
Birrozzi, A. – 46
Biscari, C. – 5, 7, 8, 38
Bisti, F. – 7, 42
Blasco, J. – 73
Blázquez-Blázquez, E. – 13
Boada, R. – 15
Boer, R. – 43, 100
Bombardi, A. – 77
Bouza, R. – 90
Bozzo, B. – 16
Brady, M. A. – 12
Breiderhoff, T. – 97
Brown, G. E. – 26
Cabeza, A. – 87, 90
Cámara-Artigas, A. – 60
Campos, J.L. – 81
Caramazza, S. – 83
Caretta, I. – 98, 99
Carlino, V. – 74, 75
Carlomagno, I. – 6, 24
Carpena, X. – 43, 100
Casanovas, A. – 93
Cascales, J. – 98, 99
Casco, M. E. – 79
Castro, G.R. – 29, 31, 32, 33, 37
Cerrada, M.L. – 13
Chislov, M. – 60
Cinque, G. – 20
Cisneros-Fernández, J. – 16
Claverie-Martin, F. – 97
Climent-Pascual, E. – 30, 55
Cocera, M. – 21
Colchero, J. – 29
Colodrero, R.M.P. – 87, 91
Concepción, P. – 69
Conesa, C. – 63
Conesa, J.J. – 43
Costa, P.M. – 84
Cotrino, J. – 75
Cremades, A. – 55
Crespi, A. – 76
Crespo, I. – 75
Cuadrado, R. – 56
Cuenca-Gotor, V.P. – 34
Cuesta, A. – 6, 36
Dardonville, C. – 80
Das, R. – 24
DeKoning, H. – 80
Díaz-Moreno, S. – 15
Díaz-Rovira, A.M. – 82
Diercks, T. – 97
Dietsch, R. – 74
Dobrynin A.N. – 77
Ducic, T. – 20, 41, 63
Ellis, G. – 73
Enrique, P. – 92
Enrique-Jiménez, P. – 72, 89
Ereño, J. – 6, 22, 97
Escudero, C. – 14, 48, 49, 50, 51, 93, 95

Authors index

- Espinós, J.P. – 7, 48
Esteban, D. - 99
Evangelio, L. – 11
Eymery, J. – 25
Ezquerro, T. – 11, 12, 70
Fabra, M.J. – 10,
Fabrizi, F. – 77
Falcon, C. – 41
Farrag, Y. – 89
Fauth, F. – 7, 44, 79, 94
Fernández, E. – 21
Fernández, J.C. – 27
Fernández-Blázquez, J.P. – 27
Fernández-Gubieda, M.L. – 23, 24
Fernández-Regúlez, M. – 11
Fernández-Romero, A.J. – 29
Ferrer, S. – 42, 95
Ferrerres, M.J. – 20
Figuera, J. de la – 7, 53, 62, 66, 78
Finizio, S. – 52
Flores, A. – 72, 88, 92
Foerster, M. - 7, 51, 52, 53, 62, 66, 96
Fontcuberta, J. – 52, 67
Förster, A. – 62
Francoual, S. – 77
Fraxedas, J. – 5, 11
Fresno, F. – 14
Frontera, C. – 5, 16
Gago, R. – 98, 99
Galceran, R. – 16
Galvez-Martinez, S. – 50
Gambardella, P. – 54
Gamino, M. – 67
García Gutiérrez, M.C. – 11, 12, 70
García, A. -14
García, C. – 14
García, J. – 73
García, X. – 94
García-Granda, S. – 33
García-Muñoz J.L. – 78, 95
García-Prieto, A. – 23
García-Saura, A.G. – 71
Gargiani, P. – 7, 51, 54, 56, 67, 70, 86
Garvey C.J. – 81
Gil-Ortiz, F. – 43, 71, 72, 100
Giménez-Mascarell, P. – 98
Giorgetti, M. – 46
Godey, S. – 54
Gómez, J. – 20
Gómez-Fatou, M.A. – 72, 88, 92
Gómez-Mascaraque, L.G. – 10
Gomis-Berenguer, A. – 6, 33
González, M.A. – 91
González, N. – 100
González-Castillo, E.I. – 72
González-Cobos, J. – 48
González-Elipe, A.R. – 48
González-Ruano, C. – 91
Gottlieb, S. – 11
Gustafson, J. – 49
Gutiérrez, E. – 11, 71
Hagman, B. – 49
Hardy, S. – 97
Heinis, D. – 44, 46
Henschel, A. – 57
Hernández, C. – 69
Hernández, J.M. – 52
Hernández, L.E. – 64
Hernández-Mínguez, A. – 52
Herrero-Martín, J. – 16, 51, 57, 73, 77, 94
Hu, Z. – 57
Huck-Iriart, C. – 49
Ibañez, J. – 34
Ilyn, M. – 49
Impérator-Clerc, M. – 81
Jang, L.Y. – 57
Jiménez, I. – 98, 100
Jiménez-Villacorta, F. – 30, 54
Jordá, J.L. – 80
Joseph, B. – 83
Juanhuix, J. – 7, 43, 71
Kamma-Lorger, C.S. – 40
Kasinathan, D. – 57
Khalaf-Nazzal, R. – 97
Kläui, M. – 52
Ko, K.T. – 57
Kostantin, E. – 97
Kowalik, I.A. – 86
Kraus, J.P. – 22
Kreuzer, M. – 20, 41, 72, 82, 85
Kuo, C.Y. – 57
Lafuerza, S. – 94
Landa-Medrano, I. – 45, 64
Laszcynski, N. – 46
Laycock, B. – 81
Lee, R. – 45

- Lendínez, S. – 52
Liras, M. – 14
Llorca, J. – 93
Llugany, M. – 26
Londono-Zuluaga, D. – 36
López, O. – 21
López-Mesas, M. – 83
López-Mir, L. – 16
López-Rubio, A. – 10
López-Vicente, R. – 29
Losilla, E.R. – 87
Lucas de-Consuegra, A. – 48
Lucas, I. – 66, 91
Luque, F.L. – 86
Machado, B. – 43, 100
Macià, F. – 52
Majtan, T. – 22
Makenji, K. – 17
Malfois, M. – 7, 40
Malmir, S. – 89
Mandziak, A. – 51, 53, 63
Manjón, F.J. – 34
Marcano, L. – 6, 23, 24
Marcilla, R. – 27
Marco, J.F. – 79
Marini, C. – 24, 26, 44, 46, 65, 82, 84
Martín Rodríguez, R. – 23
Martínez Rovira, I. – 6, 20
Martínez, B. – 16
Martínez, F. – 63
Martínez, J. C. – 13, 40
Martínez-Blanco, J. – 85
Martínez-Chantar, M.L. – 97
Martínez-Criado, G. – 6, 25
Martínez-Cruz, L.A. – 22, 97
Martínez-Escandell, M. – 79
Martínez-Moñino, A.B. – 71
Martínez-Sanz, M. – 5, 10
Martín-García, L. – 53, 62
Mascaraque, A. – 53, 66, 91
Mateo-Martí, E. – 7, 50
Mateos-Pedrero, C. – 69
Maza, de la A. – 21
Mazzoli, C. – 77
Mendez, A. – 69
Meneghini, C. – 24
Michel, E.G. – 85
Miguel de, J.J. – 86
Millán, C.R. – 80
Miravittles, C. – 76
Missiul, A. – 44, 61
Moner, V. – 6, 21
Monreal-Bernal, A. – 27
Monteseguro, V. – 34
Moreno Fernández, H. – 75, 76
Muela, A. – 23
Mugarza, A. – 54
Mukhin, A.A. – 77
Mullaliu, A. – 46
Müller, D. – 97
Muñoz, A. – 34
Muñoz, D. – 23
Munuera, C. – 53
Nemati, Z. – 24
Nicolas, J. – 42
Niño, M.A. – 87
Nistor, C. – 54
Nogales, A. – 11
Oliva, A. – 85
Olivares-Marín, M. – 45, 64
Olivera-Pastor, P. – 87, 90
Olszweski, W. – 14, 44, 46, 83
Ortega, J. E. – 49
Ortega-Villasante, C. – 63
Orue, I. – 23
Otón, J. – 43
Oyenarte, I. – 22, 97
Padilla, J. – 29, 94
Palacio, I. – 53
Pannunzio Miner, E. V. – 16
Parra, J.B. – 33
Passerini, S. – 46
Pastor, R. – 63
Pastor-Pérez, L. – 65
Pell, A. – 26, 82
Pellegrin, E. – 7, 42, 51, 57, 67, 74, 75, 96
Pellicer-Careño, I. – 15
Peña O'Shea, V. de la – 5, 14
Perea, R. – 20
Pereira, A.L.J. – 34
Pereiro, E. – 43, 45, 64
Pérez, E. – 5, 13
Pérez, L. – 53, 62, 66, 67, 91
Pérez, R. – 14
Pérez-Berná, A.J. – 43
Pérez-Dieste, V. – 14, 48, 49, 50, 51, 69, 93, 95

Authors index

- Pérez-Murano, F. – 11
Persichetti, L. – 54
Pey, A.L. – 97
Pfaendner, R. – 81
Phan, M.H. – 24
Pierucci, D. – 42
Plaza, M. – 85, 91
Plaza-Garrido, M. – 59
Ponrouch, A. – 64
Pont, M. – 7, 39
Popescu, C. – 34, 44
Porcaro, F. – 24
Postorino, P. – 83
Prados, A. – 32
Prat, J. – 95
Prezado, Y. – 20
Prieto, C. – 30, 55
Prieto, J.L. – 66
Prieto, P. – 53, 62, 78
Proenca, M. – 66
Pruneda, M. – 56
Puxeu, J. – 20
Quesada, A. – 53, 62, 66, 68
Quiles, S. – 88
Quiles-Díaz, S. – 72, 93
Quirós, C. – 85
Quitmann, C. – 6, 28
Raaij, M. van – 6, 19
Ramanan, N. – 44, 46, 83
Ramírez-Jiménez, R. – 30, 55
Ramos-Fernández, E. V. – 5, 15, 66, 79
Rebollar, E. – 12, 70
Reguero, V. – 27
Reñones, P. – 14
Resina-Gallego, M. – 82
Rey, F. – 79
Rico, V. J. – 48
Rius, G. – 11
Rius, J. – 47, 77
Robles, R. – 54
Rodríguez-Hernández, P. – 34
Rodríguez-Reinoso, F. – 79
Rodríguez-Rodríguez, A. – 5, 12, 70
Rogalev, A. – 25
Rogler, D. – 74
Rojo, T. – 45
Romaguera, A. – 94
Ronda, M. – 15
Rosanes, M. – 43
Rouziere, S. – 81
Ruano, D. – 51, 70
Rubio-Zuazo, J. – 29, 30, 31, 32, 37, 85
Ruiz de Larramendi, I. – 45
Ruiz del Arbol, N. – 49
Ruiz-Gomez, S. – 53, 62, 66, 92
Salagre, E. – 85
Salas-Colera, E. – 6, 27, 32, 33, 55
Salavagione, H.J. – 72, 88, 92
Salcedo, I.R. – 87, 90
Salinas-Garcia, M.C. – 59
Salomon, D. – 25
Sánchez de Rojas, C. – 5, 17
Sánchez, F. – 67
Sánchez, M.C. – 73
Sanchez-Arenillas, M. – 50
Sánchez-Benítez, J. – 35
Sánchez-Ferrer, A. – 71
Sánchez-Valencia, J.R. – 48
Sans, J.A. – 6, 34
Santacruz, I. – 36
Santiso, J. – 68
Santos, P. – 52
Saperas, N. – 80
Sauthier, G. – 74
Schiller, F. – 7, 49
Schirone, S. – 54
Schmidt, M. – 57
Segovia, P. – 85
Segura-Ruiz, J. – 25
Seksek, O. – 20
Senokos, E. – 27
Sepúlveda-Escribano A. – 15, 65
Serrano, A. – 23, 78, 91
Sette, F. – 5, 9
Shand, M. T. – 17
Shuttleworth, P.S. – 72
Silvestre-Albero, J. – 79
Simonelli, L. – 7, 14, 23, 24, 26, 44, 46, 82, 83
Skumryev, V. – 77
Solano, E. – 40
Soler, L. – 93
Sorrentino, A. – 43, 45, 46, 65
Srikanth, H. – 24
Statuto, N. – 52
Steadman, P. – 77
Stec, M. – 81

Stievano, L. – 45
Stremper, J. – 77
Stuiver, M. – 97
Subías, G. – 74
Subirana, M.A. – 6, 26, 82
Sulé-Suso, J. – 20
Tallarida, M. – 42
Tanaka, A. – 57
Tesio, A. Y. – 45
Thomasset, M. – 74
Tjeng, L.H. – 57
Toledo, C. – 29
Tonti, D. – 7, 45, 46, 64
Torre de la, A.G. – 36
Torrelles, X. – 68
Tremblay, M.L. – 97
Urbina, A. – 29
Valbuena, M.A. – 7, 54, 86
Valcárcel, R. – 43, 100
Valencia, S. – 23
Valido, I.H. – 26, 82
Valiente, M. – 26, 82
Vallcorba, O. – 7, 36, 44, 47, 76
Valvidares, S.M. – 51, 56, 57, 67, 70, 73
Vasili, H.B. – 51, 56, 57, 68
Vila, M. – 6, 32
Vilatela, J. – 6, 31
Villanueva, J. – 100
Villar, I. - 14
Wang, C. – 12
Washbrook, S. – 17
Webb, S.M. – 26
Wu, N. – 45
Yousef, I. – 7, 20, 21, 41, 63, 72
Zapata-Pérez, R. – 71
Zea-Garcia, J.D. – 36